Metadata of the chapter that will be visualized online

Chapter Title	Binary Systems and Their Nuclear Explosions	
Copyright Year	2018	
Copyright Holder	The Author(s)	
Author	Family Name	**Isern**
	Particle	
	Given Name	**Jordi**
	Suffix	
	Organization	Institute of Space Sciences (ICE, CSIC)
	Address	Barcelona, Spain
	Organization	Institut d'Estudis Espacials de Catalunya (IEEC)
	Address	Barcelona, Spain
	Email	isern@ieec.uab.es
Corresponding Author	Family Name	**Hernanz**
	Particle	
	Given Name	**Margarita**
	Suffix	
	Organization	Institute of Space Sciences (ICE, CSIC)
	Address	Barcelona, Spain
	Organization	Institut d'Estudis Espacials de Catalunya (IEEC)
	Address	Barcelona, Spain
	Email	hernanz@aliga.ieec.uab.es
Author	Family Name	**José**
	Particle	
	Given Name	**Jordi**
	Suffix	
	Organization	Universitat Politècnica de Catalunya (UPC)
	Address	Barcelona, Spain
	Organization	Institut d'Estudis Espacials de Catalunya (IEEC)
	Address	Barcelona, Spain
	Email	jordi.jose@upc.edu

Author's Proof

Abstract	The nuclear energy supply of a typical star like the Sun would be ~ 10^{52} erg if all the hydrogen could be incinerated into iron peak elements.

Chapter 5
Binary Systems and Their Nuclear Explosions

Jordi Isern, Margarita Hernanz, and Jordi José

5.1 Accretion onto Compact Objects and Thermonuclear Runaways

The nuclear energy supply of a typical star like the Sun would be $\sim 10^{52}$ erg if all the hydrogen could be incinerated into iron peak elements. Since the gravitational binding energy is $\sim 10^{49}$ erg, it is evident that the nuclear energy content is more than enough to blow up the Sun. However, stars are stable thanks to the fact that their matter obeys the equation of state of a classical ideal gas that acts as a thermostat: if some energy is released as a consequence of a thermal fluctuation, the gas expands, the temperature drops and the instability is quenched. The first researchers to discuss the scenario under which stars could explosively release their nuclear energy were Hoyle and Fowler (1960). They showed that this could occur under conditions of dynamic compression, as a consequence of collapse, or under electron degeneracy. They also pointed out in their seminal paper that hydrogen could only be responsible for mild explosions, like novae, as a consequence of the necessity to convert two protons into two neutrons, and that only the thermonuclear fusion of carbon could be energetic enough to feed a strong explosion. They did not consider helium because by this epoch the He-burning mechanism was not yet known.

J. Isern · M. Hernanz (✉)
Institute of Space Sciences (ICE, CSIC), Barcelona, Spain

Institut d'Estudis Espacials de Catalunya (IEEC), Barcelona, Spain
e-mail: isern@ieec.uab.es; hernanz@aliga.ieec.uab.es

J. José
Universitat Politècnica de Catalunya (UPC), Barcelona, Spain

Institut d'Estudis Espacials de Catalunya (IEEC), Barcelona, Spain
e-mail: jordi.jose@upc.edu

R. Diehl et al. (eds.), *Astrophysics with Radioactive Isotopes*, Astrophysics and Space Science Library 453, https://doi.org/10.1007/978-3-319-91929-4_5

AQ2

Intermediate and low-mass stars ($M < 10$–$12\,M_\odot$) are able to get rid of their envelope and end their life as a white dwarf. On the contrary, massive stars form an iron core that grows until it reaches the Chandrasekhar mass and collapses to a neutron star or a black hole. The degenerate core of white dwarfs can have different chemical compositions, He, C-O or O-Ne, and different size depending on the mass and the single or binary nature of the progenitor. Single stars with masses in the range of 8–9 to 10–12 $M_\odot$ produce oxygen-neon cores, those in the mass range 0.5 to 8–9 $M_\odot$ produce carbon-oxygen cores, while stars with a mass in the range 0.08–0.5 $M_\odot$ produce helium cores, but the lifetime of such stars is so large that they cannot produce a white dwarf in a Hubble time. Members of a close binary system can be strongly perturbed by their companion and thereby produce different outcomes. For instance, stars with a mass of the order of 2.5 $M_\odot$ can end their life as He white dwarfs with a mass of the order of 0.4 $M_\odot$.

The destiny of isolated white dwarfs is to cool forever. However, if they are members of a close binary system, they can revive as a consequence of mass transfer from their companion. As the mass grows, the radius of the white dwarf shrinks and the density increases, as can be derived from simple dimensional arguments. The hydrostatic and the degenerate, non-relativistic electron pressures have the functional form $P \sim M^2 R^{-4}$, and $P \sim M^{5/3} R^{-5}$, respectively. Thus it is always possible to find an equilibrium configuration defined by a mass-radius relation $R \sim M^{-1/3}$. However, as the density grows, the Fermi energy increases and electrons become relativistic. In the extreme case, the electron pressure takes the form $P \sim M^{4/3} R^{-4}$ and, since it has the same dependence on R as hydrostatic pressure, there is no longer a definite lengthscale. Furthermore, according to the virial theorem, stars supported by relativistic particles are not gravitationally bound and the injection or removal of small amounts of energy can cause a large expansion or contraction of the star.

The behavior of the different cores depends on the net rate at which energy is injected by the burning front or removed by electron captures on the ashes that were left from the previous burning cycle. Both quantities depend on the chemical composition of the stellar cores. Helium cores always experience a thermonuclear explosion because of the large energy content and the extreme flammability of He. Carbon-oxygen cores can explode or collapse, depending on the ignition density (Canal et al. 1990). If this density is larger than some critical value, $\sim(5$–$8) \times 10^9$ g/cm^3, the electron captures become dominant and they collapse to a neutron star (Bravo and García-Senz 1999). ONe-cores ignite at such a density that they always tend to collapse (Nomoto and Kondo 1991; Gutierrez et al. 1996) and Fe-cores always collapse because of their inability to release nuclear energy. Recently, however, 3D models of explosion have cast some doubts to this picture and the possibility that C-O and O-Ne-Mg cores could experience a mild explosion leaving a gravitationally bound remnant made of iron-peak elements has emerged.

5.1.1 Evolution of Degenerate Cores Before Ignition

The behavior of the white dwarf interior during the accretion phase depends on the competition between the physical processes that increase the temperature of the material (compression, nuclear reactions in the inner core and possible burning of the freshly accreted matter) and those that cool the star (via neutrino and photon losses). Since the energy transport is dominated by electron conduction, one of the relevant timescales is the time taken by a thermal signal to cross the star, given by Henyey and L'Ecuyer (1969):

$$\tau_{\mathrm{TH}} = \frac{3\kappa\rho^2 c_{\mathrm{P}}}{64\sigma T^3} l^2 \tag{5.1}$$

where κ, ρ, T, σ and c_{P} have their usual meanings and l is the linear extent of the region considered, the radius of the white dwarf in this case.

The effects of the compression induced by the accreted mass can be separated into two terms (Nomoto 1982). The first term is due to the increase in density at a fixed mass fraction as a consequence of the increase in mass, and its effects are quite uniform throughout the whole star. The second term corresponds to compression as matter moves inward in mass fraction space. It is negligible in the inner, strongly degenerate regions, where the major part of the compression work is invested in increasing the Fermi energy of electrons, but is very large in the external semi-degenerate layers. This means that a thermal wave generates in the outer layers and propagates towards the interior. A rough estimate of the compression-induced luminosity is: $L_{\mathrm{c}}/L_{\odot} = 1.4 \times 10^{-3} T_7 \dot{M}_{10}$, where T_7 is the temperature in units of 10^7 K, and $\dot{M}_{10}$ is the mass accretion rate in units of 10^{-10} $\mathrm{M}_{\odot}$/year.

The effects of this thermal wave on the physical state of the white dwarf interior depend on the time this wave takes to reach the center of the star, τ_{TH}, as compared with the time required for the star to reach the Chandrasekhar mass, τ_{comp} (Hernanz et al. 1988). For low accretion rates, $\dot{M} \leq 3 \times 10^{-10}$ $\mathrm{M}_{\odot}$/year, the thermal wave has time to reach the center, but normal cooling through the photosphere is dominant and the white dwarf evolves nearly isothermally with a temperature determined by the balance between compression and cooling, with the contribution of neutrinos and nuclear reactions. For high accretion rates, $5 \times 10^{-8} \leq \dot{M} \leq 10^{-6}$ $\mathrm{M}_{\odot}$/year, compression heating dominates but, if the mass of the white dwarf is large enough, the thermal wave has no time to reach the center and, since there $\tau_{\mathrm{TH}} \gg \tau_{\mathrm{comp}}$, these layers evolve with an adiabatic index:

$$\Gamma_3 - 1 = \frac{0.815 + 0.251\Gamma^{1/4}}{0.945 + 0.646\Gamma^{1/4}} \tag{5.2}$$

where Γ is the Coulomb coupling constant. For typical values of $\Gamma \sim$100–200, this index is $\sim$0.5 and degenerate matter is heated gently. For intermediate accretion rates, the thermal wave has sufficient time to arrive at the central layers and they

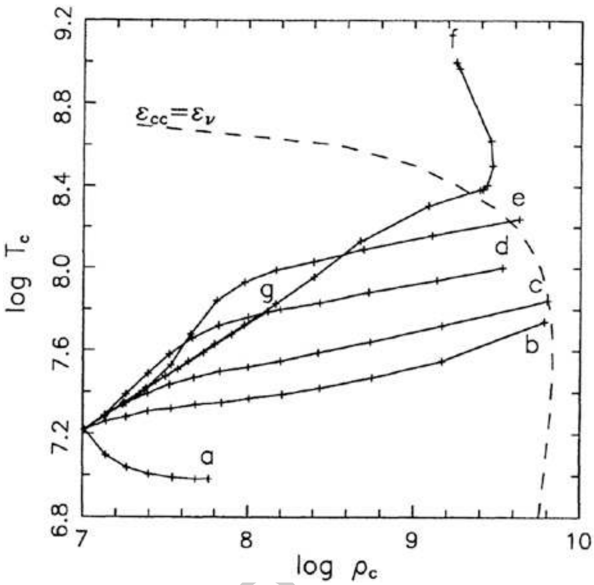

Fig. 5.1 Evolution of the center of a C-O white dwarf in the $\log T$-$\log \rho$ plane for several accretion rates of pure C-O: (a) 10^{-10} $M_\odot$/year; (b) $5\,10^{-10}$ $M_\odot$/year; (c) 10^{-9} $M_\odot$/year; (d) $5\,10^{-9}$ $M_\odot$/year; (e) $5\,10^{-8}$ $M_\odot$/year; (f) $5\,10^{-7}$ $M_\odot$/year; (g) $5\,10^{-6}$ $M_\odot$/year (Bravo et al. 1996). The dashed line represents the ^{12}C ignition curve

experience a sudden heating, followed by an evolution in the ρ-T diagram governed by the balance between the heating and cooling agents already mentioned (see Fig. 5.1).

As the temperature increases, fusion reactions start to become important. At low temperatures, neutrino emission is able to control them, but due to the different temperature dependences the energy production by nuclear reactions overwhelms neutrino losses and matter burning becomes unstable. This critical temperature, commonly called ignition temperature, T_{ig}, is defined as $\epsilon_{CC}(T_{ig}) = \epsilon_\nu(T_{ig})$. If ignition happens under degenerate conditions, a thermonuclear runaway occurs. The nature of this instability can be understood with the following argument. Assume that $P = P_e(\rho) + P_i(\rho, T)$, where P_e and P_i are the electron and ion pressure, respectively, and that ions behave as an ideal gas. Also assume that nuclear reactions release isochorically an amount of energy δq, and that matter expands adiabatically until pressure equilibrium is reached. The corresponding density change is:

$$\frac{\delta\rho}{\rho} = -\frac{2}{3\Gamma_1}\frac{P_i}{P_e + P_i}\frac{Q}{kT}\frac{\delta N}{N} \tag{5.3}$$

where Γ_1 is the first adiabatic index, Q is the energy released per fused nucleus and δN is the number of nuclei that have fused. Since $Q \sim 1\,\mathrm{MeV}$ and $kT \sim 1\,\mathrm{keV}$, if the ideal gas is dominant a small energy release will cause a large expansion with an associated cooling. On the contrary, if $P_e \gg P_i$ adiabatic cooling is not efficient and matter will heat until $P_e \sim P_i$. At this point, if $\tau_{nuc} \ll \tau_{HD}$, nuclear reactions will continue until incineration of matter is complete. Here $\tau_{nuc}^{-1} = d\ln(\epsilon_{nuc})/dt$, and $\tau_{HD} = l/c_s$ is the hydrodynamic time, l the dimension of the burning region

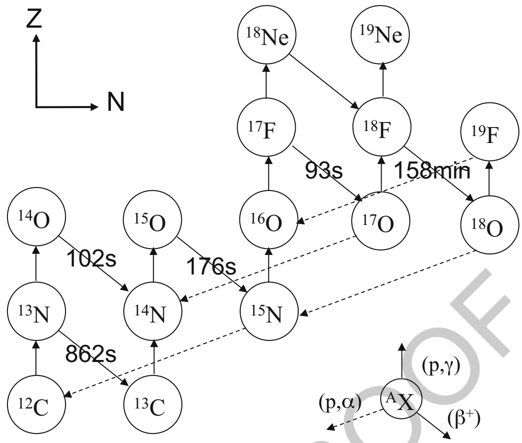

Fig. 5.2 Scheme of the carbon-nitrogen-oxygen (CNO) cycle of hydrogen burning, which operates out of equilibrium in stellar explosions. The lifetimes of the β^+-unstable nuclei, which act as *bottlenecks* of the cycle, are displayed

and c_s the sound velocity. Under hydrostatic equilibrium, $\tau_{HD} \sim \tau_{ff}$, where $\tau_{ff} = (24\pi G\rho)^{-1/2} \sim 444\rho^{-1/2}$ is the free-fall time.

It is important to realize here that in the case of H-burning two protons have to be converted into two neutrons and that β-decays will control the total rate. At high temperatures, the longest β-decay timescale is that of ^{15}O, with a mean lifetime of $\tau_{15O} = 178$ s (see Fig. 5.2) and the maximum energy production rate is:

$$\epsilon_{CNO} \leq 1.3 \times 10^{14} \frac{X_{CNO}}{0.01} \text{ erg/g/s} \tag{5.4}$$

for an assumed energy release of 28 MeV per reaction (Mazurek and Wheeler 1980). Therefore, complete burning cannot be achieved in a short time in comparison to the hydrodynamic time and H-driven explosions cannot involve all of the star.

5.1.2 The Thermonuclear Runaway

When the central regions cross the ignition line, the temperature starts to rise and nuclear reactions accelerate. Conduction is rapidly overwhelmed by energy production and a convective core forms. This core grows very quickly as a consequence of the energy release enhancement and cannot prevent the continuous rise of the temperature. When the turnover timescale of the convective eddies is longer than the heating timescale, one or several bubbles enter into the dynamical regime (Nomoto et al. 1984; García-Senz and Bravo 2005; Woosley et al. 2004), a thermonuclear runaway occurs, and a flame begins to propagate (Timmes and Woosley 1992).

The igniting zone can be imagined as a highly turbulent region where the evolution of turbulent elements towards the thermonuclear runaway is governed by the balance between heating by nuclear burning and collision of turbulent eddies, and cooling by electron conduction and expansion pdV-work. In principle it is possible to assume a distribution of fluctuations characterized by their size, δ, and their temperature excess, ΔT. These fluctuations will be able to grow only if the conductive cooling is not able to evacuate the nuclear energy generated at the center of the bubble. Consequently their size has to be larger than:

$$\delta = \sqrt{\frac{2\sigma \Delta T}{\rho \epsilon_{\rm nuc}}} \tag{5.5}$$

where σ is the thermal conductivity and $\epsilon_{\rm nuc}$ is the nuclear energy generation rate. For background temperatures in the range $(6-8) \times 10^8$ K, fluctuations must have a minimum size of 4 m–30 cm, respectively, to be able to grow. When this condition is satisfied, the temperature increases, the burning propagates by conduction (see next section) and the buoyancy accelerates the bubble to a substantial fraction of the sound speed (García-Senz and Bravo 2005). During this time other bubbles can develop similar runaways, grow and float away when they reach a critical size of $\sim$1 km, such that the final outcome is an asynchronous ignition at multiple points.

The runaway of hydrogen is responsible for nova explosions. The mechanism for such explosions can be better understood after evaluating some relevant timescales (Starrfield 1989): the accretion timescale, defined as $\tau_{\rm acc} \sim \rm M_{acc}/\dot{M}$ (which is of the order of 10^4–10^5 years, depending on the accretion rate $\dot{M}$ and accreted mass $M_{\rm acc}$), the nuclear timescale $\tau_{\rm nuc} \sim c_{\rm p}T/\epsilon_{\rm nuc}$ (which is as small as a few seconds at peak burning) and the hydrodynamic timescale ($\tau_{\rm HD} \sim H_{\rm p}/c_{\rm s} \sim (1/g)\sqrt{P/\rho}$; $H_{\rm p}$ is the pressure scale height). During the accretion phase, $\tau_{\rm acc} \leq \tau_{\rm nuc}$, accretion proceeds and the envelope mass increases. When degenerate ignition conditions are reached, degeneracy prevents envelope expansion and the thermonuclear runaway occurs. As temperature increases, the sudden release of energy would lift degeneracy in the envelope and ultimately halt the thermonuclear runaway, but this is not the case because $\tau_{\rm nuc} \ll \tau_{\rm HD}$. Therefore, the value of the nuclear timescale is crucial for the development of the thermonuclear runaway (TNR) and its final fate. In fact there are two main types of nuclear timescales: those related to β^+-decays, $\tau_{\beta+}$, and those related to proton capture reactions, $\tau_{({\rm p},\gamma)}$. In the early evolution towards the TNR, $\tau_{\beta+} < \tau_{({\rm p},\gamma)}$ and the CNO cycle operates at equilibrium. But as temperature increases up to $\sim 10^8$ K, the reverse situation occurs, ($\tau_{\beta+} > \tau_{({\rm p},\gamma)}$), and thus the CNO cycle is β-limited (see Fig. 5.2). In addition, since the large energetic output produced by nuclear reactions can not be evacuated by radiation only, convection sets in and transports the β^+-unstable nuclei to the outer cooler regions where they are preserved from destruction and where they will decay later on ($\tau_{\rm conv} < \tau_{\beta+}$), leading to envelope expansion, luminosity increase and mass ejection if the attained velocities are larger than escape velocity.

5.1.3 Physics of the Burning Front

An explosion is the mechanical disruption of a system as a consequence of a rapid release of energy. In the case of an exploding white dwarf, enough mass, $\sim 0.3\,M_\odot$, has to be quickly embraced by the burning region to unbind the star. This can be accomplished either through detonation (Arnett 1969) or through deflagration (Nomoto et al. 1976). A detonation is shock-induced burning propagating supersonically into an unburned medium, while a deflagration is a burning front that propagates by thermal conduction at subsonic velocities. Both, detonation and deflagration, are driven by a physical mechanism. However, there is a third possibility: spontaneous burning. This case occurs when the ignition conditions are reached nearly simultaneously in several points in such a way that burning spreads over a large region without any transport mechanism (Blinnikov and Khokhlov 1986; Woosley and Weaver 1986). The propagation velocity, a phase velocity in fact, can be estimated as $v_{\rm sb} = (d\tau_{\rm nuc}/dr)^{-1}$, where $\tau_{\rm nuc}$ plays a critical role at the onset of burning. This velocity increases when the absolute values of the temperature and density gradients decrease. Thus, regions with $v_{\rm sb} \geq c_{\rm s}$ ignite spontaneously and the burning front propagates supersonically. Because of the strong dependence on T, the most important factor is the temperature profile.

In order to describe the properties of the burning front, either supersonic or subsonic, it is usually assumed (Landau and Lifshitz 1959) that the unburned material is separated from the combustion products by a region of width δ where reactions take place. If $\delta \ll l$, where l is the typical scale length of the system, it is possible to connect both sides of the front by means of conservation laws of mass, momentum and energy. In the frame associated with the front, these equations, known as the Rankine-Hugoniot jump conditions, can be written as (Landau and Lifshitz 1959; Mazurek and Wheeler 1980):

$$\rho_1 u_1 = \rho_0 u_0 \tag{5.6}$$

$$P_1 + \rho_1 u_1^2 = P_0 + \rho_0 u_0^2 \tag{5.7}$$

$$\varepsilon_1 + \frac{P_1}{\rho_1} + \frac{u_1^2}{2} = \varepsilon_0 + \frac{P_0}{\rho_0} + \frac{u_0^2}{2} + q \tag{5.8}$$

that are similar to those describing shock waves except for the presence of the term q that represents the amount of energy released by reactions. The subscripts 0 and 1 denote fuel and ashes, respectively, u is the matter velocity, ε is the specific internal energy, and the remaining symbols have their usual meaning. The mass flux crossing the front is given by:

$$j = \rho_0 u_0 = \rho_1 u_1 \tag{5.9}$$

which can be written, using the mass and momentum conservation equations (Eqs. (5.6) and (5.7) respectively), as:

$$j^2 = -\frac{P_0 - P_1}{V_0 - V_1} \tag{5.10}$$

where $V = 1/\rho$ is the specific volume. The mass flux (and the velocity of the front with respect to the unburned material) is determined by the ratio between the difference of pressures and specific volumes at both sides of the burning front. Therefore, real solutions must satisfy: $(P_1 > P_0,\ V_1 < V_0)$ or $(P_1 < P_0,\ V_1 > V_0)$. The first solution corresponds to a detonation and the second one to a deflagration (Landau and Lifshitz 1959).

The velocity at which a detonation propagates can be obtained from the energy conservation equation. Equation (5.8) can be written as:

$$\varepsilon_0 + q - \varepsilon_1 + \frac{1}{2}(P_0 + P_1)(V_0 - V_1) = 0 \tag{5.11}$$

which is called the detonation adiabat (the case $q = 0$ is called the shock adiabat). The final state is obtained equating (5.10) and (5.11), once the properties of the front have been specified (see Fig. 5.3). The physical meaning of this solution is clear. A shock heats and compresses the material to a state (P_{sh}, V_{sh}) given by the intersection of Eq. (5.10) with the shock adiabat. Because of the temperature increment, material burns and reaches the state (P_1, V_1), defined by the intersection of Eq. (5.10) with the detonation adiabat. Since $q \geq 0$, then $P_1 < P_{sh}$, $V_1 > V_{sh}$ and the post-shock burning produces a rarefaction.

The family of solutions obtained from Eqs. (5.10) and (5.11) and j as a free parameter has an extremum for which j and the front velocity are minima. This solution, called the Chapman-Jouguet detonation, corresponds to the case where Eq. (5.10) is tangent to (5.11). This extremal solution has the following properties: (1) it is only determined by the thermodynamic properties of the material, including

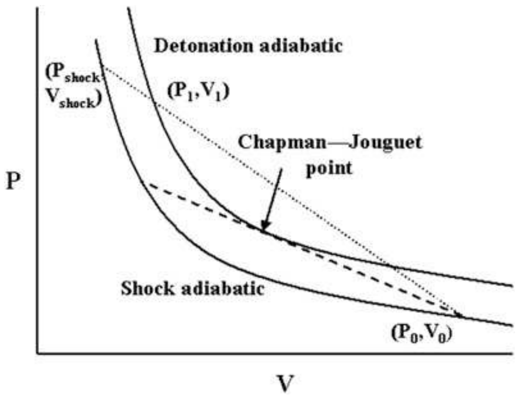

Fig. 5.3 Adiabatic of a shock and a detonation in the P–V diagram. The dotted and dashed lines represent the condition of conservation of mass and momentum ($-j^2$ = constant)

q, (2) the entropy is maximum and (3) the velocity with respect to the unburned material is minimal and equal to the sound velocity of the material behind the front. All the remaining solutions, called strong detonations, move supersonically with respect to the burned material and subsonically with respect to the unburned material. Therefore, if a detonation starts at the center of the white dwarf, all the material, from the center to very near the surface, will be incinerated to ^{56}Ni.

Strong detonations are not allowed in stars. Since material must be at rest at the centre, the velocity has to decrease from a positive value behind the front to zero at the centre. This means that a rarefaction wave has to follow the detonation. Since the velocity of a rarefaction wave is equal to the sound velocity of the material, it is necessary that the front moves at least with the sound velocity with respect to the burned material in order to not be overtaken by the rarefaction wave. Thus, due to the boundary conditions, the only acceptable detonations in stars are those of Chapman-Jouguet type.

In the case of deflagration solutions matter is subsonic on both sides of the front. Thus, any perturbation behind or ahead the front can affect it. As an example, consider a spherically symmetric burning front propagating outwards with a velocity D and the unburned matter at rest. From Eqs. (5.6) and (5.7) it is possible to write:

$$V_0(P_1 - P_0) = v_1 D \tag{5.12}$$

where v_1 is the velocity measured in the frame fixed to the center of the star. Since $P_1 - P_0 < 0$ in deflagrations, and $D > 0$, the velocity of the burned matter must be negative, $v_1 < 0$, in contradiction to the boundary condition that requires matter to be at rest at the center. Thus a deflagration can only exist if it generates a shock precursor that boosts matter outwards (Mazurek and Wheeler 1980).

The speed of the laminar flame can be estimated as follows (Landau and Lifshitz 1959): the velocity of the burning front is $D \sim \delta/\tau_{\rm burn}$, where δ is the width of the front, and $\tau_{\rm burn}$ is the lasting time of the burning ($\tau_{\rm burn} \sim \varepsilon/\varepsilon_{\rm nuc}$, where $\varepsilon_{\rm nuc}$ has to be evaluated at the critical temperature). Since a stationary flame can only exist if $\tau_{\rm burn} \sim \tau_{\rm diff}$, where the diffusion time is given by $\tau_{\rm diff} \sim \delta^2/\chi$ and χ is the thermometric conductivity, the width of the front has to be

$$\delta \sim \sqrt{\frac{\varepsilon\chi}{\varepsilon_{\rm nuc}}} \tag{5.13}$$

and the laminar velocity

$$D \sim \sqrt{\frac{\varepsilon_{\rm nuc}\chi}{\varepsilon}} \tag{5.14}$$

In the case when a white dwarf is near the Chandrasekhar limit, $\delta \sim 10^{-4}$ cm, $D \sim 10^7$ cm/s $\sim 10^{-2} c_{\rm s}$ and the density contrast between burned and unburned matter is $\Delta\rho/\rho \sim 0.2$. These values relax to 1 cm, 10^4 cm/s and 0.5 respectively when $\rho \sim 10^7$ g/cm^3.

As a consequence of turbulence induced by instabilities like the Rayleigh-Taylor buoyancy-driven or the Kelvin-Helmholtz shear-driven instability, for instance, the flame surface is wrinkled and stretched in such a way that, despite the flame continuing to propagate at the laminar velocity, the effective burning rate is strongly enhanced. Buoyancy induces the formation of burning bubbles that rise into the fuel and generate turbulent motions. The turbulent motions decay downward to the smaller Kolmogorov scale and the eddies of this cascade interact with the flame, further wrinkling and stretching its surface, thereby further enhancing the burning rate. This effect acts down to the Gibson scale, defined as the size of the eddy that can turn over in a nuclear burning time. Below this scale, the laminar velocity is larger than the turbulent velocity and fuel is burned before the eddies are able to change the shape of the flame. If the Gibson length is large as compared with the width of the flame, the internal structure of the flame is not altered (the flamelet regime). In the opposite case, the turbulent motion is able to modify the internal structure of the flame and burning enters the so called distributed regime.

5.1.4 Scenarios Leading to a Thermonuclear Runaway

Possible scenarios leading to a thermonuclear runaway can be classified according to the chemical composition of the donor (H, He,C+O, O+Ne) and the nature of the accretor, a white dwarf made of He, C+O, or O+Ne, or a neutron star. Some of the possible combinations are very rare, if not forbidden, and have not yet been associated with any observed astronomical event. Within the category of accreting white dwarfs it is possible to adopt the following scenarios (Iben and Tutukov 1985; Nomoto 1982; Webbink 1984; Whelan and Iben 1973):

Hydrogen accretion There are many astronomical objects containing a white dwarf that accretes hydrogen rich matter from a non-degenerate companion and that could suffer a thermonuclear runaway. The nature and the intensity of this instability depend on the accretion rate and the mass of the object. If the accretion rate is smaller than $\sim 10^{-8-9}\,\mathrm{M}_\odot$/year, hydrogen accumulates on the surface of the white dwarf and becomes degenerate. When the accumulated mass reaches a critical value, $\Delta M_\mathrm{H} \sim 10^{-4}$–$10^{-5}\,\mathrm{M}_\odot$, the exact values depending on the properties of the binary system, it experiences a strong flash that can be identified with the nova phenomenon (see Sect. 5.2). This flash expels almost all the accreted mass or even erodes the mass of the accreting object, for which reason the white dwarf is unable to reach the Chandrasekhar mass, except in the case when $M_{WD} > 1.3\,\mathrm{M}_\odot$. However, since the chemical composition of such white dwarfs is a mixture of oxygen and neon, the fate of such scenario is collapse to a neutron star.

For intermediate rates, $10^{-8-9} \leq \dot{M}_\mathrm{H}(\mathrm{M}_\odot/\mathrm{year}) \leq 5 \times 10^{-7}$, hydrogen burns steadily or through mild flashes, and helium accumulates on the surface of the star. If the accretion rate is high enough, this helium is converted into carbon and oxygen through weak flashes or steady burning and the white dwarf approaches the Chandrasekhar mass. But, if the effective accretion rate of helium is in the range $10^{-9} \leq \dot{M}_{\rm H}(\mathrm{M}_\odot/\mathrm{year}) \leq 5 \times 10^{-8}$, the helium layer becomes degenerate and when it reaches a critical mass, $\Delta M_{\rm He} \sim 0.3\,\mathrm{M}_\odot$, it ignites under degenerate conditions and experiences a thermonuclear runaway that can trigger the explosive destruction of the complete star. This scenario has been proposed for type Ia supernova progenitors (see Sect. 5.3.2).

If the accretion rate is larger than $\sim 5 \times 10^{-7}\,\mathrm{M}_\odot$/year a red giant-like envelope forms, a strong wind appears and the mass accumulates over the degenerate core at a rate (Hachisu et al. 1999):

$$\dot{M}_{\rm cr} \simeq 5.3 \times 10^{-7} \frac{1.7 - X}{X} (M_{\rm WD}/\mathrm{M}_\odot - 0.4) \;\; \mathrm{M}_\odot/\mathrm{year} \tag{5.15}$$

where X is the mass fraction of H in the accreted matter. As before, hydrogen and helium burn peacefully and the white dwarf has the possibility to reach the Chandrasekhar mass. Typical examples are cataclysmic variables, classical novae, recurrent novae, symbiotic stars and supersoft X-ray sources.

Helium accretion There are at least two scenarios in which a white dwarf can directly accrete helium from the companion. One consists of two degenerate objects, a primary made of carbon-oxygen and a secondary composed of helium, that merge as a consequence of the emission of gravitational waves. Since the mass of the secondary is small $\sim$0.3–0.4 $\mathrm{M}_\odot$, the process of merging is self-regulated. The second scenario consists of a C+O white dwarf plus a non-degenerate helium star and the mass transfer is powered by helium burning in the secondary. As mentioned above, if $10^{-9} \leq \dot{M}_{\rm H}(\mathrm{M}_\odot/\mathrm{year}) \leq 5 \times 10^{-8}$, helium ignites at the base of the freshly accreted mantle under degenerate conditions and can trigger the thermonuclear explosion of the accreting white dwarf despite the fact that its mass is smaller than the Chandrasekhar limit (see Sect. 5.3.2). A typical example is that of the AM Cvn systems.

Carbon-oxygen accretion Close enough binary systems formed by two intermediate mass stars can experience two episodes of common envelope evolution that result in the formation of two C/O white dwarfs with a separation that is smaller than the initial one.

Depending on the parameters of the system, one possibility is that the first newly formed C/O white dwarf merges with the core of the AGB companion during the second common envelope evolution. The merger has a mass of the order of the Chandrasekhar's mass and explodes after some time (Kashi and Soker 2011; Aznar-Siguán et al. 2015). Another possibility is that the two C/O white dwarf are left close enough to allow an important loss of angular momentum via the emission of gravitational waves that induces an additional reduction of the orbital radius at a rate:

$$\dot{r} = -\frac{64 G^3 m_1 m_2 (m_1 + m_2)}{5 c^5 r^3}$$

where G is the gravitational constant, c is the speed of light and r is the separation of both stars. If the separation of the two white dwarfs is smaller than $\sim 3R_\odot$, nothing can prevent their merging in less than a Hubble time and the primary will start accreting a mixture of carbon and oxygen.

During the merging process, the secondary is destroyed in a few orbital periods after filling its Roche lobe (Benz et al. 1990) and forms a hot and thick accretion disk around the primary. The impact is not able to induce prompt ignition (Guerrero et al. 2004) and the final outcome depends on the subsequent evolution of the disk. If the accretion rate is spherically symmetric and larger than about $\dot{M} \geq 2.7 \times 10^{-6}\,\mathrm{M_\odot/year}$, carbon ignites off-center, the flame propagates conductively inwards and the white dwarf is converted into an O-Ne white dwarf before central carbon ignition. Upon further accretion the white dwarf collapses to a neutron star (Nomoto and Kondo 1991). Recent calculations (Yoon and Langer 2005) indicate that, at least in some cases, neutrino cooling is able to quench off-center carbon ignition. An open question is the effective rate at which matter is accreted (Piersanti et al. 2003a,b) since it also contains angular momentum that prevents the contraction of the primary unless it is dissipated. Therefore, the interplay between disk and star is crucial for understanding the outcome of such a scenario.

Concerning the category of accreting neutron stars, Van Horn and Hansen (van Horn and Hansen 1974; Hansen and van Horn 1975) were the first to point out that nuclear burning on their surface can also be unstable. The regimes of unstable burning have been extensively discussed elsewhere (Fujimoto et al. 1981). To summarize, for a chemical mixture with Z(CNO)~ 0.01: mixed H/He-burning is expected for $\dot{\mathrm{M}} < 2 \times 10^{-10}\,\mathrm{M_\odot/year}$, triggered by thermally unstable H-ignition; pure He-shell ignition for $2 \times 10^{-10} < \dot{\mathrm{M}}\ (\mathrm{M_\odot/year}) < (4.4 - 11.1) \times 10^{-10}$, following completion of H-burning; and mixed H/He-burning for $\dot{\mathrm{M}} > (4.4 - 11.1) \times 10^{-10}\,\mathrm{M_\odot/year}$, triggered by thermally unstable He ignition. A reduction of the CNO content lowers the critical accretion rates and substantially narrows the range for pure He bursts.

5.2 Classical Novae

The origin of the term *nova* comes from the Latin *nova stella*, meaning that a *new star* appeared in the sky. But it has been known for a long time that the new star is in fact not new, and that a nova is more properly defined as an existing star that suddenly increases its luminosity—by more than $\sim$10 magnitudes, i.e., by a factor larger than 10^4—and then returns to its previous faint state in a few months, or even years. In fact, already Newton in the seventeenth to eighteenth century talked about *temporary stars* shining suddenly and then vanishing. It was not until the twentieth century that novae and supernovae were distinguished from each other, once the distances to the *nebulae* where they had been discovered were better known, and thus some extragalactic objects turned out to be novae with much larger intrinsic brightness (*super-novae*). An interesting and complete historical perspective of novae can be found in Bode and Evans (2008).

The discovery of the binarity of classical novae was made by Walker (1954), who observed DQ Her (a nova that exploded in 1934) and deduced that it was an eclipsing binary with a very short period. Later, Kraft showed that this was a common property of novae and of cataclysmic variables in general (Kraft 1964). It is now well known that nova explosions occur on white dwarfs accreting hydrogen-rich matter from a main sequence star companion, in a close binary system of the cataclysmic variable type. Accumulation of matter on the white dwarf leads to hydrogen ignition in degenerate conditions, which prevents the self-adjustment of the envelope through expansion. Therefore, a thermonuclear runaway ensues (see Sect. 5.1.2) and the final consequence is mass ejection at large velocities (hundreds to thousands of km s^{-1}) and a large increase of luminosity, even reaching the Eddington luminosity of the white dwarf (10^{34}–10^{35} erg/s).

In contrast to type Ia supernovae, which also occur on white dwarfs in binary systems, novae do not experience a complete disruption of the white dwarf, because the outburst only affects the external hydrogen-rich layers, i.e. 10^{-4}–10^{-5} $M_\odot$. Therefore, the nova phenomenon is expected to recur, with periods of a few tens or hundreds thousand years, which is the typical accretion time required to build-up again a critical H-rich envelope ready to explode. Mass transfer onto the white dwarfs in cataclysmic variables is a long-lasting phase, so that many nova explosions on a given white dwarf must occur. However, for historical reasons the term *recurrent nova* is reserved for another type of eruptive phenomena, those that have more than one *recorded* nova outburst. These systems also correspond to white dwarfs experiencing a thermonuclear runaway of their H-rich envelope, but the companion star is in general a red giant, instead of a main sequence star. The binary system is not a cataclysmic variable anymore; both its period—and the related binary separation—and the mass transfer rate onto the white dwarf are larger, thus allowing for a faster build-up of the critical mass and thus a shorter recurrence period (decades rather than thousands of years).

It is worth mentioning that the term *recurrent novae* is also applied to white dwarf explosions, with similar outburst properties and recurrence periods than *genuine* recurrent novae, but with a non thermonuclear origin. A completely different case are the so-called *dwarf novae*, which have much smaller outburst amplitudes and which are produced by accretion disk instabilities in cataclysmic variables. Here we are only concerned with novae from thermonuclear explosions, i.e., *classical novae* and the sub-class of *recurrent novae* with thermonuclear origin.

The long term evolution of the white dwarfs in classical and recurrent novae is debated, since it is not clear if the mass of the white dwarf grows towards the Chandrasekhar mass or decreases after each explosion. Observations of nova ejecta often show overabundances with respect to solar of elements such as carbon, oxygen, neon, among others, indicating that some mixing between the core and the accreted envelope occurs. Then, some core mass is in principle ejected indicating that the white dwarf mass might in fact decrease. However, in *recurrent novae* no large overabundances are observed. On the other hand, *recurrent novae* should take place on very massive white dwarfs, which only need a very small amount of added mass to explode; this combined with a larger accretion rate leads to the very short recurrence period observed. All in all, recurrent novae are one of the possible scenarios of type Ia supernova progenitors, although their internal composition (likely ONe instead of CO) presents a problem for this scenario.

Interestingly enough, there is a remarkable recurrent nova in the Andromeda Galaxy, M31N 2008-12a, with an extremely short recurrence period—of about 1 year—the shortest known to date (Darnley et al. 2015; Henze et al. 2015; Darnley et al. 2016a,b). This is the best candidate for a type Ia supernova explosion, because the deduced mass of the white dwarf is extremely close to the Chandrasekhar limit (Kato et al. 2014; Hachisu et al. 2016), but its chemical composition should be CO and not ONe. From the observational point of view, HST observations of the 2015 eruption of M31N 2008-12a yielded non detection of Neon, which may be indicative of a CO white dwarf (Darnley et al. 2017a). Theoretically, the white dwarf of M31N 2008-12a could reach near-Chandrasekhar-mass through successive eruptions with an initial CO core (Hillman et al. 2016). All in all, it is predicted that the M31N 2008-12a white dwarf could reach the Chandrasekhar mass and thus explode as a SNIa in less than 20 kyr (Darnley et al. 2017b).

5.2.1 Observational Properties

Most of the galactic classical novae have been discovered optically by amateur astronomers. In addition, some robotic telescopes, mainly devoted to search for optical counterparts of GRBs or to perform surveys are also finding novae and supernovae. Around 5 novae per year are being discovered in recent years in our galaxy, and several novae have been found as well in external galaxies (see Shara in Bode and Evans (2008) and references therein). However, most of the galactic novae suffer from large optical extinction (reddening) by interstellar dust, and hence the real nova rate is expected to be much larger; it should be determined from extrapolations, either from extragalactic or from galactic data. In the first case, the dependence of the nova rate on the type of galaxy has been derived, indicating that early-type galaxies are more prolific nova producers; the derived nova rate is 15–24 year^{-1} to 27 ± 8 year^{-1} (Della Valle and Livio 1994; Shafter et al. 2000). Larger rates are obtained when galactic data are extrapolated, taking into account the amount and distribution of galactic dust: 35 ± 11 year^{-1} or 41 ± 20 year^{-1} (Hatano et al. 1997; Shafter 1997).

From optical light curves of classical novae one finds an increase in luminosity corresponding to a decrease of m_V (apparent visual magnitude) of more than 9 magnitudes occurring in just a few days, and a pre-maximum halt 2 magnitudes before maximum, in some cases (Warner (1995) and references therein). Nova light curves are classified according to their speed class, defined from either t_2 or t_3, i.e., the time needed to decay by 2 or 3 visual magnitudes after maximum. Speed classes range from very fast ($t_2 < 10$ days) and fast ($t_2 \sim 11$–25 days) to very slow ($t_2 \sim 151$–250 days) (Payne Gaposchkin 1957). Some examples are the fast nova N Cyg 1992, which had $t_2 \sim 12$ days, the even faster nova N Her 1991 ($t_2 \sim 2$ days), and the slow nova N Cas 1993, which had $t_2 \sim 100$ days. An empirical relationship between the absolute magnitude at maximum M_V and the speed class of novae shows that brighter novae have shorter decay times (t_2 or t_3). The theoretical explanation of this relationship (Livio 1992) relies on novae reaching a maximum luminosity close to the Eddington limit and ejecting roughly all their envelope in a period similar to t_3. It was established that $L_{\rm max}$ is an increasing function of $M_{\rm wd}$ and that t_3 is a decreasing function of $M_{\rm wd}$. From these two relationships an expression relating M_V at maximum and t_3 is deduced. This empirical relation, valid both in the V and B photometric bands, is very often used to determine distances to novae, once visual extinction is known. Different calibrations of the maximum magnitude-rate of decline relationship (MMRD) exist, with that from Della Valle and Livio (1995) being the most commonly employed form.

It is worth mentioning that in fact the MMRD relationship has not been proven extensively, and can't be considered as universal. In fact, the extensive grid of nova numerical simulations by Yaron et al. (2005) first predicted that some classical novae might deviate significantly from the MMRD relation. On the observational side, Kasliwal et al. (2011) discovered a new photometric sub-class of faint and fast classical novae in the Andromeda Galaxy, M31, inconsistent with the canonical MMRD relationship. They suggested that the MMRD, characterized only by the white dwarf mass, was probably an oversimplification. Six years later, Shara et al. (2017) found a similar class of *faint, fast novae* in the giant elliptical galaxy M87; their conclusion was that the MMRD relationship should not be used to determine cosmic distances or distances to Galactic novae.

There have been efforts to improve the quality of nova optical light curves. In this respect, the *Solar Mass Ejection Imager* satellite, SMEI, has done an important contribution regarding the quality, because it provides good precision visible-light photometry at 102-min cadence; Hounsell et al. (2010, 2016) report on the SMEI nova observations between 2004 and 2009. Additionally, there is a recent catalog of 97 very-well-observed nova light curves (Strope et al. 2010), mainly from the *American Association of Variable Star Observers*, AAVSO, database, which has led to a new more sophisticated classification system, based not only on the speed class (time to decline by a given number of magnitudes), but also on the shape of the light curves. They use designations S for smooth light curves (38% of the novae), P for plateaus (21%), D for dust dips (18%), C for cusp-shaped secondary maxima (1%), O for quasi-sinusoidal oscillations superposed on an otherwise smooth decline (4%), F for flat-topped light curves (2%), and J for jitters or flares superposed on the decline (16%). Their classification consists of the corresponding single letter followed by the t_3 value in parentheses.

The optical light curves were extended with space-based observations to energy ranges not observable from the ground. An important step forward was the discovery of the luminosity increase in the ultraviolet when the optical started to decline, thanks to the IUE satellite (International Ultraviolet Explorer); the reason is that the spectral energy distribution shifts to higher energies when deeper and thus hotter regions of the expanding envelope are revealed (the photosphere recedes as a consequence of the decreasing opacity). On the other end of the spectrum, infrared observations (especially for novae which form dust) indicate an increase in luminosity once the ultraviolet luminosity starts to decline, which is interpreted as the resulting re-radiation (in the infrared) by dust grains of the ultraviolet energy they absorbed. Therefore, during optical decline the bolometric luminosity of classical novae remains constant, during a period of time which depends on the mass of the H-rich envelope remaining on the white dwarf after the nova explosion, which is expected to burn steadily. Evidence for residual H-burning came from observations in the supersoft X-ray range with ROSAT (Krautter et al. 1996; Balman et al. 1998; Orio et al. 2001), which revealed the related very hot photosphere.

After the ROSAT era, the Swift Gamma-Ray Burst satellite, launched in 2004, has been and continues to be an excellent facility for the study of novae in soft X-rays, mainly with its X-ray telescope instrument, XRT, thanks to its rapid response and its scheduling flexibility. Observations can start promptly, at about 9 h from discovery. It has observed 73 Galactic and Magellanic Clouds novae within 11 years of outburst (data up to June 2017); 43 of them were detected in X-rays and 12 have been observed more than 100 ks. Novae in M31 and M33 have also been observed. See Ness et al. (2007), Schwarz et al. (2011) and Osborne (2015) for reports on X-ray observations of novae with Swift.

Prior to Swift, the ESA and NASA X-ray satellites XMM-Newton and Chandra, both launched in 1999, have crucially contributed to the continued study of novae in X-rays, but they are not suited to do a systematic study of the duration of the supersoft X-ray phase of novae as Swift is. They have instead provided the highest-resolution spectra available for novae (see for instance the review Ness (2012) and references therein). In the supersoft X-ray range, these reveal a wealth of absorption lines, related to the hot white dwarf photospheric emission, much more complicated that the often assumed black body model. Also, plasma related emission lines have been revealed; a complete explanation of the whole X-ray spectra is still lacking. The Japanese satellite Suzaku has also provided important data, in the harder X-ray energy range not reachable with XMM-Newton and Chandra (see for instance Takei et al. (2009)). Finally, NuSTAR has also observed a few novae, searching for the prompt hard X-ray emission related to shocks (Orio et al. 2015; Mukai et al. 2017).

The bolometric luminosity deduced from observations is close to or even larger than the Eddington luminosity, and thus radiation pressure is probably responsible for ejection of nova envelopes (Kato and Hachisu 1994).

A very important result deduced from nova observations in all spectral wavelengths is that their ejecta are often enriched in carbon, nitrogen and oxygen—as well as neon in many objects (around 1/3 of the total); the global metallicities in nova ejecta are well above solar metallicities (see Gehrz et al. 1998 for a review). This observational fact is one of the main drivers of theoretical models, which should be able to explain it. These metallicity enhancements are not likely to be produced in the TNR, because the temperatures achieved in nova explosions are not high enough. An alternative and more widely accepted explanation is that there is some mixing between accreted matter, assumed to be of solar composition, and the underlying CO or ONe core (Starrfield et al. 1978b; Prialnik et al. 1978, 1979). In fact, such enrichment is also required to power the nova explosion itself except for very slow novae.

It is important to point out that there are two distinct nova populations: disk novae, which are in general fast and bright ($M_V(max) \simeq -8$), and bulge novae, slower and dimmer ($M_V(max) \simeq -7$). This was first suggested by Della Valle et al. (1992) and later corroborated by their early post-outburst spectra (Williams 1992) and based on the stronger group of emission lines they display (either FeII lines or He and N lines); FeII-type novae evolve more slowly and have a lower level of ionization, whereas He/N-type novae have larger expansion velocities and a higher level of ionization. It has been deduced that the faster and brighter He/N novae are concentrated closer to the galactic plane than those of the slower and dimmer FeII type, which would preferentially belong to the bulge population (Della Valle and Livio 1998; Della Valle 2002).

Novae have not been detected yet in γ-rays from radioactivities, but they have been, however, detected in high-energy γ-rays (energy larger than 100 MeV), with the Large Area Telescope (LAT) instrument onboard the *Fermi* satellite, launched by NASA in 2008. The first nova detected by Fermi/LAT was V407 Cyg (Abdo et al. 2010). This source is a binary system with a white dwarf and a Mira pulsating red giant companion; the emission lasted for about 2 weeks after the nova eruption. Other novae have been detected with Fermi/LAT, almost one per year on average (Ackermann et al. 2014; Cheung et al. 2016).

The main mechanisms responsible for the production of high-energy γ-rays are pion decay and Inverse Compton; neutral pions come from proton-proton collisions, when accelerated protons exist (hadronic process), whereas Inverse Compton relies on the existence of relativistic electrons (leptonic process). Protons and electrons are accelerated in the shock wave formed when the nova ejecta interacts with a dense ambient medium, either the wind of its the red giant companion (case of symbiotic recurrent novae, like RS Oph (Tatischeff and Hernanz 2007)) or with the nova ejecta itself (case of classical novae, not well understood yet; see for instance Chomiuk et al. (2014), Vurm and Metzger (2018) and references therein).

5.2.2 *Modeling Classical Novae*

The scenario of classical nova explosions consists of a white dwarf (either CO or ONe) accreting hydrogen-rich matter in a cataclysmic binary system, as a result of Roche lobe overflow from its main sequence companion. For accretion rates low enough, e.g. $\dot{M} \sim 10^{-9}$–$10^{-10}\,M_\odot$ year^{-1}, accreted hydrogen is compressed to degenerate conditions until ignition occurs, thus leading to a thermonuclear runaway (TNR, see Sect. 5.1.2). Explosive hydrogen burning synthesizes some β^+-unstable nuclei of short lifetimes (e.g. ^{13}N, ^{14}O, ^{15}O, ^{17}F, with τ = 862, 102, 176, and 93 s respectively, see Fig. 5.2) which are transported by convection to the outer envelope, where they are saved from destruction. These decays lead to a large energy release in the outer shells which causes the nova outburst, i.e. a visual luminosity increase accompanied by mass ejection with typical velocities 10^2–$10^3\,\mathrm{km\,s^{-1}}$. Another important effect of convection is that it transports unburned material to the burning shell (see Starrfield et al. (2016), Jose (2016), for recent reviews on nova modeling).

Mixing at the core-envelope interface turned out to be an essential ingredient in the simulations, both to power the TNR and to explain observed enhancements in metals in many novae. Several mechanisms have been suggested to explain this process, operating prior or during the thermonuclear runaway, but none of them is completely satisfactory (see an extensive review in Livio (1994)). Diffusion induced convection, first discussed by Prialnik and Kovetz (1984) and Kovetz and Prialnik (1985), can explain moderate enrichments but has difficulties to account for some of the largest metallicities inferred (Kovetz and Prialnik 1997). Other possibilities are shear mixing, convection induced shear mixing, and convective overshooting induced flame propagation. Two approaches have been adopted to simulate mixing in one-dimensional simulations: parameterization (Starrfield et al. 1998; José and Hernanz 1998) or follow-up of many successive eruptions, with inclusion of diffusion (Prialnik and Kovetz 1995; Yaron et al. 2005). The latter is in principle self-consistent, but the treatment of mass-loss between successive outbursts is quite uncertain.

Despite many observational features that characterize the nova phenomenon have been successfully reproduced by hydrodynamic simulations under the assumption of spherical symmetry, certain aspects like the way in which a thermonuclear runaway sets in and propagates, the treatment of convective transport, and most likely, the mixing at the core-envelope interface, clearly require a multidimensional approach.

Early semianalytic estimates, focused on the onset of localized TNRs on the surface of white dwarfs, suggested that heat transport was not efficient enough to spread a localized TNR to the entire surface, concluding that localized, volcanic-like TNRs were likely expected (Shara 1982). The first studies that tackled this question in the context of truly multidimensional nova simulations were conducted by Glasner et al. (Glasner and Livne 1995; Glasner et al. 1997): indeed, two-dimensional simulations were performed with the code VULCAN, an arbitrary Lagrangian Eulerian (ALE) code. To this end, a box ($0.1\ \pi^{\mathrm{rad}}$) in spherical-polar coordinates, with reflecting boundary conditions, was adopted. The resolution adopted near the envelope base was $5\,\mathrm{km} \times 5\,\mathrm{km}$. In the simulations, the evolution of an accreting $1\,\mathrm{M}_\odot$ CO white dwarf was initially followed with a one-dimensional code. The structure was subsequently mapped into a two-dimensional domain, when the temperature at the envelope base reached 100 MK. The two-dimensional simulations, that relied on a 12-isotope network, showed good agreement with the main results obtained with one-dimensional models: specifically, the critical role played by the β-unstable nuclei ^{13}N, ^{14,15}O, and ^{17}F in the expansion and ejection stages, and therefore, the presence of large amounts of ^{13}C, ^{15}N, and ^{17}O in the ejecta. Nevertheless, some remarkable differences were also identified: on one hand, the TNR was initiated as a handful of irregular, localized eruptions that set in at the envelope base, caused by convection-driven temperature fluctuations.

This suggested that combustion likely proceeds as a chain of multiple localized flames, rather than as a thin front, each surviving only a few seconds. However, turbulent diffusion efficiently dissipates any local burning, such that the fast stages of the TNR cannot be localized. Therefore, the runaway must finally spread along the stellar surface. On the other hand, the core-envelope interface is now convectively unstable, providing a source for the metallicity enhancement through Kelvin-Helmholtz instabilities (a mechanism that bears similarities with convective overshooting (Woosley 1986)).

Results from other 2D (and 3D) simulations were published, shortly after, by Kercek et al. (1998, 1999). They found substantially less violent outbursts (i.e., longer TNRs with lower peak temperatures and ejection velocities) caused by large differences in the convective flow patterns. Indeed, whereas in Glasner et al., a few, large convective eddies dominated the flow, most of the early TNR reported by Kercek et al. was governed by small, very stable eddies, which led to very limited dredge-up and mixing episodes. In fact, Kercek et al. concluded that mixing must take place prior to the TNR, in contrast with the simulations reported by Glasner et al. In summary, two independent studies, based upon the same initial model, yielded opposite results on the strength of the runaway and its capability to power a fast nova. The differences between both studies were carefully analyzed by Glasner et al. (2005), who concluded that the early stages of the TNR, when the evolution is quasi-static, are extremely sensitive to the adopted outer boundary conditions. Indeed, they showed that Lagrangian simulations, in which the envelope was allowed to expand and mass was conserved, led to consistent explosions. In contrast, in Eulerian schemes with a free outflow outer boundary condition (the choice adopted in Kercek et al.), the outburst was artificially quenched.

The feasibility of this mechanism was further explored by Casanova et al. through a set of independent two-dimensional simulations (Casanova et al. 2010, 2011a), proving that even in an Eulerian scheme (e.g., the FLASH code) with a proper choice of outer boundary conditions, Kelvin-Helmholtz instabilities (see Fig. 5.4) can naturally lead to self-enrichment of the accreted envelope with core material, at levels that agree with observations. It is worth noting, however, that convective transport cannot be described accurately by means of two-dimensional prescriptions. In fact, the conservation of vorticity (a measure of the local spinning motion of the particles in a fluid), imposed by a 2D geometry, forces all small convective cells to merge into large eddies, with a size of the order of the pressure scale height of the envelope. In sharp contrast, eddies become unstable in 3D in fully developed turbulent convection, and consequently break up, transferring their energy to progressively smaller scales (Pope 2000; Shore 2007). The resulting structures (e.g., vortices and filaments) undergo a similar fate down to approximately the Kolmogorov scale. In this framework, a pioneering three-dimensional simulation of mixing at the core-envelope interface during nova explosions (Casanova et al. 2011b) has shed light into the nature of the highly fragmented, chemically enriched, and inhomogeneous nova shells, observed in high-resolution spectra: such features have been interpreted as relics of the hydrodynamic instabilities that develop during the initial ejection stage, as predicted by the Kolmogorov theory of turbulence.

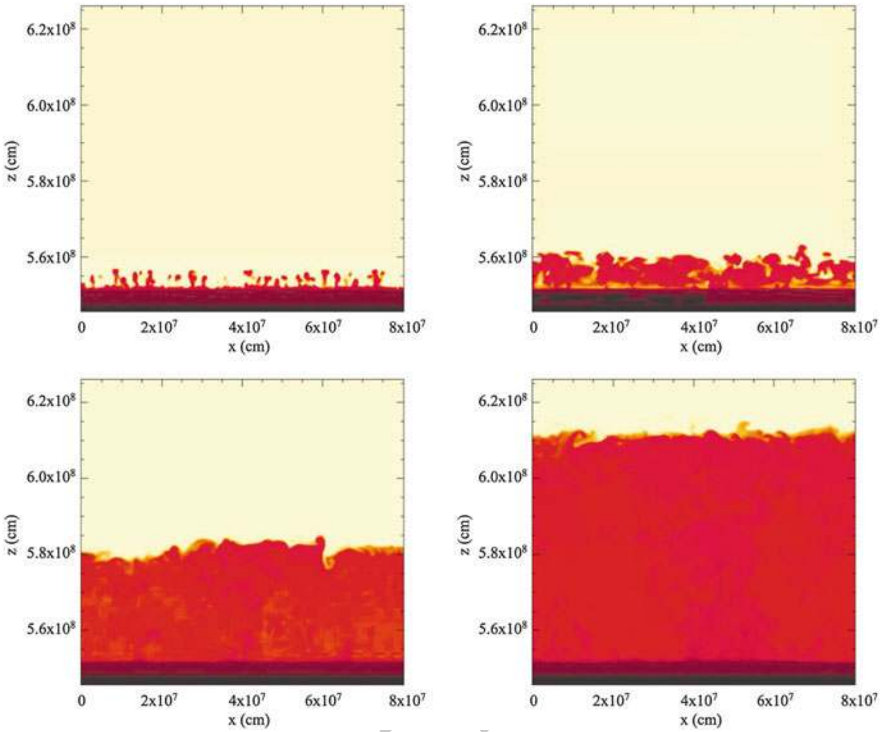

Fig. 5.4 Two-dimensional plots of the development of hydrodynamic instabilities, during a 3-D simulation of mixing at the core-envelope interface during a nova explosion, calculated with the hydrodynamic code FLASH

The inhomogeneities inferred from the ejecta have been usually attributed to uncer- 693
tainties in the observational techniques, but they may represent a real signature of 694
the turbulence generated during the thermonuclear runaway. More recently, similar 695
results have also been reported for ONe-rich substrates (3D models; Casanova et al. 696
2016) and for different white dwarf masses (2D models; Casanova et al. 2018), 697
proving that higher degrees of mixing (and therefore, more energetic outbursts) are 698
found in ONe-rich than in CO-rich substrates, and for more massive white dwarfs. 699

5.2.3 *Nucleosynthesis in Classical Novae* 700

Nova outbursts eject much less mass than supernova explosions, but novae are 701
much more frequent events than supernovae in the Galaxy; this has raised the 702
issue of the potential contribution of such stellar cataclysms to Galactic abundances. 703
Although the mass injected into the ISM per novae into is small, detailed numerical 704
simulations have indicated novae as major players in the synthesis of some specific 705

nuclear species, largely overabundant in their ejecta, such as ^{13}C, ^{15}N, and ^{17}O, with a minor contribution to Galactic levels of other nuclei with A < 40, such as ^{7}Li, ^{19}F, or ^{26}Al (Starrfield et al. 1998; José and Hernanz 1998).

Radioactivities present in nova ejecta, previously synthesized during the explosion, also constitute a major source of positrons. Indeed, ^{13}N and ^{18}F, and to a lesser extent, ^{22}Na, are the major contributors. The synthesis of ^{13}N and ^{18}F naturally occurs during the operation of the CNO cycle. Actually, the triggering reaction that powers the onset of the thermonuclear runaway is ^{12}C(p,γ)^{13}N, leading to ^{13}N synthesis. The exact amount transported to the outer envelope and contributing to γ-ray emission once transparency allows for the escape of photons, depends on details of the evolution, specially on convection. Therefore, detection of positrons from ^{13}N, through the associated electron-positron annihilation emission, would provide an important diagnostic of the dynamics of nova explosions.

The synthesis of ^{18}F in novae proceeds through the hot CNO cycle. Regardless of the nature of the white dwarf hosting the explosion (CO or ONe), the initial abundance of ^{16}O is large, and thus ^{16}O is the main source for ^{18}F formation, which can take place either through the reaction chain ^{16}O(p,γ)^{17}F(p,γ)^{18}Ne(β^+)^{18}F or via ^{16}O(p,γ)^{17}F(β^+)^{17}O(p,γ)^{18}F. The ^{18}F yields are severely constrained by its destruction mode, whatever the production channel is. During the runaway, ^{18}F destruction by beta decays can be neglected when compared to its destruction by proton captures (mainly through ^{18}F(p,α)^{15}O, which is faster than ^{18}F(p,γ)^{19}Ne (Hernanz et al. 1999). Other nuclear reactions affecting ^{18}F synthesis are proton captures on ^{17}O, i.e. ^{17}O(p,γ)^{18}F and ^{17}O(p,α)^{14}N (Coc et al. 2000).

Another interesting isotope likely produced during nova outbursts is ^{7}Li. Its synthesis is believed to proceed through the so-called *beryllium transport mechanism* (Cameron 1955), in which the previously synthesized ^{7}Be transforms into ^{7}Li through electron capture ($\tau = 77$ days, see Table 5.1) releasing a γ-ray photon of 478 keV. For this mechanism to be effective, ^{7}Be has to be transported to the outer, cooler envelope layers, with a timescale shorter than its decay time, in order to preserve its fragile daughter ^{7}Li from destruction. This mechanism requires a dynamic situation like the one encountered in novae.

Table 5.1 Radioactive isotopes synthesized in explosive events

Isotope	Decay chain	Disintegration process	Lifetime	Line energy (keV)
^{7}Be	^{7}Be $\to$ ^{7}Li	e^--capture	77 days	478
^{22}Na	^{22}Na $\to$ ^{22}Ne	β^+	3.8 years	1275
^{26}Al	^{26}Al $\to$ ^{26}Mg	β^+	1.0×10^6 years	1809
^{44}Ti	^{44}Ti $\to$ ^{44}Sc $\to$ ^{44}Ca	e^--capture, β^+	89 years (5.4 h)	78, 68, 1157
^{56}Ni	^{56}Ni $\to$ ^{56}Co	e^--capture	8.8 days	158, 812, 750, 480
^{56}Co	^{56}Co $\to$ ^{56}Fe	β^+	111 days	847, 1238
^{57}Ni	^{57}Ni $\to$ ^{57}Co $\to$ ^{57}Fe	e^--capture	(52 h) 390 days	122, 136
^{60}Fe	^{60}Fe $\to$ ^{60}Co $\to$ ^{60}Ni	β^-	2.0×10^6 years (7.6 years)	1173, 1332

The production of ^{7}Li in novae was in some way debated during years, but the recent detections of both ^{7}Li and ^{7}Be in novae (first in 2015, see below) have confirmed that novae produce it. The first studies based on parameterized one-zone models (Arnould and Norgaard 1975), were followed by hydrodynamic computations (Starrfield et al. 1978b), which did not follow the accretion phase (i.e., they had an initial envelope already in place). These models indicated that the final amount of ^{7}Li synthesized depends on the initial abundance of ^{3}He and on the treatment of convection. Later works based on one or two-zone models (Boffin et al. 1993) pointed out the critical role played by the photodisintegration reaction ^{8}B(γ,p)^{7}Be. Finally, a complete hydrodynamic study, following both the accretion and the explosion phases, was performed (Hernanz et al. 1996). Formation of ^{7}Be proceeds through α-captures on ^{3}He, ^{3}He(α, γ)^{7}Be, since (p,γ) reactions can not bridge the A=5 gap; destruction occurs via ^{7}Be(p,γ)^{8}B; however, at high temperatures (T$\approx$ 10^{8} K) this rate achieves quasi-equilibrium with the inverse photodisintegration reaction, ^{8}B(γ,p)^{7}Be. Indeed, it was shown that a critical issue is the amount of ^{7}Be surviving the TNR, thanks to the efficient role played by ^{8}B photodisintegration (Hernanz et al. 1996). ^{7}Li formation is favored in CO novae with respect to ONe novae, because their faster evolution prior to the TNR (driven by the larger amount of ^{12}C injected in the envelope) favors ^{7}Be survival and thus final ^{7}Li production.

A tentative detection of ^{7}Li in the optical band, through the LiI doublet at 6708 Å, was reported for Nova Vel 1999 (Della Valle et al. 2002), but it was later suggested that the spectral feature could instead correspond to a doublet from neutral nitrogen (Shore et al. 2003). More than 10 years later, Tajitsu et al. (2015) provided the first observational evidence of ^{7}Li synthesis in novae (see comment in Hernanz (2015)). They detected ^{7}Be, the parent nucleus of ^{7}Li, during the nova explosion of Nova Del 2013 (V339 Del) with the High Dispersion Spectrograph (HDS) of the 8.2 m Subaru Telescope, in Mauna Kea (Hawaï). Observations were done at four epochs from 2013 September to October 7: 38, 47, 48 and 52 days after maximum. The HDS provided high spectral resolution in the near-UV (from 60,000 to 90,000), allowing them to distinguish the near-UV absorption lines of the resonance doublet of singly ionized ^{7}BeII at 313.0583 and 313.1228 nm, from those of the ^{9}BeII doublet at 313.0422 and 313.1067 nm, ruling out ^{9}Be. The ^{7}BeII lines were observed with blueshifts of 1103 and 1268 km s^{-1}, the same as for the Hη and CaII K lines.

Tajitsu et al. (2016) reported additional detections of the ^{7}BeII doublet with Subaru, in Nova Sgr. 2015 No.2 (V5668 Sgr) and in Nova Oph 2015 (V2944 Oph). The same year, Molaro et al. (2016) detected the same ^{7}BeII doublet with UVES, the high-resolution spectrograph of the ESO Very Large Telescope (VLT). They reported on the detection of highly blueshifted resonance lines of ^{7}BeII at 313.0583 and 313.1228 nm in Nova Sgr. 2015 No.2 (V5668 Sgr).

It is remarkable that ^{7}Li itself has also been detected for the first time in 2015 (Izzo et al. 2015): the detection of the ^{7}LiI doublet at 6708 Å, in Nova Cen 2013 (V1369 Cen), thanks to early observations getting high resolution spectra, was reported. Alternative identifications, however, are not discarded by the authors.

Large overabundances of ^{7}Be-^{7}Li with respect to solar are obtained in general from most of the observations, larger by factors that can reach 10 than the theoretically predicted ones (see below). However, these abundances from observations are not absolute but relative to Ca; also, in some cases—like for Nova Sgr 2015 No.2 (V5668 Sgr)—the optical light curve showed several maxima, which makes the computation of the time origin for the ^{7}Be decay into ^{7}Li ambiguous, impacting the value of the final ^{7}Li abundance.

Overproduction factors of ^{7}Li with respect to solar values around 1000 are predicted by CO nova models, meaning that novae can be important contributors to the Galactic ^{7}Li (Hernanz et al. 1996) (up to 20% of the Galactic content) and may help to reproduce the steep rise of the observed lithium abundance between the formation of the Solar System and the present (Romano et al. 1999; Alibés et al. 2002).

Classical nova explosions are also sources of two important radioactive isotopes: ^{22}Na and ^{26}Al. In the pioneering work by Clayton and Hoyle (1974), it was mentioned that novae are potential emitters of 1275 keV γ-rays resulting from ^{22}Na decay. They assumed ^{22}Na mass fractions in the ejecta of the order of 10^{-3}, from the conversion of ^{20}Ne to ^{22}Na. In the last 15 years it has been shown that this conversion is not so efficient, but interestingly, the current accepted ^{22}Na yields in the most prolific novae are not far from those historic predictions. The synthesis of ^{22}Na in novae proceeds through ^{20}Ne(p,γ)^{21}Na followed either by the decay of ^{21}Na to ^{21}Ne, i.e. ^{21}Na(β^{+})^{21}Ne(p,γ)^{22}Na, or by a proton capture on ^{21}Na, i.e. ^{21}Na(p,γ)^{22}Mg(β^{+})^{22}Na (José et al. 1999).

The amount of ^{22}Na synthesized during nova explosions has not yet been determined reliably. The first hydrodynamic models of nova outbursts did not include complete nuclear reaction networks covering the Ne-Na and Al-Mg regions. In the 80's, the crucial role played by some uncertain nuclear reaction rates for the yields of ^{22}Na (and ^{26}Al, see below) was finally pointed out, and extensive nova nucleosynthesis models were computed, with parameterized models (i.e. through simplified one-zone models) with representative temperature-density temporal profiles taken from evolutionary nova models (Starrfield et al. 1978a). In the 90s, new one-zone models for nova nucleosynthesis were developed, adopting various initial compositions which included the possibility of mixing with massive white dwarf cores. These models (Weiss and Truran 1990; Nofar et al. 1991) investigated in detail the synthesis of ^{22}Na and ^{26}Al, in view of the then recent detection of galactic ^{26}Al (and non detection of ^{22}Na). Prompted by the recent discovery of large enrichments of neon in the spectra of some novae, these calculations explored the outcome of nova outbursts on massive, ONeMg white dwarfs. Interestingly, Weiss and Truran (1990) obtained ^{22}Na yields as large as 10^{-4}, which combined with envelope masses of 2×10^{-5} M$_\odot$ gave 4×10^{-9} M$_\odot$ of ^{22}Na ejected into the interstellar medium. The most recent hydrodynamic models of ONe (or ONeMg) nova outbursts on masses larger than 1.0 M$_\odot$ provide ^{22}Na yields in the range 10^{-4} to 10^{-3} M$_\odot$ (José et al. 1999; Politano et al. 1995; Starrfield et al. 1998). It is worth mentioning that mixing can occur at various depths inside the stratified ONe white dwarf: inner ONe core, outer CO buffer or middle transition zone (José et al. 2003). If mixing occurs with the unburned CO buffer on top of the ONe core, no ^{22}Na would be expected (José et al. 2003).

^{26}Al production is complicated by the presence of a short-lived (half-life 6.3 s) isomer state, $^{26}\mathrm{Al}^m$. In fact, when the temperature is smaller than 4×10^8 K (as is the case in novae), the ground ($^{26}\mathrm{Al}^g$) and isomeric states must be treated as two separate isotopes, because they do not reach thermal equilibrium (Ward and Fowler 1980).

The first calculations of ^{26}Al synthesis during explosive hydrogen burning (Hillebrandt and Thielemann 1982; Wiescher et al. 1986) suggested that novae are likely sites for the synthesis of this radioactive isotope, but not in very large amounts; these computations relied on solar or CNO-enhanced white dwarf envelopes. Later computations, again one-zone models, demonstrated the need for initial envelope enrichment in O, Ne and Mg, dredged-up from the white dwarf cores, to obtain larger amounts of ^{26}Al (Weiss and Truran 1990; Nofar et al. 1991).

The major seed nuclei for ^{26}Al synthesis are ^{24,25}Mg. At the early phases of the thermonuclear runaway (burning shell temperatures around 5×10^7 K), the dominant reaction is $^{25}\mathrm{Mg}(\mathrm{p},\gamma)^{26}\mathrm{Al}^{g,m}$; the subsequent reaction $^{26}\mathrm{Al}^m(\beta^+)^{26}\mathrm{Mg}(\mathrm{p},\gamma)^{27}\mathrm{Al}$ produces the stable isotope ^{27}Al. At larger temperatures ($\sim 10^8$ K), the nuclear path $^{24}\mathrm{Mg}(\mathrm{p},\gamma)^{25}\mathrm{Al}(\beta^+)^{25}\mathrm{Mg}$ dominates, with again $^{25}\mathrm{Mg}(\mathrm{p},\gamma)^{26}\mathrm{Al}^{g,m}$. When temperature reaches 2×10^8K, (p,γ) reactions proceed very efficiently and reduce the amount of ^{25}Al, leading to the formation of ^{26}Si ($^{25}\mathrm{Al}(\mathrm{p},\gamma)^{26}\mathrm{Si}$) which decays into $^{26}\mathrm{Al}^m$, thus by-passing $^{26}\mathrm{Al}^g$ formation. Also ^{26}Al itself (in both states) is destroyed to ^{27}Si which decays into ^{27}Al. In summary, the final amount of $^{26}\mathrm{Al}^g$ and the ratio $^{26}\mathrm{Al}^g/^{27}\mathrm{Al}$ mainly depend on the competition between the two nuclear paths $^{24}\mathrm{Mg}(\mathrm{p},\gamma)^{25}\mathrm{Al}(\beta^+)^{25}\mathrm{Mg}(\mathrm{p},\gamma)^{26}\mathrm{Al}^{g,m}$ and $^{24}\mathrm{Mg}(\mathrm{p},\gamma)^{25}\mathrm{Al}(\mathrm{p},\gamma)^{26}\mathrm{Si}$. The first channel is the only one producing $^{26}\mathrm{Al}^g$, whereas both channels produce ^{27}Al (through $^{26}\mathrm{Al}^{g,m}(\mathrm{p},\gamma)^{27}\mathrm{Si}(\beta^+)^{27}\mathrm{Al}$ or $^{26}\mathrm{Si}(\beta^+)^{26}\mathrm{Al}^m(\beta^+)$ $^{26}\mathrm{Mg}(\mathrm{p},\gamma)^{27}\mathrm{Al}$ (José et al. 1999).

The final ^{26}Al yields from novae sensitively depend on the initial mass of the white dwarf and on the degree of mixing between the accreted envelope and the core. Recent hydrodynamic models of ONe (or ONeMg) nova outbursts on masses larger than $1.0\,\mathrm{M}_\odot$ suggest ^{26}Al yields in the range 10^{-4} to 10^{-2} (José et al. 1999; Politano et al. 1995; Starrfield et al. 1998). If mixing occurs with the CO buffer on top of the bare ONe nuclei (or in the transition zone), some ^{26}Al would be expected (but no ^{22}Na), since there is a non negligible amount of the seed nucleus ^{25}Mg both in the CO buffer and in the transition zone (José et al. 2003).

5.3 SNIa Explosions

The pyrotechnical displays of the total explosion of stars are called supernovae. They are characterized by a sudden rise of the luminosity, followed by a steep decline lasting several weeks and eventually followed by a more gradual decline lasting many years. The total electromagnetic output, obtained by integrating the light curve, is $\sim 10^{49}$ erg, while the luminosity at maximum can be as high as $\sim 10^{10}\,L_\odot$. The kinetic energy of supernovae can be estimated from the expansion velocity of the ejecta, $v_{\rm exp} \sim$ 5000–10,000 km s^{-1}, and turns out to be $\sim 10^{51}$ erg. Such an amount of energy can only be obtained from the gravitational collapse of an electron degenerate core, forming a proto-neutron star or a black hole, or from its thermonuclear incineration to iron-peak isotopes. In the former case, the gravitational binding energy of a neutron star of $\sim 1.4\,M_\odot$ and ~ 10 km radius is of the order of $\sim 10^{53}$ ergs and a weak coupling between the source of energy and matter is enough to fulfill the energetic requirements (Zwicky 1938). In the second case, the nuclear specific energy of a carbon oxygen mixture is $q \sim 10^{18}$ erg/g, sufficient to obtain the required energy from burning $\sim 1\,M_\odot$ (Hoyle and Fowler 1960).

Supernovae are classified according to their spectrum at maximum light. If hydrogen lines are absent, they are called Type I supernovae or SNI. If these lines are present, they are referred to as Type II or SNII (Minkowski 1941). Also according to their spectra, SNI are further divided into three categories. If a prominent line of SiII is present, they are labeled SNIa. If this line is absent but there is a prominent HeI line, they are denoted SNIb. If both SiII and HeI lines are absent, the classification label is SNIc (Wheeler and Harkness 1990).

The light curves of SNIa are characterized by a rapid rise in luminosity, up to an average maximum $M_V \approx M_B \approx -19.30 \pm 0.03 + 5\log(H_0/60)$ (Riess et al. 1999) in about 20 days, where H_O is the Hubble constant, followed by a comparatively gentle decline divided into two different epochs. The first epoch after maximum light lasts ~ 30 days and the luminosity typically drops by $\sim 3^{mag}$, while the second phase is characterized by a slow decline with a characteristic time of ~ 70 days. Infrared photometry shows that in the J, H and K bands there is a well defined minimum at ~ 20 days after maximum and a secondary peak ~ 30 days after maximum (Elias et al. 1985), although in some cases this secondary peak is absent.

This behavior can be understood in terms of the deposition of a large amount of energy, $\sim 10^{51}$ ergs, in the interior of a stellar envelope (Mochkovitch 1994). If it is assumed that half of this energy is invested into the expansion of the debris and half into their internal energy, the average temperature is:

$$T = 6.3 \times 10^4 \left(\frac{E_{SN,51}}{R_{15}^3} \right)^{1/4} \tag{5.16}$$

where $E_{\rm SN,51}$ is the energy released by the supernova in units of 10^{51} erg and R_{15} the radius in units of 10^{15} cm. Consequently:

$$\frac{P_R}{P_G} = \frac{{}^1\!/_3 a T^4}{\frac{\Re}{\mu} T \rho} \approx 1.6 \times 10^4 \frac{(R_{15} E_{SN,51})^{3/4}}{M} \tag{5.17}$$

which means that a supernova is, in a certain sense, just a ball of light. Typical expansion velocities are:

$$v \approx 10^9 \sqrt{\left(\frac{E_{SN}}{10^{51}} \cdot \frac{M_\odot}{M}\right)} cm/s \tag{5.18}$$

Since the internal energy is dominated by radiation and the expansion is nearly adiabatic, $T \propto R^{-1}$, the total energy will evolve as $E_{th} \propto VT^4 \propto R^{-1}$. If the initial structure is compact, $\sim 10^8$ cm, the typical size of a relativistic degenerate stellar core, the energy decreases from $\sim 10^{51}$ to $\sim 10^{44}$ erg when the radius is $\sim 10^{15}$ cm, the typical radius at maximum light; i.e. the energy deposited by the shock is invested in the adiabatic expansion of material. On the contrary, if the initial structure is extended,

$$E_{th} \approx E_{th,0} \frac{R_0}{R_{env}} \approx \frac{E_{SN}}{2} \frac{R_0}{R_{env}} \tag{5.19}$$

the luminosity will be given by

$$L_P \approx \frac{E_{th}}{\tau_{diff}} \approx \frac{2\pi c}{9k_{Th}} \frac{E_{SN}}{M_{env}} R_0 \tag{5.20}$$

where the diffusion time has been estimated as:

$$\tau_{diff} \approx \frac{3R_{env}^2}{\lambda c} \approx \frac{9\kappa M_{env}}{4\pi c R_{env}} \tag{5.21}$$

and the thermal energy will provide a luminosity plateau or a broad peak after maximum.

Therefore, the explosion of a compact object is able to account for the light curve of Type Ia supernovae, but an additional source of energy is necessary to explain the tail. Although in the past some other possibilities were considered, there is now broad consensus that this energy source is provided by the radioactive decay of ^{56}Ni (Truran et al. 1967; Colgate and McKee 1969):

$$^{56}\mathrm{Ni} \rightarrow ^{56}\mathrm{Co} \rightarrow ^{56}\mathrm{Fe}$$

with $q_{Ni} \sim 7 \times 10^{49}$ erg/M$_\odot$, $q_{Co} \sim 1.5 \times 10^{50}$ erg/M$_\odot$ and $\tau_{1/2}(Ni) = 6.1$ days, $\tau_{1/2}(Co) = 77.1$ days. This hypothesis has been recently confirmed with the observation by *INTEGRAL* of the emission of ^{56}Ni around the maximum of the light curve (Diehl et al. 2014; Churazov et al. 2015; Isern et al. 2016), see Fig. 5.5, and that of ^{56}Co 60 days after the explosion (Churazov et al. 2014) of SN2014J.

The majority of the energy released by the decay of ^{56}Ni and ^{56}Co is in the form of γ-rays of $\sim$1 MeV that are scattered and eventually thermalized via Compton scattering and photoelectric absorption. The resulting thermal photons diffuse and

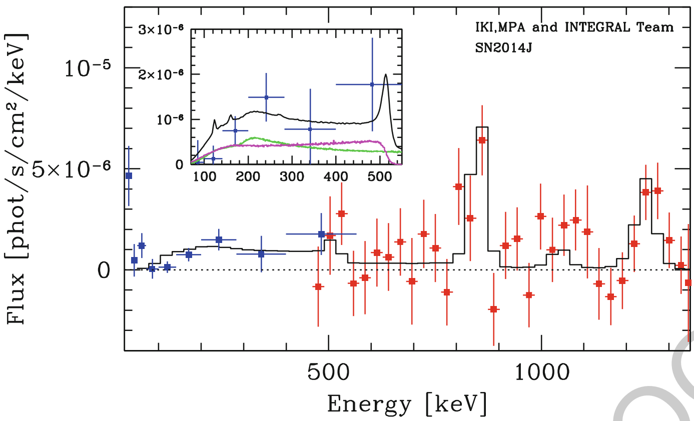

Fig. 5.5 ^{56}Co gamma lines from SN 2014J obtained with the *INTEGRAL* instruments, with data points from INTEGRAL SPI (red) and IBIS (blue) instruments; the black histogram is a fiducial model of the spectrum expected for day 75 after the explosion (Churazov et al. 2015)

eventually escape. The observed light curve thus results from a competition of two time scales describing diffusive energy transport and dynamic expansion. As before, the diffusion time scale is dominated by Thomson scattering and by absorption from bound electrons. The contribution of true absorption to the total opacity is a complicated issue because of the departures from LTE, the Doppler effect introduced by the expansion velocity and the uncertainties introduced by the chemical composition and the energy levels of different ions. Nevertheless, the opacity seems to be confined within the range 0.2–0.03 cm^2/g. If it is assumed that the envelope expands with constant velocity, $R_{env} \sim R_0 + v_{exp}t$, the hydrodynamic time scale is $\tau_h \sim R_0/v_{exp}$.

Initially the ejecta are opaque, $\tau_{diff} \gg \tau_h$, and the luminosity is small. As time goes by, $\tau_{diff} \sim \tau_h$, and photons begin to escape. Since the energy output decreases exponentially, a peak appears in the light curve that is equal to the instantaneous deposition of energy and therefore $L_{max} \propto M_{Ni}$. After the peak, the radiation trapped in the envelope diffuses outwards and the luminosity exceeds the instantaneous energy deposition rate. The width of the peak is determined by an effective diffusion time:

$$\tau_m = \sqrt{2\tau_{diff}\tau_h} \propto \kappa^{1/2} M_{env}^{3/4} M_{Ni}^{-1/4} \tag{5.22}$$

Later, when the density is small enough, an increasing fraction of the γ-photons (and later also positrons) can escape and, consequently, the luminosity is smaller than the energy output of radioactive decays. Some radioactive energy may be stored in the form of ionization, and defer luminosity originating from radioactive energy. See Arnett (1996) and references therein for a complete discussion.

The observation of the bolometric light curves together with these simple relationships allow estimates of the mass expelled and the mass of the radioactive elements synthesized by SNIa: $M_{env} = 0.4\text{–}1.4\,M_\odot$ and $M_{Ni} = 0.1\text{–}1\,M_\odot$ (Stritzinger et al. 2006). One of the most striking properties of SNIa is their photometric homogeneity i.e. the light curve of the majority shows a very small dispersion at maximum, $\sigma_M \leq 0.3^{mag}$ (Cadonau et al. 1985; Hamuy et al. 1996) when they are normalized to the peak. All these properties together immediately suggest that the most plausible scenario is the explosion of a CO white dwarf near the Chandrasekhar mass in a close binary system. This hypothesis has been confirmed in the case of SN 2011fe, which shows that the properties of the early light curve are only compatible with the explosion of a white dwarf (Bloom et al. 2012)

Spectroscopic observations at different epochs enable tomography of supernovae. During maximum light, the spectra of SNIa are characterized by various lines of neutral and singly ionized atoms of Si, Ca, Mg, S and O moving at high velocities ($v \sim 8000\text{–}30{,}000\,\mathrm{km\,s^{-1}}$) indicating that the outer layers are mainly composed of intermediate mass elements, i.e. that thermonuclear burning was not complete (Filippenko et al. 1992). Two weeks after maximum, permitted FeII lines are prominent, indicating that the photosphere has reached regions where the star was able to completely incinerate matter (Harkness 1991). The nebular phase starts 1 month after the maximum, roughly when the tail of the lightcurve begins. During this epoch, the spectrum is dominated by forbidden FeII, FeIII and CoIII emission lines (Axelrod 1980). The decrease of the Co lines, together with the relative intensity of CoIII with FeIII (Kuchner et al. 1994) provide support for the idea of a light curve tail powered by the decay of ^{56}Co. In general, the lines of different elements have different expansion velocities, indicating a layered structure where the central regions are occupied by completely burned material, i.e. the iron peak elements. This property rules out the hypothesis of a prompt detonation since in this case the white dwarf would be completely converted to ^{56}Ni.

Despite their remarkable photometric homogeneity, SNIa do exhibit some degree of heterogeneity. Already in 1973, it was proposed (Barbon et al. 1973) to sub-divide SNIa into a fast and slow class according to the rate of decline of their light curve just after maximum, the transition from the peak to the tail, and the decline of the tail. The slow class is characterized by a broader and more luminous peak than the fast class. The most extreme cases are SN1991T, considered until recently the most energetic event with the broadest peak, and SN1991bg and SN1992K, which are the reddest, fastest and most subluminous Type Ia supernovae known to date (Phillips et al. 1992; Ruiz-Lapuente et al. 1992). The difference in brightness between the extreme cases is $\sim 2^{mag}$. The large majority of SNIa also display a remarkable spectroscopic homogeneity (Branch et al. 1993) not only during the maximum but also during subsequent months. They are classified as *Branch-normal* and represent 85% of the total, although there are suggestions that this value should be reduced to 70%. The prototypes are SN1972E, 1981B, 1989B and 1994D. On the contrary, 91T-like events display FeIII lines before maximum while the 91bg-like supernovae lack the characteristic secondary maximum in the infrared. At present the question is to decide if they can be considered as different subtypes or just extreme cases of the normal events

This mildly inhomogeneous set of SNIa exhibits a correlation between peak magnitude, the width of the peak, and the expansion velocity, in the sense that the brightest SNIa show the largest expansion velocities (Pskovskii 1977; Branch 1981). The correlation between the brightness and the shape of the light curve was settled definitively when a clear relationship between the maximum of light and the magnitude decline during the first 15 days after maximum (Δm_{15}) was firmly established (Phillips 1993). This correlation (which can be parameterized in terms of the decline rate (Phillips 1993; Hamuy et al. 1996), the stretch parameter (Perlmutter et al. 1997), or via a multi-parameter fit of colors (Riess et al. 1996)) is used to renormalize the peak magnitudes and thereby substantially reduces the dispersion of the absolute magnitudes, making SNIa one of the most powerful tools for measuring cosmological distances.

In principle, these variations in the shape of the light curve can be understood in terms of the total amount of ^{56}Ni synthesized, if the ejected mass is kept constant. Since the maximum of the luminosity is proportional to the ^{56}Ni mass, the brightest events are those that have synthesized the largest amount of this material and consequently have larger expansion velocities and broader peaks since the opacity of iron peak elements is very large. In any case, this diversity of properties poses the question whether there are two explosion mechanisms, one for the *Branch-normal* supernovae and another for the peculiar events, or if there is a unique mechanism able to account for the broad range of behaviors.

The recent systematic searches of supernovae have revealed the existence of new subtypes besides the Branch-normal ones (Taubenberger 2017). The most relevant are the so called SNIax, the Super-Chandrasekhar, and the CSM types but several other exist although their relevance has not been elucidated yet. One example of the last ones is that of the Ca-rich transients, which have a luminosity in between novae and normal supernovae and display prominent Ca lines in the late spectra. All of them are thought to have a thermonuclear origin.

Type Iax supernovae (SNIax) were proposed by Silverman et al. (2012) as a true subclass. The prototype is SN 2002cx, their spectrum at maximum is similar to that of SM 1991T but they are as subluminous as SN 1991bg. The expansion velocity at maximum is $\sim$6000 km s^{-1}, that is half of that of normal supernovae, indicating a smaller kinetic energy per unit mass and do not display a secondary maximum in the infrared. The amount of ^{56}Ni synthesized in this case is $\sim$0.25 M$_\odot$. They also present a correlation between the luminosity at maximum and the early decline of the light curve, but is different from that of the normal ones. Their maximum luminosity and expansion velocity lie in the range $-14.2 > M_V > -18.4$ and $2000 < v < 8000$ km s^{-1} respectively, suggesting a large range in explosion energies, ejected masses and ^{56}Ni masses. It is suspected that their contribution to the total number of SNIa could be as large as 1/3.

The 'Super-Chandrasekhar' SNIa are $\sim$1 mag brighter than the normal ones and have low expansion velocities, $\sim$8000 km s^{-1}, around the maximum. According to the Arnett's rule the mass of ^{56}Ni synthesized during the event should be $\sim$1.3 M$_\odot$.

This value, together with the low velocities suggest that the mass of the object that exploded was larger than the Chandrasekhar's mass. This class contains few events, being SN 2003gz (Howell et al. 2006) the first one to be discovered. This, together with their high luminosity suggests that their frequency is very low.

SNIa-CSM are characterized by the coexistence of a normal SNIa spectrum, often 91T-like, with a blue continuum and the presence of hydrogen Balmer lines, suggesting an interaction between the supernova and the circumstellar material. The first event discovered was SN 2002ic (Hamuy et al. 2003). Since then, several different events have been added to the group, but the sample is still small, suggesting they are rare events that not represent more than ∼1% of the total.

The frequency and the impact on the chemical content of galaxies provide additional constraints on the different supernova mechanisms. The rate of supernovae in galaxies is usually normalized to the galaxy blue luminosity (Tammann 1970) or to the mass assuming an average M/L-ratio for each galaxy type (Cappellaro et al. 2003). The most striking feature is that SNIb/c and SNII only appear in spiral— and irregular galaxies, and are associated with a young populations, while SNIa can appear in all galaxy types, indicating that they are related to the old stellar populations. Nevertheless, the SNIa rate per unit mass is almost three times larger in late spirals than in ellipticals, thus implying that at least a fraction of SNIa must be related to the young stellar population (Cappellaro et al. 2003). Furthermore, there is some evidence that, on average, SNIa in red or early type galaxies are dimmer, have faster light curves and slower expansion velocities than those in blue or late type galaxies (Hamuy et al. 1995, 1996; Branch et al. 1996). On the other hand, the frequency of supernovae in the Milky Way has been estimated (van den Bergh and Tammann 1991) to be: $R_{\rm II} = 3.32 \times 10^{-2}$ year^{-1}, $R_{\rm Ib/c} = 0.65 \times 10^{-2}$ year^{-1} and $R_{\rm Ia} = 0.41 \times 10^{-2}$ year^{-1}. Taking into account that the mass of ^{56}Ni ejected per event is roughly 0.07, 0.3 and 0.6 $M_\odot$ for SNII, SNIb/c and SNIa, respectively, it turns out that nearly half of the galactic iron was synthesized by Type Ia supernovae. This means that SNIa have to produce the right amount of iron peak isotopes to account for the observed isotopic Solar abundances.

5.3.1 Chandrasekhar-Mass Models

As discussed in Sect. 5.1.3, the outcome of carbon ignition under degenerate conditions in a white dwarf near the Chandrasekhar limit can be a detonation or a deflagration, depending on the particular structure at the moment of ignition, represented by density, temperature, chemical composition and velocity profiles. For instance, it is easier to generate the overpressure necessary to launch a detonation at low densities, $\sim 3 \times 10^7$ g/cm^3, than at high densities due to the degeneracy dependence on density and temperature.

The Prompt Detonation Model Even though a pure detonation seems possible from a physical point of view (Blinnikov and Khokhlov 1986), this kind of explosion cannot account for the observed SNIa spectra at maximum light.

At densities above $\sim 10^7$ g/cm^3, the fuel is completely incinerated to Fe-peak elements and it leaves only a few hundredths of a solar mass of intermediate mass elements, which is not enough to produce the characteristic strong SiII line of SNIa. The rejection of a pure detonation as the SNIa mechanism is a consequence of the simplicity of this burning mode. As discussed in Sect. 5.1.3, in the absence of external perturbations like a piston, the Chapman-Jouget detonation is the only stable solution (other than a deflagration) of the Rankine-Hugoniot equations that define the burning front. Thus, there are no free parameters left, no time for modification of the fuel pre-combustion structure, no diversity, and pure detonations always produce the wrong result. Notice however that the presence of a shallow thermal gradient close to the ignition profile might induce the formation of shocks that could burn a large mass in a short time, starting the dynamical phase of the supernova (Blinnikov and Khokhlov 1986; Bravo et al. 1996) and a mixture of deflagration and detonation regimes might be the result.

The Deflagration Model Deflagrations are less constrained from a physical point of view, but their properties are strongly conditioned by the hydrodynamics of the explosion process itself. As described in Sect. 5.1.3, at the microscopic scale the speed of the flame only depends on the local physical conditions. Thus, the laminar velocity of the flame can be determined as a function of density (Timmes and Woosley 1992): $v'_{\rm lam} = \alpha\rho_9^{\beta}$ cm/s, where ρ_9 is the density in units of 10^9 g/cm^3, and α and β are fit parameters. For $\rho_9 < 0.36$, $\alpha = 5.68 \times 10^6$ and $\beta = 1.46$, while for $2 \geq \rho_9 \geq 0.36$, $\alpha = 3.68 \times 10^6$ and $\beta = 1.03$. A further correction can be obtained taking into account the effect of Coulomb interactions: $v_{\rm lam} = K_{\rm cc} v'_{\rm lam}$, where $K_{\rm cc} = 0.894 - 0.0316 \log(\rho_9)$ (Bravo and García-Senz 1999). The situation becomes extremely complicated when the flame is accelerated by the deformation induced by hydrodynamic instabilities. This acceleration is difficult to describe because it implies many length scales, from the global length scale, $\sim 10^7$–10^8 cm, to the microscopic width of the laminar flame, which strongly depends on the density as shown before.

One possibility (Woosley and Weaver 1986) is to parameterize the velocity of the deflagration as a function of flame radius, r, as: $v_{\rm def,W} = A v_{\rm sound}\left(1 - e^{-Br}\right)$. The parameters A and B are constrained by the condition that the flame should propagate at a small Mach number close to the center but should reach velocities as high as 0.1–0.5 Mach in the outer layers of the white dwarf. A second possibility (Khokhlov 1995), assumes that the rate of surface creation by the turbulence is balanced by the rate of surface destruction due to flame propagation. The deflagration velocity should then be given by $v_{\rm def,K} = 0.5\sqrt{g_{\rm eff} L}$, where L is the driving scale, $g_{\rm eff} = g{\rm At}$, g is the gravitational acceleration and At is the Atwood number (Timmes and Woosley 1992). Such kind of self-regulating regime has been implemented in several ways in many multidimensional simulations of SNIa (Gamezo et al. 2003; García-Senz and Bravo 2005). A third possibility (Niemeyer and Woosley 1997) is that the deflagration moves at the speed of the Rayleigh-Taylor bubbles in the nonlinear scale, the so-called Sharp-Wheeler model, in which the velocity increases linearly with time t, $v_{\rm def,NW} = 0.1 g_{\rm eff} t$. Finally, the concept of a subgrid-scale model that takes into account the dissipation of turbulent energy at microscopic scales has been adopted in many multidimensional simulations performed to date (Schmidt and Niemeyer 2006; Röpke et al. 2006). In spite of the differences in the treatment of the flame, most three-dimensional simulations of SNIa produce quite homogeneous results.

The success or failure of a deflagration model depends on its ability to consume the fuel with the same speed as the front engulfs it, such that it does not leave unburned pockets of carbon and oxygen behind (Niemeyer and Woosley 1997). High-resolution simulations aimed to explore the multipoint ignition scenario (Röpke et al. 2006) indicate that when the number of initial seeds increases, the ignition volume becomes saturated and the gross features of the explosion converge towards a unique solution. The optimal number of flame seeds is estimated to be in the range ∼100–400 per octant distributed in radius following a Gaussian up to ∼100–150 km. However, even in the most favorable case it is difficult to obtain more than 0.7 $M_\odot$ of ^{56}Ni and a kinetic energy above 0.7×10^{51} ergs, which is too small to account for the bulk of bright-normal SNIa. In addition, the deflagration always leaves a large mass of carbon and oxygen unburned, $M_{\rm ub} > 0.57\ M_\odot$ (Schmidt et al. 2006).

The present three-dimensional simulations of Type Ia supernovae based on a pure deflagration algorithm have to face the following problems when confronted with observations: (i) although the amount of Fe-group elements synthesized in the explosion is sufficient, the mass of ^{56}Ni is not. (ii) the final kinetic energy is always smaller than the canonical value of 10^{51} ergs. (iii) the synthesis of intermediate-mass elements is scarce. (iv) the ejecta lack chemical stratification. (v) big clumps of radioactive ^{56}Ni are present at the photosphere at the time of maximum luminosity.

Before discarding deflagrations as the main mode of Type Ia supernovae it is necessary to examine some still poorly understood aspects. For instance, it might be that the theoretical description of subsonic flames included in the hydrodynamical codes and used in the simulations is incomplete as is the case when they enter the distributed regime at densities lower than $\sim(1\text{–}3) \times 10^7$ g/cm^3. It is also important to notice that the influence of the initial conditions at the onset of the ignitions has not yet been clarified.

The Delayed Detonation Model In 1974, a burning regime was proposed (Ivanova et al. 1974) in which the initial flame was not able to unbind the star, leading to a pulsation and a delayed transformation of the deflagration into a detonation (deflagration-detonation transition or DDT). The DDT concept was later extended (Khokhlov 1991; Khokhlov et al. 1993) to include the possibility of a transition to detonation without an intervening pulsation. The essential ingredient for the formation of a detonation is the existence of a non-uniformly preheated region with a level of fluctuations of temperature, density, and chemical composition such that a sufficiently large mass would be burnt before a sonic wave could cross it. The thermal gradient needed (Khokhlov 1991) is:

$$\nabla T < \frac{\Theta T}{A v_{\rm sound} \tau_i} \tag{5.23}$$

where A is a numerical coefficient, $A \sim 0.2$–5.0, $\tau_i = T/\dot{T}$ is the induction time at the temperature T, and $\Theta \sim 0.04$–0.05 is the Frank-Kameneetskii factor:

$$\Theta = -\frac{\partial \ln \tau_i}{\partial \ln T} \tag{5.24}$$

There are several mechanisms that can produce such fluctuations: adiabatic pre-compression in front of a deflagration wave, shock heating, mixing of hot ashes with fresh fuel (Khokhlov 1991), accumulation of pressure waves due to a topologically complex geometrical structure of the flame front, or transition to the distributed burning regime (Niemeyer and Woosley 1997). Among these possibilities the turbulence pre-conditioning has received more attention. In the case of a white dwarf expanding as a consequence of a deflagration, the turbulent velocity has to exceed the laminar flame velocity by a factor 1–8 at a length scale comparable to the detonation wave thickness (Khokhlov et al. 1997). This criterion is fulfilled for flame densities in the range 5×10^6 g/cm^3 $< \rho < (2 - 5) \times 10^7$ g/cm^3 for reasonable assumptions. At densities above 10^8 g/cm^3, a DDT transition is unlikely (Khokhlov et al. 1997) although the bubble fragmentation could increase the flame surface and facilitate a DDT at $\rho \sim 2 \times 10^8$ g/cm^3 (Zingale and Dursi 2007). Despite the difficulties to justify the DDT models, the one-dimensional delayed detonation simulations are particularly successful in reproducing many key observational characteristics of SNIa (Hoeflich and Khokhlov 1996), like the light curves and photospheric expansion velocities.

The Pulsational Delayed Detonation Model The 3D formulation of the pulsational delayed detonation model is the so-called Pulsational Reverse Detonation model or PRD. In this scenario the detonation is triggered by an accretion shock that forms above a quasi-hydrostatic core composed mainly of C-O with a mass of 0.8–1.15 $M_\odot$. Heating by the accretion shock ignites the fuel slightly below the core's surface. Because of the inertial confinement provided by the material falling through the accretion shock, the core cannot expand and cool efficiently. As a consequence, a detonation propagating inwards forms and burns most of the core. The resulting energetics as well as the nucleosynthesis are roughly in agreement with observations, specially concerning the observed stratification.

5.3.2 *Super-Chandrasekhar Models, Sub-Chandrasekhar, and White Dwarf-White Dwarf Collisions*

The only way known to push the mass of a degenerate structure beyond the Chandrasekhar limit is through rotation. If it is assumed that the white dwarf rotates as a rigid body, it is possible to delay the ignition up to masses of the order of 1.4–1.5 $M_\odot$ (Piersanti et al. 2003a,b). If differential rotation is allowed, the ignition can be delayed up to masses $\sim 2\,M_\odot$ (Piersanti et al. 2003a). A follow-up of rigid rotation models has been calculated with a 1D hydrodynamic code modified to take into account the centrifugal force (Domínguez et al. 2006) and a weak dependence on the rotation period has been found. The problem is that these calculations assume that the transition from deflagration to detonation occurs at a fixed density and it is not known how rotation affects this change of regime of the burning front.

Sub-Chandrasekhar models assume a white dwarf with a mass $M_{WD} \leq 1.1$–$1.2\,M_{\odot}$ that accretes helium rich matter at a rate in the range $10^{-9} \leq \dot{M} \leq 5 \times 10^{-8}\,M_{\odot}\,\mathrm{year}^{-1}$. These rates allow the formation of a degenerate helium mantle around the initial CO core. When this mantle reaches a critical mass, $\sim$0.2–0.3 $M_{\odot}$, a thermonuclear runaway starts at its bottom and triggers the explosion of the star before reaching the Chandrasekhar limit. Notice that white dwarfs with an initial mass larger than $1.2\,M_{\odot}$ could reach the Chandrasekhar mass before exploding and experience central ignition.

One dimensional models indicate that before the thermonuclear runaway occurs, the base of the helium layers becomes convective and transports energy and part of the reactants away from the inner core boundary in such a way that He ignites above the interface. The high flammability of helium together with the low density of the envelope guarantees the formation of a detonation that incinerates the envelope and launches a shock wave inwards through the CO core. Because of the focusing effect of the spherical symmetry, this shock strengthens and induces the detonation of C in the central region that leads to a supernova explosion.

These explosions reproduce the gross features of SNIa explosions, specially sub-luminous ones like SN 1991bg and allow to explain with a single parameter, the initial mass of the white dwarf, their observed diversity. Despite such advantages, Sub-Chandrasekhar models were not the favorite to account for SNIa outbursts. The reason was that they predicted the existence of a very fast moving layer composed of ^{56}Ni and ^{4}He that is not observed, as well resulting in light curves that rise too fast (Hoeflich and Khokhlov 1996). The situation changed when it was shown (Bildsten et al. 2007; Shen et al. 2010; Shen and Moore 2014) that it was possible to induce a detonation with a He-envelope as small as $\simeq 10^{-2}\,M_{\odot}$, thus removing the constrain introduced by the lack of ^{56}Ni lines in the spectrum at maximum light. Multidimensional calculations by Fink et al. (2007), Sim et al. (2007, 2010, 2012) in 2D, and Moll and Woosley (2013) in 3D, have confirmed these results and, furthermore the recent work by Blondin et al. (2017) and Goldstein and Kasen (2018) has shown that this scenario can reproduce the faint end of the Phillips relationship. From the observational point of view it has been shown that the companion of the white dwarf star that exploded as SN 2012Z, a Type Iax supernova, was probably a He-star (McCully et al. 2014) and that the protuberance recently found in the early light curve of SN 2017a could be due to the presence of ^{56}Ni in the outer layers (Jiang et al. 2017). To these evidences it has to be added the excess of gamma-ray emission near the maximum of the optical light curve that seems to be produced by the presence of ^{56}Ni in the outer layers (Diehl et al. 2014; Isern et al. 2016).

Another possibility that has emerged within the context of the double degenerate scenario is the collision, not the merging, of two white dwarfs with velocities of the order of the free-fall time. Such collisions can produce events that can be assimilated to standard and non standard SNIa (Benz et al. 1989; Raskin et al. 2009; Rosswog et al. 2009a; Lorén-Aguilar et al. 2010; Aznar-Siguán et al. 2013, 2014; García-Senz et al. 2013; Kushnir et al. 2013), but it was believed they were very rare and only could occur inside dense ambients like globular clusters. However, very recently it has been suggested that triple systems containing an inner close binary white dwarf could experience significant pericenter changes with time scales of the order of the orbital period that could end with a violent collision (Antonini and Perets 2012), although the frequency of such scenario has not been elucidated yet.

The outcome of the collision strongly depends on the size of the He-layer of white dwarfs. Papish and Perets (2016) have found that if the mass of the helium layer is larger than $\sim 0.1\,M_{\odot}$, the detonation of He propagates on the white dwarf surface before triggering the central ignition of the core. Since the burning of helium at these densities is not efficient enough, important amounts of ^{44}Ti and ^{48}Cr are synthesized. If the He-shells are low mass, there is not a helium detonation, but helium burning precedes the detonation of the C/O core, and important amounts of material enriched with intermediate mass elements are ejected at high velocities.

5.3.3 Nucleosynthesis in Thermonuclear Supernovae

The abundances of the elements synthesized in SNIa events depend on the peak temperature reached by the material and on the excess of neutrons versus protons. Roughly speaking, the SNIa material undergoes four burning regimes: (i) nuclear statistical equilibrium (NSE), (ii) incomplete Si burning, (iii) incomplete O burning and (iv) incomplete C-Ne burning (Woosley 1986). The neutron excess depends on the initial abundance and distribution of the neutron rich isotopes like ^{22}Ne, which depend on the metallicity and thermal history of the white dwarf, and on the extent of electron captures on the burned material, which mainly depends on the ignition density and on the burning regime. Another complication comes from the additional degrees of freedom introduced by 3D flames that open a variety of possible ignition modes as well as the possibility of leaving pockets of unburned material. Finally, the adopted nuclear reaction and electron capture rates are an important source of uncertainty. Despite all these factors it is possible to obtain some insight into the problem using parameterized 1D models with different propagation velocities of the burning front, different ignition densities and different initial metallicities. Three dimensional models still need some additional work.

The chemical composition of matter in nuclear statistical equilibrium (NSE) with equal number of protons and neutrons, i.e. with electron mole number $Y_e = 0.5$, peaks around ^{56}Ni. When Y_e takes values in the range 0.470–0.485, the peak moves towards ^{58}Ni, and ^{54}Fe; values in the interval 0.46–0.47 produce predominantly ^{56}Fe; values in the range of 0.45–0.43 are responsible of the formation of ^{58}Fe, ^{54}Cr, ^{50}Ti and ^{64}Ni, while values below 0.43–0.42 are responsible for ^{48}Ca. Parameterized models indicate that the amount of mass with $Y_{\rm e} < 0.45$ depends on the ignition density, while that with $0.47 < Y_{\rm e} < 0.485$ depends on the deflagration velocity.

Therefore ^{58}Fe, ^{54}Cr, ^{50}Ti, ^{64}Ni and ^{48}Ca are a measure of $\rho_{\rm ig}$ while ^{58}Ni, ^{54}Fe are a measure of $v_{\rm def}$ (Thielemann et al. 2004). It is important to realize that the change from using the Fuller et al. (1985) rates to the Langanke and Martínez-Pinedo (2000) rates strongly alleviates the chronic problem of producing an excess of neutronized species. In any case, to correctly evaluate the implications of the nucleosynthesis resulting from the different mechanisms and explosion scenarios it is necessary to integrate them into a galactic chemical evolution model that takes into account the contributions of all the iron-peak producers (Bravo et al. 1992; Matteucci et al. 1993). The nucleosynthesis yields also depend on a more subtle parameter, the abundance profiles of carbon and oxygen, which in turn are a function of the mass and initial metallicity of the progenitor of the white dwarf. In general, low mass progenitors produce white dwarfs with oxygen abundances in the center as large as $X_{\rm O} = 0.7$ (D'Antona and Mazzitelli 1989; Salaris et al. 1997). This abundance can be enhanced as a consequence of the sedimentation induced by crystallization (Canal et al. 1990) if the white dwarf has had time to solidify before the start of the accretion phase. The differences in the energetic contents of carbon and oxygen nuclei translates into different ^{56}Ni yields (Domínguez et al. 2001). A similar effect is produced by the abundance and distribution of ^{22}Ne across the star (Bravo et al. 1992). These differences in the final production of ^{56}Ni translate into a dispersion of the peak SNIa luminosities of $\sim$0.2 magnitudes. This value is smaller than the observed differences at high redshift and thus does not invalidate the use of SNIa for measuring distances but introduces some caution in the context of their use to determine the cosmological equation of state (Domínguez et al. 2001).

5.4 X-ray Bursts and Superbursts

X-ray bursts were serendipitously discovered in 1975 by Grindlay and Gursky (1976), and independently, by Belian et al. (1976). In contrast to standard transient sources, characterized by lifetimes ranging from weeks to months, these new cosmic X-ray sources (a subset of the low-mass X-ray binary class, or LMXB) exhibit brief *bursts*, lasting from seconds to minutes (see Bildsten 1998; Lewin et al. 1993, 1995; Strohmayer and Bildsten 2006, for reviews).

The two bursting episodes reported by Grindlay et al. were based on observations performed with the Astronomical Netherlands Satellite (ANS) on a previously known X-ray source, 3U 1820-30, located in the globular cluster NGC 6624. Similar events were reported by Belian et al., from X-ray observations of sources in the Norma constellation, performed with two military *Vela-5* satellites, covering the 15-month period from May 1969 to August 1970.

One year later, three additional burst sources, one of them, the enigmatic *Rapid Burster* (XBT 1730-335), were identified within a few degrees of the Galactic center (Lewin et al. 1976). Within a year, 20 additional burst sources were discovered, mainly by SAS-3 and OSO-8 satellites. To date, $\sim$110 Galactic (Type I) X-ray

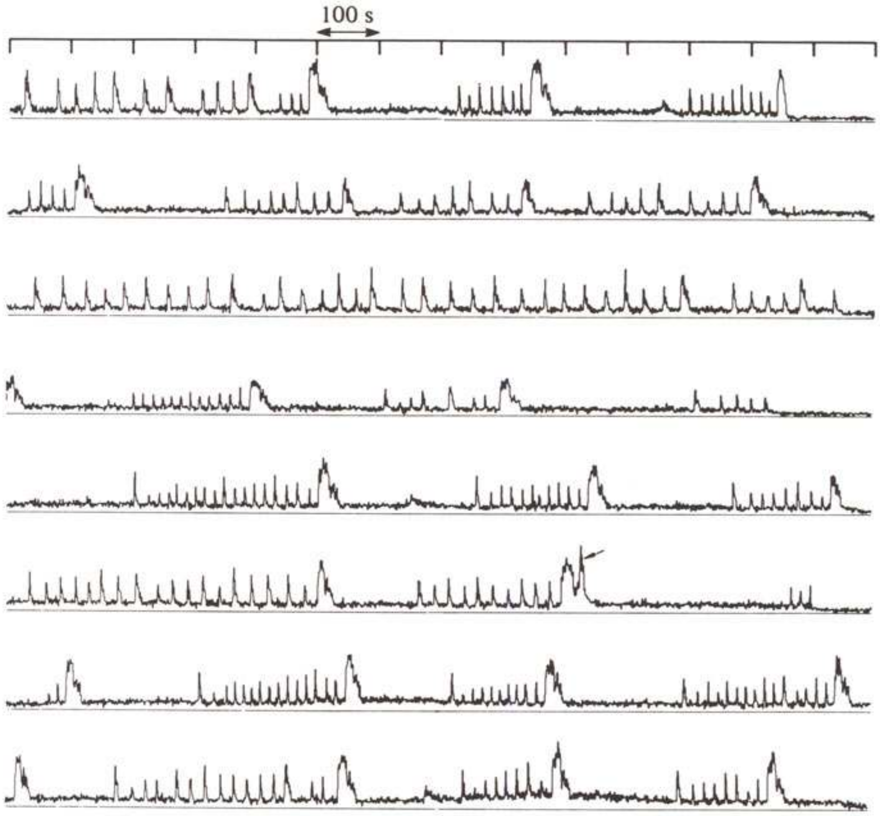

Fig. 5.6 Type II bursts from the Rapid Burster, based on SAS-3 observations performed in March 1976. The burst pinpointed with an arrow is actually a type I burst. Image from Lewin (1977)

burst sources (hereafter, XRBs) have been identified[1] with burst durations of ∼10–100 s, and recurrence periods ranging typically from hours to days. Some bursts have been reported with extremely short recurrence times, ranging from 4 to 10 min; their ignition has been linked to rotational mixing (Keek et al. 2010). On the other hand, longer duration bursts have also been identified more recently (Galloway et al. 2008; Keek and in't Zand 2008): intermediate-duration bursts, for instance, can last for about 15–40 min and are characterized by a total energy output of $\sim 10^{40}$–10^{41} erg, and recurrence periods of tens of days (Linares et al. 2009; in't Zand et al. 2005; Falanga et al. 2008); superbursts, in turn, have typical durations of about a day, a total energy output of $\sim 10^{42}$ erg, and recurrence periods of about a year (Cornelisse et al. 2000; Strohmayer and Brown 2002). These differences have been suggested to result from different fuels and ignition depths (Fig. 5.6).

[1] See http://www.sron.nl/$\sim$jeanz/bursterlist.html, for an updated list of known bursting sources.

5.4.1 The Nature of Type I X-ray Bursts

Maraschi and Cavaliere (1977), and independently, Woosley and Taam (1976), were the first to suggest the possibility that XRBs are powered by thermonuclear runaways on the surface of accreting neutron stars. However, it was soon realized that the quick succession of flashes exhibited by the Rapid Burster (with recurrent times as short as ∼10 s), didn't match the general pattern shown by these bursting sources. A major breakthrough in the understanding of the nature of these cataclysmic events was the discovery of two different kinds of bursts associated with the Rapid Burster (Hoffman et al. 1978): a classification of type I and type II bursts was then established, the former associated with thermonuclear flashes, the later linked to accretion instabilities. In fact, during many years, type II bursts were unequivocally linked with the Rapid Burster, the only object that showed both type I and type II bursts. More recently, a second member of the type II class, the bursting pulsar GRO J1744-28, has been identified. Hereafter, we will focus on type I X-ray bursts, the most frequent type of thermonuclear stellar explosion in the Galaxy (the third, in terms of total energy output after supernovae and classical novae).

The first evidence of the thermonuclear origin of type I XRBs came from lightcurve analysis, in particular the ratio between time-integrated persistent and burst fluxes, α. It was soon realized that the ratio between the gravitational potential energy released by matter falling onto a neutron star (G M_{NS}/R_{NS} ∼ 200 MeV/nucleon) during the accretion stage and the nuclear energy liberated during the burst (∼5 MeV/nucleon, for a solar mixture transformed into Fe-group nuclei), match the values inferred for α, in the range ∼40–100.

The spatial distribution of type I XRBs matches that of LMXBs, with a clear concentration towards the Galactic center. A significant fraction of XRBs is indeed found in globular clusters. This pattern suggests that they are associated with an old stellar population (Lewin et al. 1993). The donors transferring material onto the neutron stars in XRBs are faint, low-mass stars ($M < 1\,M_\odot$), either Main Sequence or Red Giant stars. Recently, the first extragalactic XRBs were discovered in two globular cluster source candidates of the Andromeda galaxy (M31) (Pietsch and Haberl 2005).

It is believed that mass transfer episodes are driven by Roche-lobe overflow, hence leading to the build-up of an accretion disk around the neutron star. The maximum mass-accretion rate is set by the Eddington limit ($\dot{M}_{Edd} \sim 2 \times 10^{-8}\,M_\odot$/year, for H-rich accretion onto a 1.4 $M_\odot$ neutron star). Typically, XRB sources have orbital periods ranging from 1 to 15 h (White et al. 1995).

The nature of the underlying primary star was initially a matter of debate. A model involving accretion onto massive black holes (>100 $M_\odot$) was proposed in the 70s (Grindlay and Gursky 1976). Nevertheless, XRB observations in globular clusters (from which reasonably accurate distance estimates can be obtained), performed with the OSO-8 satellite, best fitted with a blackbody spectrum with kT ∼ 0.87–2.3 keV (Swank et al. 1977), suggested a source with much smaller dimensions than a super-massive black hole (either a neutron star or a stellar mass black hole).

Other features, such as the harder X-ray spectra of XRB sources compared with most of the X-ray transients hosting black hole candidates, as well as the masses inferred from those systems, point towards a neutron star primary (van Paradijs and McClintock 1995).

Indeed, the masses inferred for neutron stars in XRBs are quite uncertain. However, two lines observed in the XRB spectra of EXO 0748-676 (suggested to be H- and He-like Fe lines; see Cottam et al. 2002), plus the measurement of a 45 Hz neutron star spin frequency in the same source, allowed mass estimates in the range $1.5 < M_{NS}(\mathrm{M}_\odot) < 2.3$, with a best fit for 1.8 $\mathrm{M}_\odot$ (Villarreal and Strohmayer 2004) (Fig. 5.7).

Light curves from X-ray bursts show a large variety of shapes (with single, double, or triple-peaked bursts). Generally speaking, they are characterized by a fast

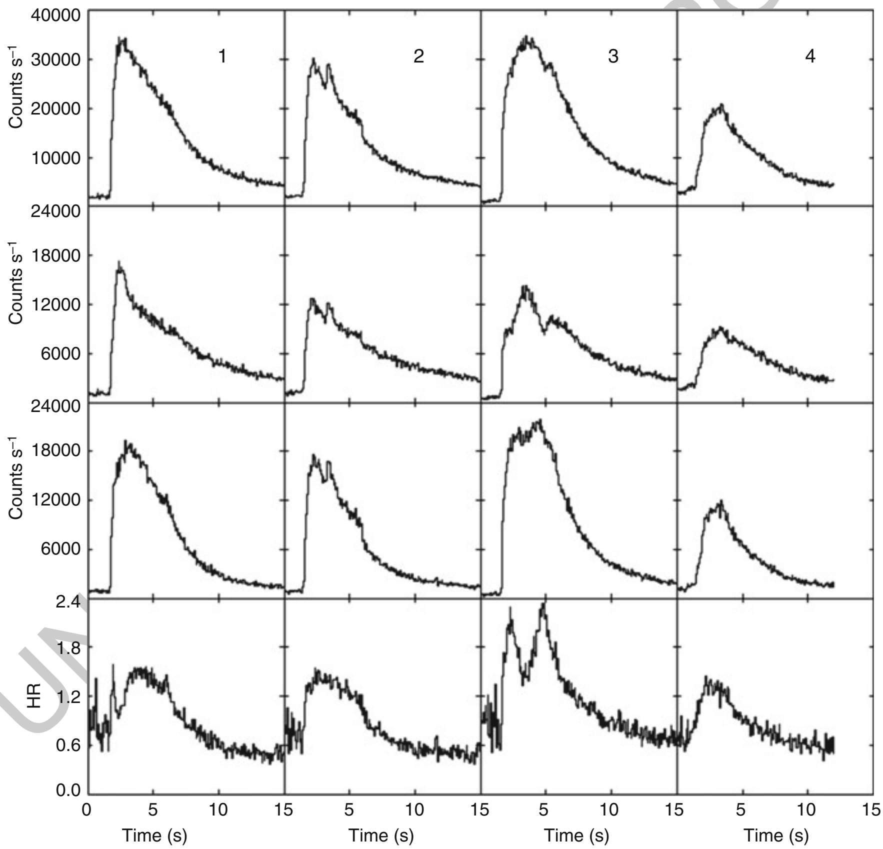

Fig. 5.7 A suite of XRB lightcurves from the LMXB source 4U1728-34 as observed with the RXTE satellite. Each sequence (top to bottom), shows the overall count rates in the energy bands 2–60, 2–6, 6–30 keV, and the ratio (6–30 keV)/(2–6 keV). Figure from Strohmayer and Bildsten (2006)

rise (∼1–10 s), a peak luminosity of $\sim 3\times10^{38}$ erg s^{-1} (Galloway et al. 2008; Lewin et al. 1993; Kuulkers et al. 2003), followed by a slower (sometimes exponential-like) decline (∼10–100 s).

An interesting feature, observed in the spectra of many XRBs, is a 4.1 keV emission line (Waki et al. 1984), interpreted as Lyman α lines of helium-like Fe atoms, broadened by Doppler and gravitational effects, likely originating at the inner edge of the accretion disk. Indeed, it has been suggested that time-resolved spectroscopy can in principle allow measurements of the surface gravitational redshift (Damen et al. 1990; Smale 2001).

The fact that XRB sources do not exhibit X-ray pulsations suggest that the underlying neutron stars have weak magnetic fields ($< 10^{11}$ G). Indeed, pulsations are assumed to result from misalignment between the magnetic axis and the rotation axis of the neutron star. Moreover, it is unlikely that XRBs will originate from highly magnetized neutron stars, as a strong magnetic field would funnel the infalling charged plasma towards a small fraction of the neutron star surface, close to the magnetic caps; the effective accretion rate (per unit area) would be so high, that suppression of thermonuclear flashes be expected (Joss 1978; Taam and Picklum 1978).

The understanding of the nature of XRBs requires also multiwavelength observations beyond the X-ray domain: in 1978, the first simultaneous optical/X-ray burst was detected from the source 1735-444 (Grindlay et al. 1978). The fluence in the optical burst was $\sim 2\times10^{-5}$ times that of the X-ray band, too large to be explained by the low-energy tail of the blackbody X-ray burst emission (Lewin et al. 1993). More important, the optical burst was delayed by ∼3 s with respect to the X-ray peak (McClintock et al. 1979). A similar delay (∼1.4 s) was also reported from Ser X-1 (Hackwell et al. 1979), and later, from many other sources (Lewin et al. 1993). These results suggest that optical emission observed from XRBs corresponds to reprocessing of X-rays in material within a few light-seconds from the source. Likely sites for this reprocessing include the accretion disk that surrounds the neutron star as well as the hemisphere of the secondary star directly illuminated by the X-ray source. Hence, the delay in the optical wavelengths results from travel-time differences between the X-rays leading directly to the observer and those that first intercept the disk, lose energy (becoming optical photons), and finally reach the observer.

The situation is less clear at other wavelengths: infrared emission has been suggested to accompany type I X-ray bursts. Indeed, detection of infrared burst from the Rapid Burster has been claimed in the past (Kulkarni et al. 1979), although an unambiguous confirmation is lacking (Lewin et al. 1980). Also, although radio bursts have been reported from the Rapid Burster, no X-ray bursts were seen simultaneously (Hayakawa 1981). More detailed observations at these wavelengths are required to disentangle the controversy.

5.4.2 *Modeling X-ray Bursts*

Modeling of type I XRBs and their associated nucleosynthesis has been extensively addressed by different groups. This reflects the astrophysical interest in determining the nuclear processes that power such explosions as well as in providing reliable estimates for the composition of the neutron star surface (Maraschi and Cavaliere 1977; Woosley and Taam 1976; Joss 1977). Nonetheless, several thermal, radiative, electrical, and mechanical properties of the neutron star depend critically on the specific abundance pattern of its outer layers. Moreover, the diversity of shapes of XRB lightcurves is also probably due to different nuclear histories (see Heger et al. (2007), for a detailed analysis of the interplay between long bursts and the extension of the rp-process), suggesting that the final chemical composition, at the end of the burst, is not unique.

The properties of the bursts are also affected by *compositional inertia*; that is, they are sensitive to the fact that accretion proceeds onto the ashes of previous bursts (Taam 1980; Woosley et al. 2004). Indeed, this compositional inertia reduces the recurrence times between bursts, especially for scenarios involving accretion of metal-poor matter. Another critical quantity is the emerging heat flux from deeper layers of the neutron star (Ayasli and Joss 1982; Fushiki and Lamb 1987; Brown 2000), which proved critical to the burst properties of pure He bursts (Bildsten 1995).

The first studies of localized TNRs on neutron stars (Shara 1982) suggested that heat transport was too inefficient to spread a local flame to the overall stellar envelope. Therefore, localized, volcanic-like explosions were predicted during X-ray bursts. However, it is worth noting that these studies relied only on radiative and conductive transport, ignoring the crucial role played by convection on the lateral thermalization of a TNR. The scenario was revisited by Fryxell and Woosley (1982b), who suggested that the most likely outcome involves TNRs propagated by small-scale turbulences, in a deflagrative regime, leading to the horizontal spread of the front at typical velocities of $\sim 5 \times 10^6\,\mathrm{cm\,s^{-1}}$. Such speeds suggest that the time required for a flame to engulf the entire stellar surface is much longer than the characteristic spin periods of accreting neutron stars ($\sim$milliseconds). Hence, it was predicted that fast rotation of the neutron star could modulate localized burning regions, eventually allowing for a direct observation of the neutron star spin. Indeed, the discovery of high-frequency, burst oscillations in the X-ray source 4U1728-34 (360–600 Hz; see Strohmayer et al. 1996) provided first observational evidence for millisecond rotation periods in accreting neutron stars. Since then, burst oscillations have been claimed for many additional sources. Studies to constrain neutron star properties based on modeling of such oscillations are currently underway.

5.4.3 *Nucleosynthesis in Type I X-ray Bursts*

In contrast to classical nova outbursts, where the main nuclear activity is driven by proton-capture reactions in competition with β^+-decays, X-ray bursts are triggered by a combination of nuclear reactions, including H-burning (via rp-process) and He-burning (that initiates with the triple α-reaction, and is followed both by the breakout of the CNO cycle through ^{14,15}O+α, plus a competition of proton captures and (α,p) reactions—the so-called αp-process). Moreover, with a neutron star as the underlying compact object hosting the explosion, temperatures and densities in the accreted envelope reach quite high values: $T_{peak} > 10^9$ K (an order of magnitude higher than in nova outbursts), and $\rho \sim 10^6$ g cm^{-3}. As a result, detailed nucleosynthesis studies require the use of hundreds of isotopes, up to the SnSbTe mass region (Schatz et al. 2001), or even beyond (the nuclear activity in Koike et al. (2004) reaches ^{126}Xe), and thousands of nuclear interactions extending to the proton drip line. In sharp contrast, the main nuclear activity for classical novae is limited to Ca, and runs close to the valley of stability (Fig. 5.8).

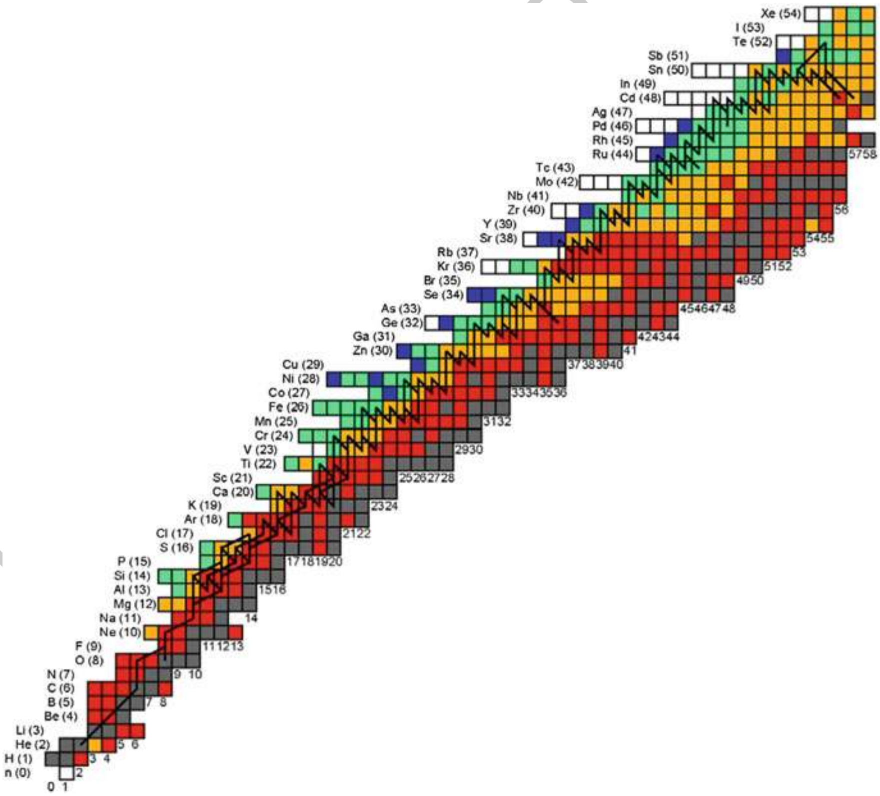

Fig. 5.8 Main nuclear path during a typical X-ray burst. Figure from Schatz et al. (1999)

Because of computational limitations, studies of XRB nucleosynthesis have usually been performed with limited nuclear reaction networks. More recently (Schatz et al. 1999, 2001), detailed nucleosynthesis calculations have been carried out with networks containing more than 600 isotopes (up to Xe, in Schatz et al. 2001), but using a one-zone approach, or also one-zone nucleosynthesis calculations with temperature and density profiles obtained with spherically symmetric evolutionary codes, linked to a 1270-isotope network extending up to ^{198}Bi (Koike et al. 2004). Other attempts (Parikh et al. 2008) include one-zone nucleosynthesis calculations, with temperature and density profiles obtained from the literature, and a large nuclear reaction network, containing 606 isotopes (up to ^{113}Xe) and more than 3500 nuclear processes. Note however that different numerical approaches and approximations have been adopted in all those works (hydrodynamic simulations with limited networks or one-zone calculations with detailed networks) and hence, the predicted nucleosynthesis in each case has to be taken with caution. Indeed, recent attempts have been made to couple hydrodynamic stellar calculations (in 1-D) and detailed networks (with $\sim$300 isotopes, up to ^{107}Te (Fisker et al. 2008; Tan et al. 2007), with 1392 nuclear processes and 325 isotopes, up to ^{107}Te (José et al. 2010), or with networks containing up to 1300 isotopes in an adaptive framework (Woosley et al. 2004).

To date, no fully multidimensional calculation for realistic XRB conditions has been performed. So far, a number of efforts have focused on the analysis of flame propagation on the envelopes accreted onto neutron stars and on *convection-in-a-box* studies aimed at characterizing convective transport prior to ignition. Some of the pioneering studies of thermonuclear flame propagation on neutron stars (Shara 1982) suggested that the onset of a localized ignition on a neutron star would likely propagate as a deflagration front, incinerating the whole envelope in a timescale of 100 s. The dichotomy between detonations and deflagrations was subsequently explored by different groups (Fryxell and Woosley 1982a,b; Simonenko et al. 2012a,b; Zingale et al. 2001), but their results depend critically on the assumed initial density at the ignition point (frequently, too extreme and therefore not representative of X-ray burst conditions). The current consensus, however, suggests that TNRs in X-ray bursts propagate subsonically (i.e., a deflagration front). The early development of convection in the stages preceding thermonuclear ignition has been recently analyzed in a multidimensional framework, in an attempt to assess the possibility of dredge up of ashes enriched in heavy elements to the neutron star photosphere (in't Zand and Weinberg 2010). Several efforts in this direction have been undertaken by different groups. In particular, simulations of pure He bursts and mixed H/He bursts in two and three dimensions (Malone et al. 2011, 2014; Zingale et al. 2015) have been performed in the last years with the MAESTRO code. The latter assumed an outer envelope composed of a mixture of H and He, slightly overabundant in CNO nuclei with respect to solar values, on top of an inert nickel substrate. The simulation assumed a plane-parallel geometry on a uniform grid, with a spatial resolution of only $\sim$6 cm. Comparison between 2D and 3D turbulent convection shows similar peak temperatures and Mach numbers, but different convective patterns, with evidence of the energy cascade into smaller scales that characterizes 3D convection. Further multidimensional studies of X-ray bursts under realistic conditions are really needed to shed light into the way ignition initiates and propagates, as well as in the way convection sets in and extends throughout the accreted envelope.

The relevant nuclear reaction path in XRBs has been extensively discussed in the literature (José et al. 2010; Iliadis 2007; Fisker et al. 2008): the most interesting nucleosynthesis is achieved for mixed H/He bursts, because of the complex nuclear reaction interplay (see details in Fisker et al. 2008; José et al. 2010). For illustrative purposes, we describe the main nuclear activity achieved for typical XRB conditions: a 1.4 $M_\odot$ neutron star, accreting solar-like material at a constant rate of 1.75×10^{-9} $M_\odot$ year^{-1}. In general, such bursts are initiated by H-burning, specifically the cold mode of the CNO cycle (mainly through ^{12}C(p,γ)^{13}N(β^+)^{13}C(p,γ)^{14}N). At moderate temperatures, the main nuclear flow proceeds close to the valley of stability. When T$\sim 2 \times 10^8$ K, the nuclear activity already reaches ^{40}Ca, with the most abundant species being H, ^{4}He, and ^{14,15}O. When T approaches $\sim 3 \times 10^8$ K, the 3α reaction dominates the nuclear flow, together with a combination of (p,γ) and (p,α) reactions, and some β^+ decays (mainly ^{32,33}Cl). At T$\sim 4 \times 10^8$ K, CNO-breakout ensues, initially led by ^{15}O(α,γ)^{19}Ne (see Fisker et al. (2006), for a study of the impact of the ^{15}O(α,γ) rate on the bursting behavior of an accreting neutron star), and followed by two consecutive proton-captures on ^{20}Na and ^{21}Mg, where the flow recedes due to the strong photodisintegration reactions on ^{22}Al. Following ^{21}Mg-decay, the flow shifts to ^{21}Na(p,γ)^{22}Mg, moving away from the valley of stability, towards the proton-drip line. As the rise of the temperature continues, and enough ^{14}O is build-up through the triple-α reaction, followed by ^{12}C(p,γ)^{13}N(p,γ)^{14}O, the alternative path through ^{14}O(α,p)^{17}F dominates the flow (Champagne and Wiescher 1992; Woosley et al. 2004), by-passing the ^{15}O(α,γ)^{19}Ne link to ^{21}Na through ^{17}F(p,γ)^{18}Ne(α,p)^{21}Na, with ^{18}Ne(α,p)^{21}Na representing the main path towards heavier species.

When T$\sim 1.5 \times 10^9$ K, the most abundant species in the envelope become ^{18}Ne, ^{21,22}Mg (from ^{18}Ne(α,p)^{21}Na(p,γ)^{22}Mg), ^{25}Si, ^{28}S-^{28}P, ^{33}Ar-^{33}Cl, and ^{37}K, the first isotope that achieves an abundance of 10% by mass. At this stage, the flow has reached ^{64}Ge. Shortly after, the envelope achieves peak temperature, $T_{peak} \sim 1.7 \times 10^9$ K. The most abundant isotope (except for H) is ^{54}Ni, and later, ^{64}Ge and ^{68}Se. During the subsequent decline, the nuclear flow is dominated by a cascade of β-decays. The final composition of the envelope, which is not ejected by the TNR, is essentially composed of elements with $A = 60$–70, mainly ^{64}Zn (originally as ^{64}Ge, and ^{64}Ga), and ^{68}Zn (^{68}Se), with traces of other species. Explosions in lower metallicity envelopes are characterized by an extension of the main nuclear path by the rp-process, much beyond ^{56}Ni, up to the SnSbTe region (Schatz et al. 2001) or beyond, according to a recent reanalysis of the role of photodisintegration reactions in this mass region (Elomaa et al. 2009).

Most of the reaction rates required for these extensive nucleosynthesis calculations rely on theoretical estimates from statistical models, and may be affected by significant uncertainties. Efforts to quantify the impact of such nuclear uncertainties on the overall abundance pattern accompanying XRBs have been undertaken by different groups (Iliadis et al. 1999; Thielemann et al. 2001; Amthor et al. 2006), revealing a complex interplay between the nuclear activity and the shape of the light curve (Hanawa et al. 1983; Woosley et al. 2004). The most extensive work to date (Parikh et al. 2008), has helped to identify the most influential nuclear processes: ^{65}As(p, γ)^{66}Se, ^{61}Ga(p, γ)^{62}Ge, ^{12}C(α, γ)^{16}O, ^{96}Ag(p, γ)^{97}Cd, and in a lesser extent, ^{30}S(α, p)^{33}Cl, ^{56}Ni(α, p)^{59}Cu, ^{59}Cu(p, γ)^{60}Zn, ^{86}Mo(p, γ)^{87}Tc, ^{92}Ru(p, γ)^{93}Rh, ^{102}In(p, γ)^{103}Sn, and ^{103}In(p, γ)^{104}Sn.

A major drawback in the modeling of X-ray bursts comes from the lack of observational nucleosynthetic constraints (beyond the obvious implications for the physics of the neutron star crusts, outlined at the beginning of this section). The potential impact of XRB nucleosynthesis on Galactic abundances is still a matter of debate: although ejection from a neutron star is unlikely because of its large gravitational potential, radiation-driven winds during photospheric radius expansion may lead to ejection of a tiny fraction of the envelope, containing nuclear processed material (Weinberg et al. 2006; MacAlpine et al. 2007). Indeed, although it has been claimed that XRBs may help to explain the Galactic abundances of the problematic light *p-nuclei* (Schatz et al. 1998), new calculations have ruled out this possibility (Bazin et al. 2008; José et al. 2010). Finally, it has been proposed that a way to overcome the lack of observational constraints may come from the identification of gravitationally redshifted atomic absorption lines, which could be identified through high-resolution X-ray spectra (Bildsten et al. 2003; Chang et al. 2005, 2006; Weinberg et al. 2006). Indeed, although specific features have been reported in the spectra of 28 XRBs detected from EXO 0748-676 during a 335 ks observation with XMM-Newton (Cottam et al. 2002), interpreted as gravitationally redshifted absorption lines of Fe XXVI (during the early phase of the bursts), Fe XXV, and perhaps O VIII (during the late stages), no evidence for such spectral features was found neither after a 200 ks observation of GS 1826-24, from which 16 XRBs were detected (Kong et al. 2007), nor after a 600 ks observation of the original source EXO 0748-676 (Cottam et al. 2008; Rauch et al. 2008).

5.4.4 Superbursts

Whereas regular, type I XRBs are characterized by common features in terms of duration, energetics, and recurrence times, a few extremely energetic events have recently been detected thanks to better performances in monitoring achieved with X-ray satellites (i.e., BeppoSAX, Chandra, or XMM-Newton). These rare and rather violent events are known as *superbursts* (see Kuulkers 2004; Cumming 2005; in't Zand 2017, for reviews). The first observation of a superburst was reported by Cornelisse et al. (2000) in the framework of a "common" type I bursting source (c.f., the BeppoSAX source 4U1735-44) (Fig. 5.9).

About 26 superbursts from 15 different bursting sources have been discovered, including GX 17+2 and 4U 1636-536, for which 4 superbursts have been identified (in't Zand 2017). Although the term *superburst* was first used by Wijnands (2001)

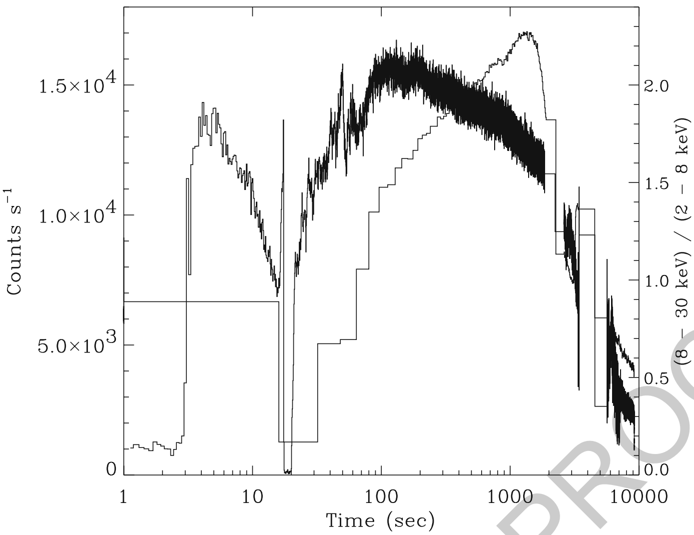

Fig. 5.9 Two superbursts observed with the RXTE satellite, in the (2–30) keV band. Figure from Strohmayer and Brown (2002)

to describe these very long X-ray bursts, historically the same name was applied to a relatively strong type I XRB reported from 4U 1728-34 by Basinska et al. (1984).

Superbursts represent some sort of extreme X-ray bursts: they have long durations, with a typical (exponential) decay time ranging from 1 to 3 h (including an extreme case, KS 1731-260, that lasted for more than 10 h; see Kuulkers et al. 2002), extremely energetic (about ∼1000 times more than a typical XRB, that is, $\sim 10^{42}$ erg), and with much longer recurrence periods (4.7 years for the system 4U 1636-53, for which two superbursts have been observed to date; see Wijnands 2001). Although superburst sources also exhibit regular type I XRBs, their occurrence is quenched for about a month after each superburst.

The duration and energetics of superbursts suggest that they result from thermonuclear flashes occurring in deeper fuel layers than those from typical X-ray bursts (at densities exceeding 10^9 g cm^{-3}; see Cumming and Bildsten (2001)), more likely, in the C-rich ashes resulting from type I X-ray bursts (first proposed by Woosley and Taam 1976; see also Brown and Bildsten 1998; Cumming and Bildsten 2001; Weinberg and Bildsten 2007; Keek et al. 2012).

Controversy remains over how much carbon is left after a type I burst: some studies (Schatz et al. 1999, 2001) have indeed shown than most of the C is burnt during the previous H/He burning episodes. However, other analyses (Cumming and Bildsten 2001) led to the conclusion that even small amounts of carbon are enough to power a superburst (especially in neutron star oceans enriched from the heavy ashes driven by the rp-process). Recent studies suggest that both stable and unstable burning of the accreted H/He mixture are required to power a superburst (in't Zand et al. 2003). Alternative models have also been proposed to account for the origin of such superbursts, including TNRs on strange quark matter stars (Page and Cumming 2005).

5.5 Observational Diagnostics of Binary-Systems

5.5.1 Gamma-Rays from Radioactivity

Novae and supernovae emit γ-rays because some of the nuclei they synthesize and eject into the interstellar medium are radioactive, either β^+-unstable (i.e., emitting a positron when decaying) or undergoing electron captures. Radioactive isotopes decay to excited states of their daughter nuclei, which de-excite to their ground states by emitting γ-ray photons with energies around one MeV, over a wide range of timescales. Table 5.1 shows the most relevant radioactive isotopes produced in novae and supernovae. Two additional isotopes, the β^+-unstable ^{13}N and ^{18}F (τ=862 s and 158 min, respectively), are also important in the case of novae. The emitted γ-rays can be potentially detected, either in individual objects or as diffuse emission from the cumulative γ-ray output of many objects in the galaxy, whenever the lifetime of a given isotope is longer than the average period between two successive events producing it (see Sect. 5.5.1.3). In addition, the positrons emitted when β^+-unstable nuclei decay annihilate with electrons and thus emit γ-rays, powering a 511 keV line plus a continuum below this energy.

The shape and intensity of the γ-ray output of novae and supernovae, as well as its temporal evolution, depend not only on the number of γ-ray photons produced, but also on how they propagate through the expanding envelope and ejecta. The first step to compute the spectrum is to generate γ-rays according to the decay schemes of the corresponding radioactive isotopes. The number of photons generated in a particular object depends on the isotopic abundances and decay rates of the relevant nuclei. In addition to these *direct* γ-ray photons, positrons emitted as a consequence of the radioactive decays of the β^+-unstable nuclei (see Table 5.1) should be traced. Once photons are generated, their trip across the expanding ejecta should be simulated by taking into account the various interaction processes affecting their propagation, i.e., Compton scattering, e^-–e^+ pair production, and photoelectric absorption.

The treatment of positron annihilation deserves particular attention. The role of magnetic fields is crucial, but it is not well known how to handle it. Thus, some drastic approximations are often made. When a positron is emitted, it can either escape without interacting with the expanding envelope or annihilate with an ambient electron. In nova envelopes, it is safe to assume that positrons thermalize before annihilating. This approximation is wrong in less than 1% of cases in an electronic plasma (Leising and Clayton 1987). In a neutral envelope, the excitation cross-section dominates any other interaction at energies above ~100 eV (Bussard et al. 1979), and thus positrons lose energy until they reach this value. In order to reproduce this braking effect, positrons should be propagated until they cross an equivalent column of $\sim 0.2\,\mathrm{g\,cm^{-2}}$, measured along a straight line (Chan and Lingenfelter 1993). This is the mean range expected for a 0.6 MeV positron slowing to energies ∼100 eV through elastic collisions with the surrounding medium, when the effect of magnetic fields on its propagation is neglected. Once thermalized, the positron covers a negligible distance and then annihilates.

For densities and temperatures typical of novae and SNIa envelopes, positrons form positronium (positron-electron system) in ∼90% of annihilations (Leising and Clayton 1987), while in the remaining 10% of cases they annihilate directly. Positronium is formed in the singlet state 25% of the time, leading to the emission of two 511 keV photons, and in the triplet state 75% of the time, leading to a three-photon annihilation continuum. The spectrum of photons produced from the triplet state was obtained by Ore and Powell (1949). Therefore, once a positron is produced, its trip should be followed until it escapes or covers the average energy-loss distance. In the latter case it produces positronium 90% of the time, resulting in triplet or singlet annihilations in a 3:1 ratio, while in 10% of the cases it annihilates directly. Monte Carlo codes, based for instance on the method described in Pozdnyakov et al. (1983) and Ambwani and Sutherland (1988), are well suited to compute the γ-ray output of novae and type Ia supernovae (Gómez-Gomar et al. 1998b,a).

5.5.1.1 Gamma-Ray Emission from Individual Classical Novae

The potential of novae as γ-ray emitters was first pointed out by Clayton and Hoyle (1974), who stated that observable γ-rays from novae would come from electron-positron annihilation, with positrons from ^{13}N, ^{14}O, ^{15}O and ^{22}Na decays, as well as a result of the decay of ^{14}O and ^{22}Na to excited states of ^{14}N and ^{22}Ne nuclei, which de-excite by emitting photons at 2.312 and 1.274 MeV respectively. Some years later, Clayton (1981) noticed that another γ-ray line could be expected from novae when ^{7}Be transforms (through an electron capture) to an excited state of ^{7}Li, which de-excites by emitting a photon of 478 keV. The original idea came from Audouze and Reeves (1982), and both works were inspired by the contemporaneous papers mentioning the possibility of ^{7}Li synthesis in novae (Arnould and Norgaard 1975; Starrfield et al. 1978b). In fact, ^{7}Li production in novae was, and continuous to be, a crucial topic (Hernanz et al. 1996), since Galactic ^{7}Li is not well accounted for by other sources, either stellar (AGB stars), interstellar (spallation reactions by cosmic rays) or cosmological (Big Bang). The main ideas presented in these pioneering studies have remained unchanged; but some aspects have changed in the last years, mainly related to new detailed nucleosynthesis studies of novae.

The γ-ray signatures of classical novae depend on their yields of radioactive nuclei (see the reviews Leising (1991, 1993), Hernanz (2002)). CO and ONe novae differ in their production of ^{7}Be, ^{22}Na and ^{26}Al, while they synthesize similar amounts of ^{13}N and ^{18}F. In both nova types, there should be line emission at 511 keV related to e^-–e^+ annihilation, and a continuum produced by Comptonized 511 keV emission and positronium decay.

The yields of radioactive nuclei adopted to compute the γ-ray spectra and light curves presented here are from José (unpublished) based on Iliadis et al. nuclear reaction rates; see Hernanz (2014). The main change with respect to previous models is that ^{18}F yields are lower, thus impacting the 511 keV line and the continuum below it, as seen when compared with γ-ray spectra and light curves from the first edition of this book (also published in Hernanz (2012)).

The temporal evolution of the whole γ-ray spectrum of four representative nova models is shown in Fig. 5.10. The most prominent features of the spectra are the annihilation line at 511 keV and the continuum at energies between 20–30 keV and 511 keV (in both nova types), the ^{7}Be line at 478 keV in CO novae, and the ^{22}Na line at 1275 keV in ONe novae. Therefore, the main difference between spectra of CO and ONe novae are the long-lived lines, which directly reflect the different chemical composition of the expanding envelope (^{7}Be-rich in CO novae and ^{22}Na-rich in ONe ones).

The early γ-ray emission, or *prompt* emission, of novae is related to the disintegration of the very short-lived radioisotopes ^{13}N and ^{18}F. The radiation is emitted as a line at 511 keV (direct annihilation of positrons and singlet state positronium), plus a continuum (Gómez-Gomar et al. 1998a; Hernanz et al. 2002). The continuum is related to both the triplet state positronium continuum and the Comptonization of the photons emitted in the line. There is a sharp cut-off

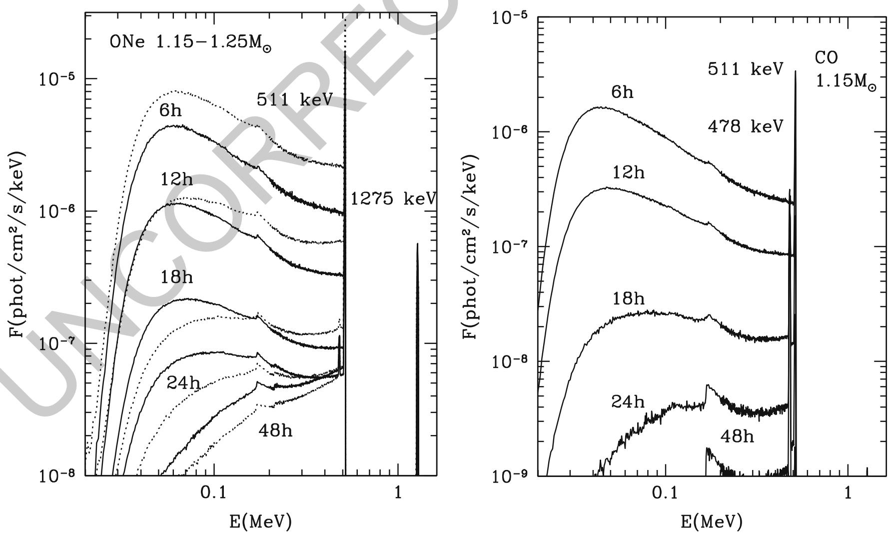

Fig. 5.10 Left: spectra of ONe novae of masses 1.15 (solid) and 1.25 $M_\odot$ (dotted) at different epochs after T_{max} (labels for dotted lines follow the same sequence as those for solid lines: from top to bottom 6, 12, 18, 14 and 48 h). Right: same for a CO nova of mass 1.15 $M_\odot$ (solid). Distance is 1 kpc

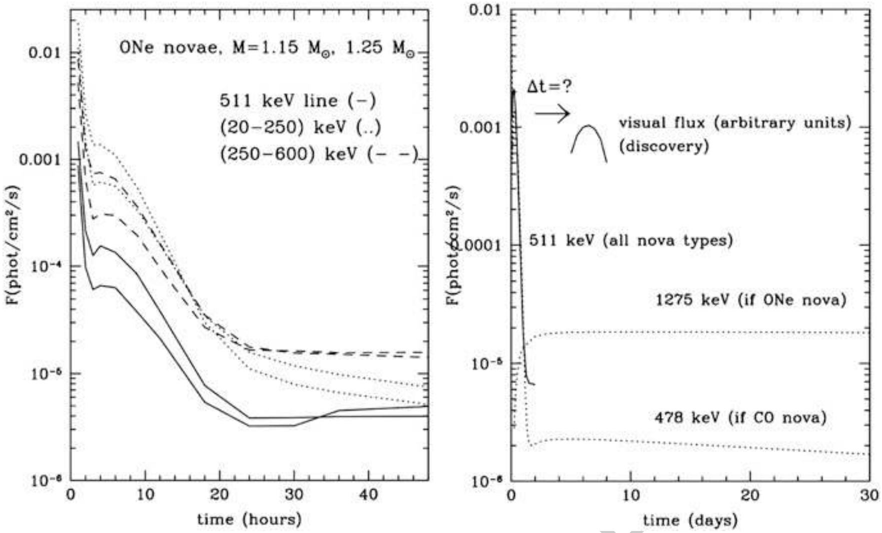

Fig. 5.11 Left: light curve of two continuum bands below 511 keV for ONe novae. The upper curves correspond to the larger mass, at early times; but at later epochs the most massive nova emits a slightly smaller flux, because of larger transparency. The light curve of the 511 keV line is also shown. Distance is 1 kpc. Right: nova γ-ray light curves, as compared with visual ones. The vertical scale for the visual light curve is arbitrary

at energies 20–30 keV (the exact value depending on the envelope composition) because of photoelectric absorption (see Fig. 5.10). The largest flux is emitted in the (20–250) keV range, since the continuum has its maximum at ~60 keV (ONe novae) and at ~45 keV (CO novae), followed by the flux in the (250–511) keV range (excluding the 511 keV line) and the flux in the 511 keV line (see Fig. 5.11). The two maxima in the light curves of the 511 keV line correspond to ^{13}N and ^{18}F decays, but the first maximum is difficult to resolve because its duration is extremely short; in addition, it is very model dependent: only ^{13}N in the outermost zones of the envelope could be seen in γ-rays because of limited transparency at very early epochs and, therefore, the intensity of the first maximum depends on the efficiency of convection. This first maximum thus provides important insight into the dynamics of the envelope after the peak temperature is attained at its base.

The annihilation emission is the most intense γ-ray feature expected from novae, but unfortunately it has a very short duration, because of the short lifetime of the main positron producers (^{13}N and ^{18}F). There are also positrons available from ^{22}Na decay in ONe novae, but these contribute much less (they are responsible for the *plateau* at a low level, between 10^{-6} and 10^{-5} phot cm^{-2} s^{-1}, for d=1 kpc; see Fig. 5.11). However, after roughly 1 week the envelope is so transparent that ^{22}Na positrons escape freely without annihilating. In summary, annihilation radiation lasts only ~1 day at a high level, and 1–2 weeks at a lower level *plateau* (the latter only in ONe novae). Another fact preventing easy detection is the early (before

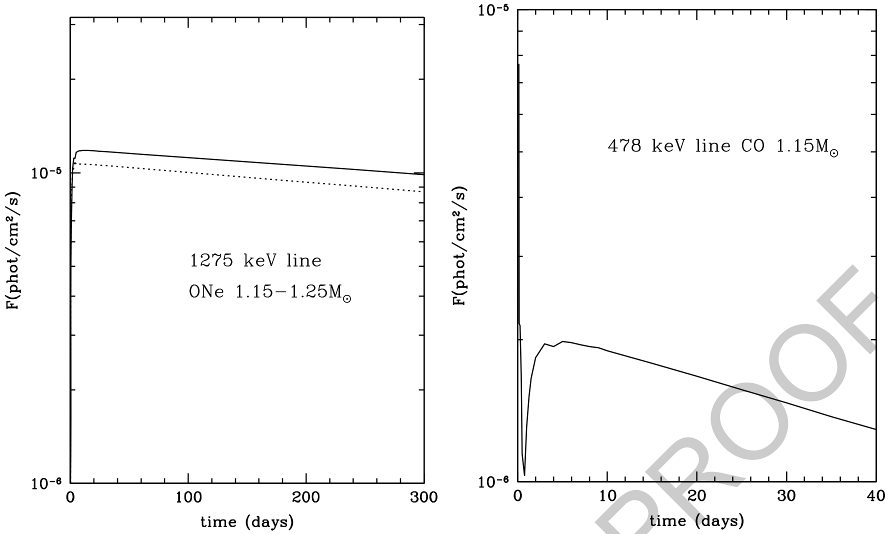

Fig. 5.12 Left: light curve of the 1275 keV line for two ONe nova models. Right: light curve of the 478 keV line for a CO nova model. Distance is 1 kpc

the nova is discovered optically) appearance of γ-rays from electron-positron annihilation (see Fig. 5.11).

The most distinctive feature in the γ-ray spectra of CO novae is line emission at 478 keV, related to de-excitation of the ^{7}Li which results from an electron capture on ^{7}Be. The light curves of the 478 keV line are shown in Fig. 5.12: the flux reaches its maximum at day 13 and 5 in the more and less opaque models, with total masses 0.8 and 1.15 $M_\odot$, respectively. The width of the line is 3 and 8 keV for the 0.8 and 1.15 $M_\odot$ CO novae, respectively. The maximum flux is around 10^{-6} phot cm^{-2} s^{-1}, for d=1 kpc.

The ^{22}Na line at 1275 keV appears only in ONe novae, because CO novae do not synthesize this isotope. The rising phase of the 1275 keV line light curves (see Fig. 5.12) lasts between 10 (1.25 $M_\odot$) and 20 days (1.15 $M_\odot$). Soon after the maximum, the line flux declines with the lifetime of ^{22}Na, 3.75 years. The line intensities directly reflect the amount of ^{22}Na ejected mass during this phase. The corresponding fluxes at maximum are typically around 10^{-5} phot cm^{-2} s^{-1}, at d=1 kpc, and the width of the line is around 20 keV, which poses severe problems for its detectability with instruments having high energy resolution, like SPI onboard INTEGRAL.

There have been many unsuccessful attempts to detect γ-rays from novae. The main efforts have focused on the 1275 keV line from ^{22}Na in individual objects, but searches of the cumulative emission have also been performed. The annihilation line has also been searched for whenever wide field of view instruments were available, scanning zones of the sky where novae had exploded.

The most recent observational search for the 1275 keV line from novae was performed with the COMPTEL instrument onboard the Compton Gamma-Ray Observatory (CGRO) (Iyudin et al. 1995). COMPTEL observed a number of recent novae during the period 1991–1993, five of which of the neon type (i.e. those expected to emit the 1275 keV line). None was detected. The average 2σ upper limit for any nova of the ONe type in the galactic disk was around 3×10^{-5} phot cm^{-2} s^{-1}, which translated into an upper limit of the ejected ^{22}Na mass around 3.7×10^{-8} M$_{\odot}$, for the adopted distances. This limit was constraining for models available at the time (Starrfield et al. 1992, 1993; Politano et al. 1995), but is not so for current models (José and Hernanz 1998). The main reason for the discrepancy between models of different groups (José and Hernanz (1998) versus Politano et al. (1995) and Starrfield et al. (1998)) is the following: old models were based on the explosion on ONeMg white dwarfs, with some mixing between the accreted H-rich matter and the underlying material, whereas recent models adopt ONe white dwarfs as underlying cores, because more recent evolutionary calculations of stellar evolution predict much lower magnesium abundances (Ritossa et al. 1996; Dominguez et al. 1993). The smaller initial content of neon and magnesium makes ^{22}Na synthesis much less favored. Different reaction networks also have an impact on the final yields obtained by different groups.

The first search for the 478 keV line from the galactic center and from some particular novae was performed with SMM/GRS (Harris et al. 1991), yielding upper limits around 10^{-3} phot cm^{-2} s^{-1}, corresponding to ^{7}Be ejected masses around 10^{-7} M$_{\odot}$. These fluxes and masses are well above the current theoretical predictions and thus do not constrain the models. More recent analyses of novae during the period 1995–1997, have been possible thanks to the Transient Gamma-Ray Spectrometer (TGRS) on board the Wind satellite. The flux limits from TGRS were a factor of 10 smaller than those from SMM observations, but the upper limits on ^{7}Be ejected masses did not improve by the same factor, mainly because novae observed with TGRS were at larger distances than those observed with SMM (Harris et al. 2001).

It is worth noticing that the detection of the 478 keV line from ^{7}Be in novae would provide unambiguously the amount of ^{7}Be, and thus of ^{7}Li, ejected by the corresponding nova, without the problems mentioned from UV-optical detections: these give relative amounts, e.g., with respect to Ca, and also depend on the delicate process of abundance determinations from equivalent widths of the different lines of ^{7}BeII.

As mentioned above, the emission resulting from e^{-}-e^{+} annihilation is the most intense γ-ray outcome of classical novae, but γ-rays are emitted well before the visual maximum of the nova, i.e. typically before the nova is discovered, and have a very short duration (see Fig. 5.11). Therefore, they can not be detected through observations pointing to a particular nova already discovered. Wide field of view instruments monitoring the sky in the appropriate energy range, like the Burst and Transient Source Experiment (BATSE) on board CGRO or TGRS on board Wind, are best suited for the search of the 511 keV line and the continuum below it.

TGRS was very convenient to search for the 511 keV line, because of its large field of view, and also because its germanium detectors had enough spectral resolution to separate the cosmic 511 keV line from the nova line, provided that the latter is a bit blueshifted (this happens only at the beginning of the emission phase, when material is not completely transparent yet) (Harris et al. 1999). TGRS's field of view contained five new novae during the period 1995–1997; upper limits were obtained by Harris et al. (1999), who deduced that their method was sensitive enough to detect novae occurring out to about 0.8 kpc, for any nova type (CO and ONe).

Another instrument that was well suited for the detection of the prompt γ-ray emission from novae was BATSE on board CGRO. Before the launch of CGRO in 1991, a prediction was made (Fishman et al. 1991) on the detectability of low-energy γ-rays from novae with the BATSE instrument, based on the models of γ-ray emission from Leising and Clayton (1987). BATSE had the advantage of continuously covering almost the whole sky, but on the other hand it was less sensitive and had poor energy resolution. More recently, a posteriori analyses of the background data at the explosion epoch of all classical novae discovered optically during the whole period of CGRO operation (1991–2000), searching for some signal, were performed (Hernanz et al. 2000). The 3-σ sensitivity using the 511 keV data only is similar to that with WIND/TGRS (Harris et al. 1999), but TGRS's sensitivity required a particular line blueshift, whereas BATSE is independent of it. The 3-σ sensitivity using the (250–511) keV data is a little more than a factor of 2 better than that from TGRS (Harris et al. 1999).

The 2002 launch of the ESA satellite International Gamma-Ray Laboratory, INTEGRAL, opened new perspectives for the detection of γ-rays from explosive events, with its two major instruments, the spectrometer SPI and the imager IBIS. SPI is made of 19 germanium detectors; its 3σ sensitivity at 1 MeV, for 10^6 s observation time and narrow lines, is around 2.4×10^{-5} phot cm^{-2} s^{-1}, with 2 keV energy resolution. However, this sensitivity degrades considerably for broad lines. Detection of γ-rays from novae with INTEGRAL is not too likely, because its detectability distance limits are small and, therefore, few novae are expected (Hernanz and José 2004). This is due to both the small fluxes expected and the reduced (with respect to pre-launch estimates) inflight measured sensitivities at the relevant energies. Very small distances are needed to obtain a secure detection: around 0.2 kpc for the 478 keV line from ^{7}Be and around 0.7 kpc for the 1275 keV line from ^{22}Na.

There is a new mission concept, named *e-ASTROGAM*, presented to ESA call M5, which if accepted would represent an important step forward for γ-ray astrophysics in the MeV and GeV range. Sensitivities better by factors of around 10 would be reached for the MeV lines, leading to detectability distances larger by factors of about 3, with respect to those with INTEGRAL/SPI. The mission proposal description, with a detailed insight into the instrumentation, can be found in De Angelis et al. (2017b) and Tatischeff et al. (2016), whereas a more detailed view of the science is reported on the Science White Book (De Angelis et al. 2017a)

5.5.1.2 Gamma-Ray Emission from Individual Type Ia Supernovae

In Type Ia supernova ejecta, the dominant radioactive chains are ^{56}Ni $\rightarrow^{56}$ Co $\rightarrow^{56}$ Fe and ^{57}Ni $\rightarrow^{57}$ Co $\rightarrow^{57}$ Fe (see Table 5.1). The amount of radioactive material, its distribution within the ejecta as well as the density, velocity and chemical composition profiles are different for each model described in Sect. 5.3 and these differences affect the total intensity and the evolution of the different lines, as well as the importance and extension of the continuum component of the spectrum (Burrows and The 1990; Kumagai and Nomoto 1997; Gómez-Gomar et al. 1998b).

In 1D geometry, the predicted γ-emission can be roughly described as follows: Twenty days after the explosion all models involving a prompt or a delayed detonation display strong lines because their high expansion rates induce a rapid decrease of the density, as shown in Fig. 5.13. Lines are particularly intense for those models containing ^{56}Ni and ^{56}Co in the outer layers (pure detonation and sub-Chandrasekhar models). The maximum intensity of these lines is model dependent since it is a function of the expansion rate and of the distribution of ^{56}Ni. Pure deflagration models only display a continuum since they efficiently Comptonize high energy γ-rays. The shape of the continuum at low energies is limited in all models by the competing photoelectric absorption, which imposes a cut-off below 40–100 keV. The energy of the cut-off is determined by the chemical composition of the external layers where most of the emergent continuum is formed at this epoch. Consequently, the continuum of those models containing low Z elements in the outer layers will extend to lower energies than that of those containing high Z elements. Therefore, it is possible to use these differences to discriminate among the different burning modes.

AQ5

Two months after the explosion, Fig. 5.13, the ^{56}Ni lines have disappeared and the emission is dominated by the ^{56}Co lines, which reach their maximum of intensity roughly 2 months after the explosion in all models except for the pure deflagration ones. At maximum, the intensity of the lines in pure detonations, delayed detonations and sub-Chandrasekhar models is determined by the total mass

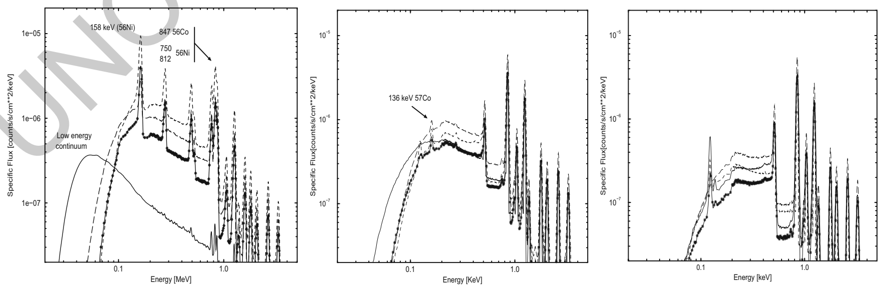

Fig. 5.13 Gamma-ray spectrum for four models of SNIa explosion at 5 Mpc 20, 60, and 120 days (from left to right) after the explosion. Pure deflagration model (solid line), delayed detonation model (long-dashed line), detonation model (dashed line) and sub-Chandrasekhar model (starred line) (Gómez-Gomar et al. 1998b)

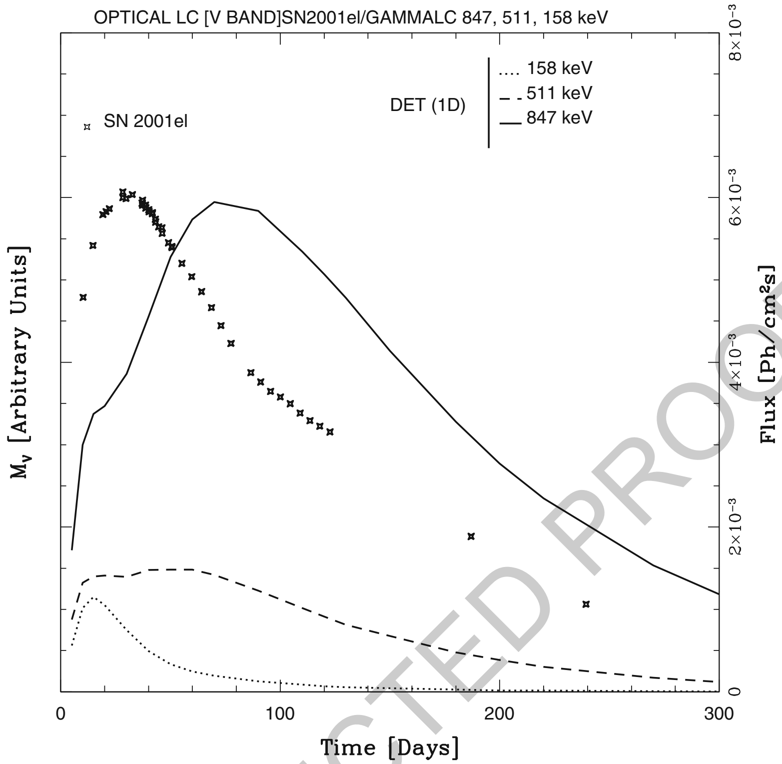

Fig. 5.14 Evolution of the different lines as a function of time for a typical delayed detonation model. The distance is assumed to be 1 Mpc. The optical light curve in the visual has also been included in order to provide a time reference. Courtesy of A. Hirschmann

of radioactive isotopes, while the differences caused by the expansion velocities are secondary. The 122 and 136 keV lines of ^{56}Co are already visible but faint.

Four months after the explosion, the ejecta are optically thin in all cases and the intensity of the lines is proportional to the parent isotopes (Fig. 5.13). The continuum is faint and dominated by the positronium annihilation component which shows a step below 170 keV, the energy of the backscattered 511 keV photons, plus a contribution of photons scattered once.

Figure 5.14 displays the temporal behavior of the ^{56}Ni and ^{56}Co lines. The 158 and 812 keV ^{56}Ni-lines peak very early, near the maximum of light and, because of absorption, they are much weaker than those of ^{56}Co Therefore, an early detection can provide information about the location of ^{56}Ni in the debris. The most prominent spectral feature is the 847 keV ^{56}Co line, which reaches maximum intensity roughly 2 months after the explosion in all models except for the pure deflagration case. Since the intensity of this line at maximum is essentially determined by the total mass of the radioactive isotopes it can be used to measure the total amount of ^{56}Ni synthesized during the explosion.

Figure 5.14 also displays the evolution of one of the most prominent lines, the 511 keV annihilation one. Positrons emitted during the decay of ^{56}Co thermalize because of ionization and excitation energy losses as well as other mechanisms, and eventually they annihilate either directly or through the formation of positronium. The degree of ionization and the structure of the magnetic field is crucial to determine the fraction of positrons that escape from SNIa. After 200 days almost all the high energy photons escape and the energy deposited by the annihilation of positrons is the only available source to power the light curve. Therefore, a careful determination of the 511 keV line is fundamental to understand the evolution of the supernova debris (Milne et al. 2001).

The decay chain ^{44}Ti$\rightarrow$^{44}Sc$\rightarrow$^{44}Ca ($\tau_{1/2} = 60.0$ years and $\tau_{1/2} = 3.97$ h, respectively) offers an additional opportunity to obtain information about the explosion although, as a consequence of the relatively long lifetime of ^{44}Ti, the observation has to be performed in young supernova remnants. This isotope is synthesized during the α-rich freeze out in a low density ambient, similar to those found in delayed detonation and sub-Chandrasekhar models.

The early X-ray emission in the 6–8 keV region can also provide an important diagnostic for discriminating between Chandrasekhar and sub-Chandrasekhar models. The γ-rays produced by disintegration of ^{56}Ni and ^{56}Co, together with the thermalized photons with energies above $\sim$7 keV, induce strong emission of the K$_{\alpha}$-lines of Fe, Co and Ni. In the case of the Chandrasekhar models, ^{56}Ni is so deeply placed that these photons are absorbed before escaping while in the sub-Chandrasekhar models they are produced in the outermost layers from where they freely escape producing a distinctive feature in the spectra. The total expected flux in the 5–10 keV band at 15 Mpc is $\sim 2 \times 10^{-7}$ photons/s/cm^2, which means that it could be detected from a reasonably close supernova (Pinto et al. 2001). Another feature that could also be used to distinguish among these two families of models is the 14.4 keV emission of ^{57}Co, which is only expected in sub-Chandrasekhar models.

XMM and Chandra allow high spectroscopic and angular resolution studies of some galactic remnants of SNIa. In particular, for the X-rays from the Tycho supernova remnant the best fit is obtained with a one dimensional delayed detonation characterized by a quite high density transition placed in the range $(2.2 - 2.5) \times 10^7$ g/cm^3 (Badenes et al. 2006), while in the case of G337.2-07 the best fit is obtained for a pulsational delayed detonation with a density transition at 7.7×10^6 g/cm^3 (Rakowski et al. 2006). In both cases, the X-ray spectrum strongly suggests a high degree of chemical stratification, a property that is lacking in most current three-dimensional models of SNIa.

Interestingly enough, DDT models also provide the best fit to the X-ray spectra of 22 clusters of galaxies (de Plaa et al. 2007) and is the only model able to match the observed Ar/Ca and the Ca/Fe ratios. It is important to remember that the chemical composition of the intracluster medium is representative of the average supernova yields, since it is the result of the contributions from many supernovae during the clusters life time.

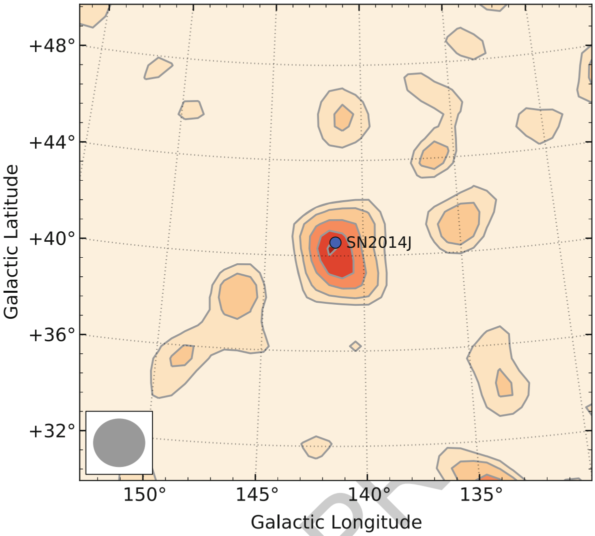

Fig. 5.15 Gamma-ray signature of SN 2014J in the SPI data during the period 16–35 days after the explosion. The excess in the supernova position is 5σ (Isern et al. 2016)

SN2014J was discovered by Fossey et al. (2014) on January 21st 2014 in M82 (d $= 3.5 \pm 0.3$ Mpc). The moment of the explosion was estimated to be on January 14.72 UT 2014 or JD 2456672.22 (Zheng et al. 2014) and was observed three times by the *INTEGRAL* instruments SPI and IBIS/ISGRI. During the first observation run, 16.5–35.2 days after the explosion, *INTEGRAL* obtained a robust detection of the gamma emission near the maximum of light, as illustrated in Fig. 5.15 (Churazov et al. 2014; Diehl et al. 2014; Churazov et al. 2015; Isern et al. 2016). Effectively, the analysis of the data obtained by INTEGRAL during this epoch, in the position of the supernova, revealed the existence of emission excesses with a significance of $\sim 5\,\sigma$ in the energy bands 70–190 (SPI and IBIS) and 650–1380 keV (SPI) that were not present during the observations performed before the explosion. The excess found a low energies is associated to the ^{56}Ni 158 keV gamma ray line and has completely unexpected properties. Diehl et al. (2014) found that the 158 keV ^{56}Ni line was very near to the laboratory value, the Doppler shift was below 2100 km s^{-1} and the broadening modest, less than 6000 km s^{-1}, suggesting the existence of a disk or ring containing ^{56}Ni placed almost perpendicularly to the line of sight. A behavior consistent with these values was also found in the 812 keV line. On the contrary, Isern et al. (2016) found a broad and redshifted feature associated to this emission excess. When the temporal evolution of the spectrum was taken into account and the secondary photons were removed, a line of intensity $(1.59 \pm 0.57) \times 10^{-4}$ photons cm^{-2} s^{-1} centered at 154 ± 0.64 keV and a width of 3.7 ± 1.5 keV appeared. This line almost disappeared during the period 22.6–28.2 days after the explosion and reappeared in the period 28.6–35.2 after the explosion, although at this epoch is too weak to obtain any conclusion. Interestingly enough, the IBIS/ISGRI displayed a similar behavior in the energy band 67.5–189 keV, during the same time intervals, but with a better signal to noise ratio. This behavior suggested a blobby ring receding from the observer.

The observations during the late period, 50–162 days after the explosion allowed the detection of the ^{56}Co 847 an1238 keV lines at 4.7 σ and 4.3 σ of confidence level, thus confirming the hypothesis that the light curves of SNIa are powered by the ^{56}Ni decay chain. The spectra and the light curve obtained in this way, were broadly consistent with the standard spherical deflagration or delayed detonation models near the Chandrasekhar's mass (Churazov et al. 2014, 2015). The mass of ^{56}Ni obtained from the intensity of this line is completely consistent with the value obtained from the Arnett's rule.

5.5.1.3 Contribution of Classical Novae to Diffuse Radioactivities

Some radioactive nuclei have lifetimes larger than the typical time elapsed between successive novae or type Ia supernova explosions in the Galaxy. For such cases, diffuse emission resulting from the cumulative effect of several sources is expected. This kind of emission should trace the galactic distribution of the corresponding sources of the given isotope. If detected, it would give a valuable information, not available from observations at other wavelengths because of interstellar extinction. The Galactic nova spatial distribution and the nova rate are in fact poorly known, since their determination relies on observations of novae in other galaxies or on extrapolations of observations in our Galaxy, taking into account the distribution of extinction related to interstellar dust (Della Valle and Livio 1994; Shafter 1997, 2002). ^{22}Na and ^{26}Al from novae are potential contributors to diffuse emission at 1275 and 1809 keV, respectively. For ^{22}Na, there is the advantage that only novae are expected to contribute to its galactic content, whereas for ^{26}Al massive stars and AGBs also clearly contribute. Therefore, the galactic 1275 keV emission from ^{22}Na, should trace directly the spatial nova distribution; but unfortunately, as analyzed below, the predicted emission is too low for the performances of the current instruments. Concerning ^{26}Al, since its emission has been detected in the Galaxy, an estimate of the nova contribution to the global line flux is needed (Diehl et al. 1995; Prantzos and Diehl 1996).

The global flux at 1275 keV depends on the amount of ^{22}Na ejected per nova explosion and on the distribution and rate of ONe novae in the Galaxy (since only ONe produce ^{22}Na). A detailed study of the diffuse galactic 1275 keV line emission from novae showed that contributions from a few young and close novae dominate, yielding a very irregular distribution versus galactic longitude (Higdon and Fowler 1987). A comparison with the upper limits from HEAO 3 observations (Mahoney et al. 1982) gave 5.6×10^{-7} $M_{\odot}$ as upper limit to the mean ^{22}Na yield per nova, for a disk nova population. It was clear from this work that the results were subject to many uncertainties, such as their galactic distribution, the bulge/disk ratio, their global rate and the fraction of ONe versus CO novae. A recent analysis of the cumulative emission at 1275 keV from novae shows that the ejected ^{22}Na masses needed for a detection of this emission with the SPI spectrometer, onboard the

INTEGRAL satellite, are far above what current theoretical models predict ($\sim 10^{-7}$ versus a few $10^{-9}\,M_\odot$) (Jean et al. 2000).

The production of ^{26}Al by classical novae occurs again mainly in ONe novae, with low mass white dwarfs more prolific producers of ^{26}Al than massive ones. A crude estimate of the global contribution of novae to the ^{26}Al content in the Galaxy can be made, assuming that all novae contribute with the same amount of ^{26}Al, $M_{ejec}(^{26}Al)$, and that ^{26}Al is active during a time equal to its lifetime τ. Then the Galactic mass of ^{26}Al coming from novae would be (Weiss and Truran 1990; José et al. 1997)

$$M(^{26}Al)(M_\odot) = M_{ejec}(^{26}Al)\,\tau\,R_{nova}\,f_{ONe} = 0.12\frac{M_{ejec}}{10^{-8}\,M_\odot}\,\frac{R_{nova}}{35\ \mathrm{year}^{-1}}\,\frac{f_{ONe}}{0.33} \tag{5.25}$$

where R_{nova} is the total galactic nova rate and f_{ONe} is the fraction of ONe novae. Adopting typical ^{26}Al ejected masses (i.e., $2 \times 10^{-8}\,M_\odot$), the contribution of novae to galactic ^{26}Al would be $\sim 0.2\,M_\odot$, more than a factor of 10 below the observed mass, in agreement with the current idea (deduced from the observed 1.809 MeV line sky map) that galactic ^{26}Al comes mainly from massive stars (Knödlseder 1999) A complete analysis of the global contribution of novae to the ^{26}Al in the Galaxy was carried out by Kolb and Politano (1997), applying galactic nova population models, adopting the ^{26}Al yields from Politano et al. (1995) and taking very large ejected masses (larger than those from typical hydrodynamic models). The authors concluded that the nova contribution could range between 0.15 and $3\,M_\odot$, but this number largely depended on the unknown degree of mixing in novae, which largely influences their ^{26}Al yield, in addition to other parameters of the population synthesis code, like for instance the mass ratio (primary versus secondary star masses) distribution in zero-age main sequence binaries.

5.5.2 *Dust from Novae and Thermonuclear Supernovae*

Astrophysics has basically relied on electromagnetic radiation (collected by ground-based telescopes as well as by space-borne observatories) as the basic tool to determine stellar properties. But since the mid-80s, new methods that rely on matter rather than on radiation, have become available as well.

5.5.2.1 Stardust Mineralogy

Back in 1973, A.G.W. Cameron speculated in a seminal paper (Cameron 1973) that primitive carbonaceous chondrites may host *presolar grains*, tiny spherules of *stardust* condensed in the outflows of stars in advanced stages or in the ejecta of stellar explosions, containing a record of the nuclear history of their stellar parent bodies. Indeed, presolar grains have been isolated from meteorites, suggesting that the chemical processes that affected some meteoritic bodies were apparently mild and non-destructive to the grains.

The stellar paternity of these grains can be assessed by their anomalous isotopic composition, significantly different from that of the Solar System, and attributed to a suite of nucleosynthetic processes that took place in their parent stellar sources. In turn, the discovery of isotopically anomalous grains embedded in meteorites provided evidence of the chemical heterogeneity of the solar nebula (Cameron 1962). Moreover, although grains are difficult to date because of their low content in radioactive species, their large isotopic anomalies, including $^{14}N/^{15}N$, $^{12}C/^{13}C$, or silicon ratios far beyond the values reported from any other Solar System sample, suggest an ancient origin, with an age older than the Solar System itself (thus the label *presolar*).

Diamonds were the first presolar grains isolated from meteorites (Lewis et al. 1987). This was followed by the isolation of SiC grains (Bernatowicz et al. 1987; Tang and Anders 1988), and graphite (Amari et al. 1990). These three carbonaceous phases were identified because of their isotopically anomalous noble gas (Xe, Ne) components. So far, silicon carbide (SiC), graphite (C), diamond (C), silicon nitride (Si_3N_4), silicates (Messenger et al. 2003; Nguyen and Zinner 2004; Mostefaoui and Hoppe 2004), and oxides, such as corundum (Al_2O_3), or spinel ($MgAl_2O_4$), have been identified as presolar grains. In fact, all SiC grains extracted from meteorites are of presolar origin; approximately half of the graphite grains are presolar; only ∼2% of the spinel grains, and scarcely 0.001–0.02% of the silicates, are presolar.

Those grains, identified and extracted from meteorites, are systematically analyzed in the laboratory with ever improving precision. Such laboratory analyses revealed a variety of isotopic signatures that point towards several stellar progenitors, such as asymptotic giant branch stars and supernovae (see Clayton and Nittler 2004; Lodders 2005; Meyer and Zinner 2006, for recent reviews) (Table 5.2).

Several meteoritic bodies have been used to study presolar grains, basically very primitive, mildly metamorphosed, carbonaceous chondrites, such as Murchison, or Allende. Indeed, the anomalous size of Murchison's grains (Lodders 2005; Zinner 2005), much larger than those isolated from other meteorites (for reasons not yet understood), as well as the large number of samples available, made Murchison one of the favorite targets for studies of presolar grains.

5.5.2.2 Silicon Carbide Grains

SiC grains have been most extensively studied. They are often classified into different populations (presumably reflecting different stellar birthplaces) on the basis of their C, N, and Si isotopic ratios (Hoppe and Ott 1997).

It is widely accepted that about ∼93% of all SiC grains, the so-called *mainstream population*, are formed in the winds accompanying solar-metallicity AGB stars (Gallino et al. 1993; Lugaro et al. 2003; Ott and Begemann 1990). About ∼1%

Table 5.2 Inventory of known presolar grain types (adapted from Zinner 2005; Lodders 2005)

Grain type	Characteristic size	Potential stellar sources[a]	Discovery papers
Nanodiamond	2 nm	AGB SN	Lewis et al. (1987)
SiC	0.1–20 µm	AGB, SN, J-stars, CN	Bernatowicz et al. (1987), Tang and Anders (1988)
Graphite	1–20 µm	SN, AGB, CN	Amari et al. (1990)
Corundum	0.2–3 µm	RGB, AGB, SN	Hutcheon et al. (1994), Nittler et al. (1994)
Spinel	0.2–3 µm	RGB, AGB, SN	Nittler et al. (1997), Choi et al. (1998)
Hibonite	0.2–3 µm	RGB, AGB, SN	Choi et al. (1999)
Si_3N_4	0.3–1 µm	AGB, SN	Nittler et al. (1995)
Silicates (olivine, pyroxene)	0.1–0.3 µm	RGB, AGB, SN	Messenger et al. (2003), Nguyen and Zinner (2004)

[a]Acronyms: *AGB* Asymptotic Giant Branch Stars, *SN* Supernovae, *CN* Classical Novae, *RGB* Red Giant Branch Stars

correspond to *X grains*, which are characterized by moderate excesses of ^{12}C and ^{15}N, large ^{26}Al/^{27}Al ratios, and excesses of ^{28}Si, features pointing towards a supernova origin (Amari et al. 1992; Hoppe et al. 2000; see also Sect. 5.3.3). In addition, a variety of carbon-rich J-type stars are expected to account for ∼4–5% of the overall SiC grains, the so-called *A* and *B grains* (with born-again AGB stars, such as the Sakurai's object V4334 Sgr, or other C-rich stellar types, like R- or CH-stars, not being totally excluded; see Amari et al. (2001c)). Other populations include *Y* (∼1%) and *Z grains* (∼1%), whose origin is probably linked to low-metallicity AGB stars (Amari et al. 2001b; Hoppe et al. 1997). A rare variety of SiC grains (<1%), together with a couple of graphite grains, that exhibit a suite of isotopic signatures characteristic of classical nova outbursts, have been reported in recent years (Amari et al. 2001a; Amari 2002) (Fig. 5.16).

5.5.2.3 Supernova Grains

SiC grains of type X, low-density graphites, and the very rare silicon nitrates are believed to originate in ejecta accompanying supernovae. Many of the isotopic signatures of these grains (namely, moderate excesses of ^{12}C, and ^{15}N, large ^{26}Al/^{27}Al ratios, and excesses of ^{28}Si) are qualitatively consistent with supernova models, although some of these features can also be produced by other stellar sources. Both thermonuclear and core-collapse supernovae have been proposed as potential sources for these grains, although type II supernova models seem to be favored (Nittler and Ciesla 2016). A clear fingerprint of their supernova origin is the excess of ^{44}Ca (attributed to in situ decay of ^{44}Ti), present in ∼10–20% of the X grains (Amari et al. 1992), unaccompanied by anomalies in other stable calcium

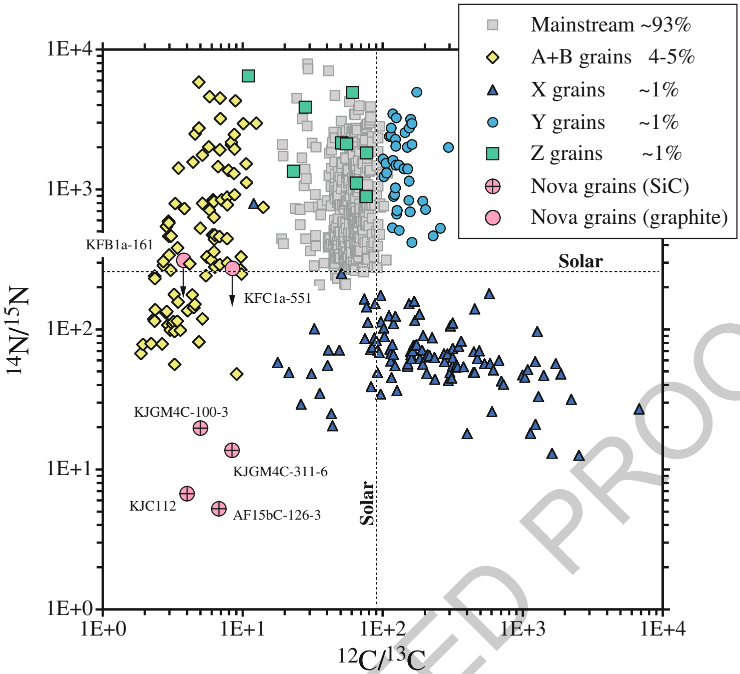

Fig. 5.16 Carbon and nitrogen isotopic ratios for the different SiC grain populations. Error bars are smaller than the symbols

isotopes. Other isotopic signatures that suggest a supernova origin include long-decayed species, such as ^{32}Si, ^{26}Al, ^{41}K, and ^{49}V (Nittler and Ciesla 2016).

A major problem to quantitatively match the grain data with supernova models (type II, in particular) is the need for selective mixing between different stellar layers (Lodders 2005; Zinner 2005), at a much larger scale than that suggested by observations and/or simulations. Efforts to quantitatively match grain data by means of supernova models have revealed a number of discrepancies. For instance, supernova SiC grains are systematically ^{15}N rich and ^{54}Fe poor with respect to model predictions. Recent simulations suggest that many isotopic features of supernova SiC and graphite grains can be reproduced by H-ingestion in the He-rich shells, that is, by the presence of residual H during explosive He-burning in supernova models (Pignatari et al. 2013; Liu et al. 2016, 2017, 2018). An alternative to selective mixing suggests the formation of supernova SiC and graphite grains in the O-rich layers of a massive star during a type II supernova explosion, where radiation may play a key role in dissociating the very stable CO molecules, hence freeing C atoms (Clayton et al. 1999, 2001; Clayton 2013). However, some isotopic features predicted in such models disagree with current presolar grain data (Nittler and Ciesla 2016). The supernova paternity of some presolar grains can also be settled by microstructural and mineralogical studies. In particular, supernova SiC and Si_3N_4 grains frequently appear as aggregates of small crystals while AGB SiC grains are typically single crystals. On the other hand, supernova graphites often present TiC subgrains that exhibit evidence of past ion irradiation (see details in Nittler and Ciesla (2016)).

A major, unsolved question is which fraction of the dust synthesized during core-collapse supernovae survives the passage of reverse shocks before being injected into the interstellar medium. Such issue will help to shed light into the specific contribution of supernovae to the dust we observe in the Universe.

5.5.2.4 Nova Grains

Infrared and ultraviolet observations have revealed dust forming episodes in the shells ejected during classical nova outbursts (Gehrz et al. 1998; Gehrz 2002). Their relatively high frequency (about ∼30–35 nova explosions per year, just in our Galaxy (Shafter 2002)), has raised the issue of the potential contribution of novae to the different grain populations.

Since the pioneering studies of dust formation in novae by D.D. Clayton and F. Hoyle (Clayton and Hoyle 1976) (a concept already suggested by A.G.W. Cameron in 1973), all efforts devoted to the identification of potential nova grains relied mainly on the search for low ^{20}Ne/^{22}Ne ratios (since noble gases, such as Ne, do not condense into grains, ^{22}Ne is frequently attributed to in situ ^{22}Na decay, a clear imprint of a classical nova explosion). Indeed, Clayton and Hoyle pointed out several isotopic signatures (large overproduction of ^{13,14}C, ^{18}O, ^{22}Na, ^{26}Al or ^{30}Si), that may help in the identification of such nova candidate grains. Forty years later, most of these signatures still hold, in view of our current understanding of nova explosions (see Jose 2016; Starrfield et al. 2016, for recent reviews), except ^{14}C, bypassed by the main nuclear path in novae, and ^{18}O, slightly overproduced by novae although grains nucleated in this environment are expected to be much more anomalous in ^{17}O (Kovetz and Prialnik 1997; José and Hernanz 1998; Starrfield et al. 1998, 2009) (Fig. 5.17).

A major step forward in the discovery of presolar nova candidate grains was achieved by Amari et al. (2001a), Amari (2002), who reported on several SiC and graphite grains, isolated from the Murchison and Acfer 094 meteorites, with an abundance pattern qualitatively similar to nova model predictions: low ^{12}C/^{13}C and ^{14}N/^{15}N ratios, high ^{30}Si/^{28}Si, and close-to-solar ^{29}Si/^{28}Si; and high ^{26}Al/^{27}Al and ^{22}Ne/^{20}Ne ratios for some of the grains (José et al. 2004). But in order to quantitatively match the grain data, one had to assume a mixing process between material newly synthesized in the nova outburst and more than ten times as much unprocessed, isotopically close-to-solar, material before grain formation.

Concerns about the likely nova paternity of these grains have been raised (Nittler and Hoppe 2005), after three additional micron-sized SiC grains were also isolated from the Murchison meteorite with similar trends (in particular, low ^{12}C/^{13}C and ^{14}N/^{15}N ratios), but with additional imprints (mainly non-solar Ti features), from which a supernova origin cannot be excluded. It is not clear, however, whether

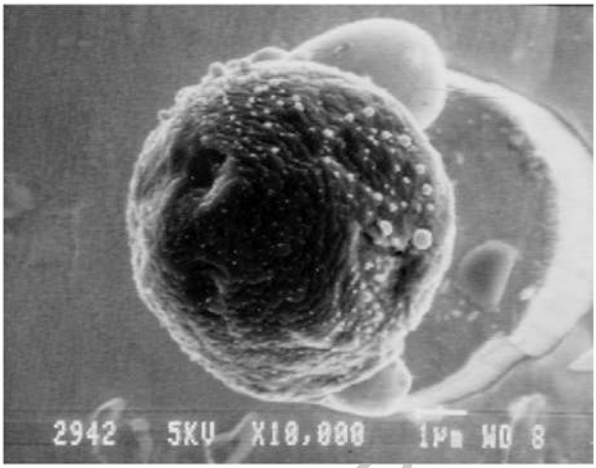

Fig. 5.17 The nova candidate graphite grain KFC1a-511 after Secondary Ion Mass Spectrometry (SIMS). Image courtesy of S. Amari

both samples (hereafter, A01 and NH05, respectively) correspond to the same progenitor. After all, their isotopic signatures are not identical: for instance, grains from the NH05 sample have much larger ^{26}Al/^{27}Al ratios and are more heavily depleted in ^{29}Si than grains from the A01 sample. Furthermore, grain M11-334-2 (NH05 sample) is deficient in ^{30}Si with respect to solar (whereas ^{30}Si excesses, characteristic of the A01 sample, are expected in the ejecta from ONe novae). Moreover, it must be stressed that the presence of anomalous Ti does not necessarily rule out a possible nova paternity (with the exception of ^{44}Ti, attributed to in situ decay of ^{44}Ca, an isotope clearly linked to a supernova explosion): titanium is, indeed, very close to the nucleosynthetic endpoint for novae (calcium), and hence, it could easily be reached by a slightly more violent outburst. This could be driven by explosions in cooler white dwarfs, or following lower mass-accretion rate episodes (José and Hernanz 2007a; Glasner and Truran 2009). Furthermore, explosions in metal-deficient envelopes, such as those expected for primordial nova systems, could have a similar effect (José et al. 2007; José and Hernanz 2007b).

Other nova candidate grains have been proposed in the last decades: for instance, the SiC grain 240-1 (Nittler et al. 2006), also isolated from Murchison, exhibits both ^{12}C/^{13}C and ^{14}N/^{15}N ratios lower than for any other presolar grain reported so far. These isotopic features are consistent with pure nova ejecta from a white dwarf with a mass ranging between 1.0 and 1.2 $M_\odot$. However, the ^{29}Si excesses measured in this grain do not match the usual predictions from nova models (which usually reflect ^{29}Si deficits, with respect to solar). A putative nova origin has also been attributed to the oxide grain T54 (Nittler 1997), with ^{16}O/^{17}O $\sim$ 71 and ^{16}O/^{18}O $\sim$ 2000, likely condensed in the shells ejected from a nova outburst on a 0.8 $M_\odot$ CO white dwarf. Unfortunately, no additional isotopic determinations were carried out on this grain. The inventory of nova candidate grains includes as well other oxide grains (two alumina and two spinel; Gyngard et al. 2011). Again, mixing between the nova ejecta and material of solar composition was required to match the composition of those grains. Finally, the presolar graphite grain LAP-149, isolated from the primitive meteorite LaPaz Icefield 031117, has also been suggested as a potential nova grain, as it exhibits one of the lowest $^{12}C/^{13}C$ ratios observed among presolar grains. Being extremely ^{13}C-rich and ^{15}N-poor, its origin suggests condensation in the ejecta of a low-mass CO nova (Haenecour et al. 2016).

The main difficulty faced in the unambiguous identification of presolar nova grains is the need for a simultaneous match of multiple isotopic ratios. Furthermore, the requirement of dilution of nova material with large amounts of unprocessed, isotopically close-to-solar material before grain formation, is considered another drawback for a proper identification of nova candidate grains. A very recent effort in this regard (Iliadis et al. 2018), based on a Monte Carlo technique, that involves the random sampling over the most important nova model parameters, has led to the identification of 18 presolar grains with measured isotopic signatures consistent with a CO nova origin, without assuming any dilution of the ejecta. Among these, the grains G270-2, M11-334-2, G278, M11-347-4, M11-151-4, and Ag2-6 have the highest plausibility of a (CO) nova paternity.

Future nova candidate grains will reveal more clues on the mechanisms powering nova explosions. To achieve this, cosmochemists will have to rely on a much wider range of isotopic determinations for proper identification of the stellar source (to disentangle, for instance, which grains are formed in supernova blasts and which in nova explosions). Novae hosting very massive white dwarfs (around 1.35 $M_\odot$) likely imprint additional signatures in the grains condensing in their ejecta (in particular, a suite of sulfur anomalies as well as severe ^{31}P overproduction). New techniques for laboratory analysis need to be developed to unambiguously identify such signatures, avoiding potential contamination of the samples by sulfuric acid, one of the standard methods used during the separation process.

5.6 Accretion in Binaries: Special Cases

It was seen in the case of the merging of two white dwarfs that if the total mass was larger than the Chandrasekhar mass, the final outcome could either be a SNIa or a collapse to a neutron star. However in the large majority of cases, the total mass is smaller than the critical value and the final result is a white dwarf "born again". The fraction of the secondary that is expelled is not yet known and, consequently, the influence of such systems on the chemical evolution of the Galaxy has not been yet elucidated. The total amount of freshly synthesized elements during the impact is small (Guerrero et al. 2004), except in the case of a secondary made of helium that shows an enhancement of Ca, Mg, Si, S and Fe, and confined to a corona around the primary.

In the collapse case, since the primary is rapidly rotating, as expected from the transfer of angular momentum from the disk to the star, a centrifugally supported disk made of heavily neutronized species, $Y_e \sim 0.1$, will form around the proto-neutron star. As a consequence of the neutrino irradiation, electron neutrino captures will increase the electron mole number to a value $Y_e \sim 0.5$ and α-particles will form inducing a wind that will blow away the disk. During this process it is expected that $\sim 10^{-2}\,\mathrm{M}_\odot$ of ^{56}Ni will be synthesized and that the event will look as a dim SNIa-like transient (Metzger et al. 2009).

Merging of close binaries as well as close encounters in densely populated stellar systems, like globular clusters or galactic nuclei, can also provide violent scenarios able to trigger a nucleosynthetic activity other than the conventional thermonuclear explosions described up to now. The center of the Milky Way, for instance, contains a massive black hole surrounded by a swarm of stars, many of them white dwarfs. Close encounters are very common and tidal torques can produce extreme deformations of the stars or even trigger an explosion.

The tidal interaction between a white dwarf and a black hole is characterized by three length scales (Carter and Luminet 1983; Rosswog et al. 2009b): (i) the stellar radius, $R_{\rm WD}$, (ii) the gravitational radius of the black hole $R_{rmg} = 2GM_{\rm BH}/c^2 \simeq 3 \times 10^{11} M_{\rm BH,6}$, where $M_{\rm BH,6}$ is the mass of the black hole in units of $10^6\,\mathrm{M}_\odot$, and (iii) the tidal radius, $R_\tau \simeq 1.2 \times 10^{11} M_{\rm BH,6}^{1/3}(R_{\rm WD}/10^9\ \mathrm{cm})(M_{\rm WD}/0.6\,\mathrm{M}_\odot)^{-1/3}$ cm, that is the distance from the black hole at which $M_{\rm BH}/R_\tau^3$ equals the mean density of the passing star.

The strength of the tidal encounter can be estimated from the dimensionless parameter $\beta = R_\tau/R_{\rm P}$, where $R_{\rm P}$ is the pericenter distance, assuming a parabolic orbit. When $\beta \geq 1$, the star is disrupted in a single flyby. The energy to tear apart the star (the binding energy of the star) is supplied by the orbital energy. In the case of white dwarfs, the ratio between the total disruption radius and the gravitational radius is

$$\beta_{\rm g} = \frac{R_\tau}{R_{\rm g}} \simeq 0.4 M_{\rm BH,6}^{-2/3}\left(\frac{R_{\rm WD}}{10^9\ \mathrm{cm}}\right)\left(\frac{M_{\rm WD}}{0.6\,\mathrm{M}_\odot}\right)^{-1/3} \qquad (5.26)$$

therefore, if the mass of the black hole is high enough, the tidal radius is inside the gravitational radius and the white dwarf is swallowed without being disrupted. This critical mass is

$$M_{\rm BH,lim} \simeq 2.5 \times 10^5 \left(\frac{R_{\rm WD}}{10^9\ \mathrm{cm}}\right)^{3/2}\left(\frac{M_{\rm WD}}{0.6\,\mathrm{M}_\odot}\right)^{-1/2} \qquad (5.27)$$

The dynamics of the encounter can be described as follows (Carter and Luminet 1983). When the star is far from the black hole, the tidal interaction is negligible and the white dwarf is in hydrostatic equilibrium. As soon as it enters the Roche lobe, tidal interaction quickly grows in strength. As a consequence, matter is compressed by the flattening of the star. When the white dwarf is flat enough, the internal energy becomes dominant and the star experiences a bounce that reduces the pressure and makes the tidal interaction dominant once more. Depending on the parameters of the encounter (M_{BH}, M_{WD}, β) and on the chemical composition of the white dwarf, a vigorous thermonuclear burning can occur during the compression phase that can even produce a substantial amount of iron peak elements (Rosswog et al.

2009b). Finally, when the star is far enough, self-gravitation recovers control and, depending on the balance between internal and gravitational energies, matter is partially swallowed by the black hole, partially ejected to the interstellar medium and partially remains bound. During the expansion phase the radioactive debris, the β-decay of ^{56}Ni, mainly, can emit light and produce some kind of peculiar, subluminous SNIa (Rosswog et al. 2009b).

The recent success of LIGO in detecting gravitational waves from the merging of two compact objects has triggered the interest on the neutron star -neutron star (NS+NS) and neutron star—black hole (NS+BH) merging. There are several reasons for such interest: the possibility to test the equation of state of nuclear matter, a site for the synthesis of r-elements, and electromagnetic events displaying a wide range of time scales and wavelengths (Fernández and Metzger 2016).

This electromagnetic counterpart can manifest itself as a beam of electromagnetic radiation, i.e. as a short Gamma Ray Burst (Narayan et al. 1992; Mochkovitch et al. 1993) and as a *kilonova* or *macronova*, i.e. a transient powered by the radioactive decay of the r-process elements produced in the expanding ejecta that can be detected at optical and infrared wavelengths (Metzger 2017). One of the main characteristics of these transients is an increase of their duration due to the presence of Lanthanid an Actynid isotopes ($A > 140$) that extraordinarily increase the opacity as compared with the usual case of iron peak elements. Since the opacity and the velocity of the ejecta control the diffusion time, magnitude, color and duration of the kilonova will depend on the composition, geometry and kinematics of the ejecta (Fernández and Metzger 2016). The first confirmed kilonova was associated to the gamma-ray burst GRB 130603B (Tanvir et al. 2013; Berger et al. 2013; Fan et al. 2013), and the first detection of the gravitational emission of a NS+NS merger was GW170817 (Abbott et al. 2017), which was associated to the short GRB 170817A and was observed at almost all wavelengths (Antonini and Perets 2012)

In principle there are two potential sources of debris: material expelled on dynamical time scales, with typical velocities of 0.1–0.3c and material coming from the remnant disk. The relative importance of both components depends on the parameters of the system (Fernández and Metzger 2016). In the case of a NS-BH mergers, the dynamical ejection is induced by the tidal forces and material is confined near the equatorial region while in the case of NS+NS, the ejection occurs in the contact interface and material is ejected over a wider solid angle. Part of this material is heated by a shock wave and irradiated with neutrinos. The chemical composition nicely fits the observed abundances of r-elements observed in the Solar System. Outflows from the remnant disk can be produced on longer time scales, depending on neutrino heating, state of the disk, presence of magnetic fields and so on. The velocity of this material is smaller, $\sim 0.05c$, than that of the dynamic component and less neutron rich as a consequence of a longer exposure to weak interaction.

References

Abbott BP, Abbott R, Abbott TD, Acernese F, Ackley K, Adams C, Adams T, Addesso P, Adhikari RX, Adya VB, et al (2017) GW170817: observation of gravitational waves from a binary neutron star inspiral. Phys Rev Lett 119(16):161101. https://doi.org/10.1103/PhysRevLett.119.161101, arXiv:1710.05832

Abdo AA, Ackermann M, Ajello M, Atwood WB, Baldini L, Ballet J, Barbiellini G, Bastieri D, Bechtol K, Bellazzini R, et al (2010) Gamma-ray emission concurrent with the nova in the symbiotic binary V407 Cygni. Science 329:817–821. https://doi.org/10.1126/science.1192537, arXiv:1008.3912

Ackermann M, Ajello M, Albert A, Baldini L, Ballet J, Barbiellini G, Bastieri D, Bellazzini R, Bissaldi E, Blandford RD, Bloom ED, Bottacini E, Brandt TJ, Bregeon J, Bruel P, Buehler R, Buson S, Caliandro GA, Cameron RA, Caragiulo M, Caraveo PA, Cavazzuti E, Charles E, Chekhtman A, Cheung CC, Chiang J, Chiaro G, Ciprini S, Claus R, Cohen-Tanugi J, Conrad J, Corbel S, D'Ammando F, de Angelis A, den Hartog PR, de Palma F, Dermer CD, Desiante R, Digel SW, Di Venere L, do Couto e Silva E, Donato D, Drell PS, Drlica-Wagner A, Favuzzi C, Ferrara EC, Focke WB, Franckowiak A, Fuhrmann L, Fukazawa Y, Fusco P, Gargano F, Gasparrini D, Germani S, Giglietto N, Giordano F, Giroletti M, Glanzman T, Godfrey G, Grenier IA, Grove JE, Guiriec S, Hadasch D, Harding AK, Hayashida M, Hays E, Hewitt JW, Hill AB, Hou X, Jean P, Jogler T, Jóhannesson G, Johnson AS, Johnson WN, Kerr M, Knödlseder J, Kuss M, Larsson S, Latronico L, Lemoine-Goumard M, Longo F, Loparco F, Lott B, Lovellette MN, Lubrano P, Manfreda A, Martin P, Massaro F, Mayer M, Mazziotta MN, McEnery JE, Michelson PF, Mitthumsiri W, Mizuno T, Monzani ME, Morselli A, Moskalenko IV, Murgia S, Nemmen R, Nuss E, Ohsugi T, Omodei N, Orienti M, Orlando E, Ormes JF, Paneque D, Panetta JH, Perkins JS, Pesce-Rollins M, Piron F, Pivato G, Porter TA, Rainò S, Rando R, Razzano M, Razzaque S, Reimer A, Reimer O, Reposeur T, Saz Parkinson PM, Schaal M, Schulz A, Sgrò C, Siskind EJ, Spandre G, Spinelli P, Stawarz Ł, Suson DJ, Takahashi H, Tanaka T, Thayer JG, Thayer JB, Thompson DJ, Tibaldo L, Tinivella M, Torres DF, Tosti G, Troja E, Uchiyama Y, Vianello G, Winer BL, Wolff MT, Wood DL, Wood KS, Wood M, Charbonnel S, Corbet RHD, De Gennaro Aquino I, Edlin JP, Mason E, Schwarz GJ, Shore SN, Starrfield S, Teyssier F, Fermi-LAT Collaboration (2014) Fermi establishes classical novae as a distinct class of gamma-ray sources. Science 345:554–558. https://doi.org/10.1126/science.1253947, arXiv:1408.0735

Alibés A, Labay J, Canal R (2002) Galactic cosmic rays from superbubbles and the abundances of lithium, beryllium, and boron. Astrophys J 571:326–333. https://doi.org/10.1086/339937, arXiv:astro-ph/0202097

Amari S (2002) Presolar grains from novae: their isotopic ratios and radioactivities. New Astron Rev 46:519–524. https://doi.org/10.1016/S1387-6473(02)00194-X

Amari S, Anders A, Virag A, Zinner E (1990) Interstellar graphite in meteorites. Nature 345:238–240. https://doi.org/10.1038/345238a0

Amari S, Hoppe P, Zinner E, Lewis RS (1992) Interstellar SiC with unusual isotopic compositions – grains from a supernova? Astrophys J 394:L43–L46. https://doi.org/10.1086/186468

Amari S, Gao X, Nittler LR, Zinner E, José J, Hernanz M, Lewis RS (2001a) Presolar grains from novae. Astrophys J 551:1065–1072. https://doi.org/10.1086/320235, arXiv:astro-ph/0012465

Amari S, Nittler LR, Zinner E, Gallino R, Lugaro M, Lewis RS (2001b) Presolar SIC grains of Type Y: origin from low-metallicity asymptotic giant branch stars. Astrophys J 546:248–266. https://doi.org/10.1086/318230

Amari S, Nittler LR, Zinner E, Lodders K, Lewis RS (2001c) Presolar SiC grains of Type A and B: their isotopic compositions and stellar origins. Astrophys J 559:463–483. https://doi.org/10.1086/322397

Ambwani K, Sutherland P (1988) Gamma-ray spectra and energy deposition for Type IA supernovae. Astrophys J 325:820–827. https://doi.org/10.1086/166052

Amthor MA, Galaviz D, Heger A, Sakharuk A, Schatz H, Smith K (2006) Sensitivity of Type I X-ray bursts to rp-process reaction rate. In: International symposium on nuclear astrophysics – nuclei in the cosmos

Antonini F, Perets HB (2012) Secular evolution of compact binaries near massive black holes: gravitational wave sources and other exotica. Astrophys J 757:27. https://doi.org/10.1088/0004-637X/757/1/27, arXiv:1203.2938

Arnett WD (1969) A possible model of supernovae: detonation of ^{12}C. Astrophys Space Sci 5:180–212. https://doi.org/10.1007/BF00650291

Arnett D (1996) Supernovae and nucleosynthesis: an investigation of the history of matter from the big bang to the present. Princeton University Press, Princeton

Arnould M, Norgaard H (1975) The explosive thermonuclear formation of 7Li and 11B. Astron Astrophys 42:55–70

Audouze J, Reeves H (1982) The origin of the light elements. In: Essays in Nuclear Astrophysics. Cambridge University Press, Cambridge, pp 355–375

Axelrod TS (1980) Late time optical spectra from the Ni-56 model for Type 1 supernovae. PhD thesis, California University, Santa Cruz

Ayasli S, Joss PC (1982) Thermonuclear processes on accreting neutron stars – a systematic study. Astrophys J 256:637–665. https://doi.org/10.1086/159940

Aznar-Siguán G, García-Berro E, Lorén-Aguilar P, José J, Isern J (2013) Detonations in white dwarf dynamical interactions. Mon Not R Astron Soc 434:2539–2555. https://doi.org/10.1093/mnras/stt1198, arXiv:1306.6559

Aznar-Siguán G, García-Berro E, Magnien M, Lorén-Aguilar P (2014) On the possible observational signatures of white dwarf dynamical interactions. Mon Not R Astron Soc 443:2372–2383. https://doi.org/10.1093/mnras/stu1309, arXiv:1407.0200

Aznar-Siguán G, García-Berro E, Lorén-Aguilar P, Soker N, Kashi A (2015) Smoothed particle hydrodynamics simulations of the core-degenerate scenario for Type Ia supernovae. Mon Not R Astron Soc 450:2948–2962. https://doi.org/10.1093/mnras/stv824, arXiv:1503.02444

Badenes C, Borkowski KJ, Hughes JP, Hwang U, Bravo E (2006) Constraints on the physics of Type Ia supernovae from the X-ray spectrum of the Tycho supernova remnant. Astrophys J 645:1373–1391. https://doi.org/10.1086/504399, arXiv:astro-ph/0511140

Balman S, Krautter J, Oegelman H (1998) The X-ray spectral evolution of classical Nova V1974 Cygni 1992: a reanalysis of the ROSAT data. Astrophys J 499:395–406

Barbon R, Ciatti F, Rosino L (1973) Light curves and characteristics of recent supernovae. Astron Astrophys 29:57–67

Basinska EM, Lewin WHG, Sztajno M, Cominsky LR, Marshall FJ (1984) X-ray observations of the burst source MXB 1728-34. Astrophys J 281:337–353. https://doi.org/10.1086/162103

Bazin D, Montes F, Becerril A, Lorusso G, Amthor A, Baumann T, Crawford H, Estrade A, Gade A, Ginter T, Guess CJ, Hausmann M, Hitt GW, Mantica P, Matos M, Meharchand R, Minamisono K, Perdikakis G, Pereira J, Pinter J, Portillo M, Schatz H, Smith K, Stoker J, Stolz A, Zegers RGT (2008) Production and β decay of rp-process nuclei Cd96, In98, and Sn100. Phys Rev Lett 101(25):252501/1–252501/4. https://doi.org/10.1103/PhysRevLett.101.252501, arXiv:0810.3597

Belian RD, Conner JP, Evans WD (1976) The discovery of X-ray bursts from a region in the constellation Norma. Astrophys J 206:L135–L138. https://doi.org/10.1086/182151

Benz W, Thielemann FK, Hills JG (1989) Three-dimensional hydrodynamical simulations of stellar collisions. II – White dwarfs. Astrophys J 342:986–998. https://doi.org/10.1086/167656

Benz W, Cameron AGW, Press WH, Bowers RL (1990) Dynamic mass exchange in doubly degenerate binaries. I – 0.9 and 1.2 solar mass stars. Astrophys J 348:647–667. https://doi.org/10.1086/168273

Berger E, Fong W, Chornock R (2013) An r-process Kilonova associated with the short-hard GRB 130603B. Astrophys J 774:L23. https://doi.org/10.1088/2041-8205/774/2/L23, arXiv:1306.3960

Bernatowicz T, Fraundorf G, Ming T, Anders E, Wopenka B, Zinner E, Fraundorf P (1987) Evidence for interstellar SiC in the Murray carbonaceous meteorite. Nature 330:728–730. https://doi.org/10.1038/330728a0

Bildsten L (1995) Propagation of nuclear burning fronts on accreting neutron stars: X-ray bursts and sub-hertz noise. Astrophys J 438:852–875. https://doi.org/10.1086/175128

Bildsten L (1998) Thermonuclear burning on rapidly accreting neutron stars. In: Buccheri R, van Paradijs J, Alpar A (eds) NATO ASIC Proc. 515: the many faces of neutron stars, p 419

Bildsten L, Chang P, Paerels F (2003) Atomic spectral features during thermonuclear flashes on neutron stars. Astrophys J 591:L29–L32. https://doi.org/10.1086/377066, arXiv:astro-ph/0303147

Bildsten L, Shen KJ, Weinberg NN, Nelemans G (2007) Faint thermonuclear supernovae from AM Canum Venaticorum binaries. Astrophys J 662:L95–L98. https://doi.org/10.1086/519489, arXiv:astro-ph/0703578

Blinnikov SI, Khokhlov AM (1986) Development of detonations in degenerate stars. Sov Astron Lett 12:131–133

Blondin S, Dessart L, Hillier DJ, Khokhlov AM (2017) Evidence for sub-Chandrasekhar-mass progenitors of Type Ia supernovae at the faint end of the width-luminosity relation. Mon Not R Astron Soc 470:157–165. https://doi.org/10.1093/mnras/stw2492, arXiv:1706.01901

Bloom JS, Kasen D, Shen KJ, Nugent PE, Butler NR, Graham ML, Howell DA, Kolb U, Holmes S, Haswell CA, Burwitz V, Rodriguez J, Sullivan M (2012) A compact degenerate primary-star progenitor of SN 2011fe. Astrophys J 744:L17. https://doi.org/10.1088/2041-8205/744/2/L17, arXiv:1111.0966

Bode MF, Evans A (2008) Classical Novae. Cambridge University Press, Cambridge

Boffin HMJ, Paulus G, Arnould M, Mowlavi N (1993) The explosive thermonuclear formation of Li-7 revisited. Astron Astrophys 279:173–178

Branch D (1981) Some statistical properties of Type I supernovae. Astrophys J 248:1076–1080. https://doi.org/10.1086/159237

Branch D, Fisher A, Nugent P (1993) On the relative frequencies of spectroscopically normal and peculiar Type IA supernovae. Astron J 106:2383–2391. https://doi.org/10.1086/116810

Branch D, Romanishin W, Baron E (1996) Statistical connections between the properties of Type IA supernovae and the B-V colors of their parent galaxies, and the value of H 0. Astrophys J 465:73–78. https://doi.org/10.1086/177402, arXiv:astro-ph/9510071

Bravo E, García-Senz D (1999) Coulomb corrections to the equation of state of nuclear statistical equilibrium matter: implications for SNIa nucleosynthesis and the accretion-induced collapse of white dwarfs. Mon Not R Astron Soc 307:984–992. https://doi.org/10.1046/j.1365-8711.1999.02694.x

Bravo E, Isern J, Canal R, Labay J (1992) On the contribution of Ne-22 to the synthesis of Fe-54 and Ni-58 in thermonuclear supernovae. Astron Astrophys 257:534–538

Bravo E, Tornambe A, Dominguez I, Isern J (1996) Clues to Type IA SN progenitors from degenerate carbon ignition models. Astron Astrophys 306:811–822

Brown EF (2000) Nuclear heating and melted layers in the inner crust of an accreting neutron star. Astrophys J 531:988–1002. https://doi.org/10.1086/308487, arXiv:astro-ph/9910215

Brown EF, Bildsten L (1998) The ocean and crust of a rapidly accreting neutron star: implications for magnetic field evolution and thermonuclear flashes. Astrophys J 496:915–933. https://doi.org/10.1086/305419, arXiv:astro-ph/9710261

Burrows A, The L (1990) X- and gamma-ray signatures of Type IA supernovae. Astrophys J 360:626–638. https://doi.org/10.1086/169150

Bussard RW, Ramaty R, Drachman RJ (1979) The annihilation of galactic positrons. Astrophys J 228:928–934. https://doi.org/10.1086/156920

Cadonau R, Tammann GA, Sandage A (1985) Type I supernovae as standard candles. In: Bartel N (ed) Supernovae as distance indicators. Lecture notes in physics, vol 224. Springer, Berlin, pp 151–165. https://doi.org/10.1007/3-540-15206-7-56

Cameron AGW (1955) Origin of anomalous abundances of the elements in giant stars. Astrophys J 121:144–160. https://doi.org/10.1086/145970

Cameron AGW (1962) The formation of the sun and planets. Icarus 1:13–69. https://doi.org/10.1016/0019-1035(62)90005-2

Cameron AGW (1973) Interstellar grains in museums? In: Greenberg JM, van de Hulst HC (eds) Interstellar dust and related topics, IAU symposium, vol 52, pp 545–547

Canal R, Isern J, Labay J (1990) The origin of neutron stars in binary systems. Annu Rev Astron Astrophys 28:183–214. https://doi.org/10.1146/annurev.aa.28.090190.001151

Cappellaro E, Barbon R, Turatto M (2003) Supernova statistics. Astrophysics. arXiv:astro-ph/0310859

Carter B, Luminet J (1983) Tidal compression of a star by a large black hole. I Mechanical evolution and nuclear energy release by proton capture. Astron Astrophys 121:97–113

Casanova J, José J, García-Berro E, Calder A, Shore SN (2010) On mixing at the core-envelope interface during classical nova outbursts. Astron Astrophys 513:L5. https://doi.org/10.1051/0004-6361/201014178, arXiv:1004.2792

Casanova J, José J, García-Berro E, Calder A, Shore SN (2011a) Mixing in classical novae: a 2-D sensitivity study. Astron Astrophys 527:A5. https://doi.org/10.1051/0004-6361/201015895, arXiv:1012.3199

Casanova J, José J, García-Berro E, Shore SN, Calder AC (2011b) Kelvin-Helmholtz instabilities as the source of inhomogeneous mixing in nova explosions. Nature 478:490–492. https://doi.org/10.1038/nature10520

Casanova J, José J, García-Berro E, Shore SN (2016) Three-dimensional simulations of turbulent convective mixing in ONe and CO classical nova explosions. Astron Astrophys 595:A28. https://doi.org/10.1051/0004-6361/201628707

Casanova J, José J, Shore SN (2018) Two-dimensional simulations of mixing in classical novae: the effect of the white dwarf composition and mass. Astron Astrophys. https://doi.org/10.1051/0004-6361/201628707

Champagne AE, Wiescher M (1992) Explosive hydrogen burning. Annu Rev Nucl Part Sci 42: 39–76. https://doi.org/10.1146/annurev.ns.42.120192.000351

Chan K, Lingenfelter RE (1993) Positrons from supernovae. Astrophys J 405:614–636. https://doi.org/10.1086/172393

Chang P, Bildsten L, Wasserman I (2005) Formation of resonant atomic lines during thermonuclear flashes on neutron stars. Astrophys J 629:998–1007. https://doi.org/10.1086/431730, arXiv:astro-ph/0505062

Chang P, Morsink S, Bildsten L, Wasserman I (2006) Rotational broadening of atomic spectral features from neutron stars. Astrophys J 636:L117–L120. https://doi.org/10.1086/499428, arXiv:astro-ph/0511246

Cheung CC, Jean P, Shore SN, Stawarz Ł, Corbet RHD, Knödlseder J, Starrfield S, Wood DL, Desiante R, Longo F, Pivato G, Wood KS (2016) Fermi-LAT gamma-ray detections of classical Novae V1369 Centauri 2013 and V5668 Sagittarii 2015. Astrophys J 826:142. https://doi.org/10.3847/0004-637X/826/2/142, arXiv:1605.04216

Choi B, Huss GR, Wasserburg GJ, Gallino R (1998) Presolar corundum and spinel in ordinary chondrites: origins from AGB stars and a supernova. Science 282:1284–1289. https://doi.org/10.1126/science.282.5392.1284

Choi B, Wasserburg GJ, Huss GR (1999) Circumstellar hibonite and corundum and nucleosynthesis in asymptotic giant branch stars. Astrophys J 522:L133–L136. https://doi.org/10.1086/312239

Chomiuk L, Linford JD, Yang J, O'Brien TJ, Paragi Z, Mioduszewski AJ, Beswick RJ, Cheung CC, Mukai K, Nelson T, Ribeiro VARM, Rupen MP, Sokoloski JL, Weston J, Zheng Y, Bode MF, Eyres S, Roy N, Taylor GB (2014) Binary orbits as the driver of γ-ray emission and mass ejection in classical novae. Nature 514:339–342. https://doi.org/10.1038/nature13773, arXiv:1410.3473

Churazov E, Sunyaev R, Isern J, Knödlseder J, Jean P, Lebrun F, Chugai N, Grebenev S, Bravo E, Sazonov S, Renaud M (2014) Cobalt-56 γ-ray emission lines from the Type Ia supernova 2014J. Nature 512:406–408. https://doi.org/10.1038/nature13672, arXiv:1405.3332

Churazov E, Sunyaev R, Isern J, Bikmaev I, Bravo E, Chugai N, Grebenev S, Jean P, Knödlseder J, Lebrun F, Kuulkers E (2015) Gamma-rays from Type Ia Supernova SN2014J. Astrophys J 812:62. https://doi.org/10.1088/0004-637X/812/1/62, arXiv:1502.00255

Clayton DD (1981) Li-7 gamma-ray lines from novae. Astrophys J 244:L97. https://doi.org/10.1086/183488

Clayton DD (2013) Analytic approximation of carbon condensation issues in Type II Supernovae. Astrophys J 762:5. https://doi.org/10.1088/0004-637X/762/1/5

Clayton DD, Hoyle F (1974) Gamma-ray lines from novae. Astrophys J 187:L101+. https://doi.org/10.1086/181406

Clayton DD, Hoyle F (1976) Grains of anomalous isotopic composition from novae. Astrophys J 203:490–496. https://doi.org/10.1086/154104

Clayton DD, Nittler LR (2004) Astrophysics with presolar stardust. Annu Rev Astron Astrophys 42:39–78. https://doi.org/10.1146/annurev.astro.42.053102.134022

Clayton DD, Liu W, Dalgarno A (1999) Condensation of carbon in radioactive supernova gas. Science 283:1290. https://doi.org/10.1126/science.283.5406.1290

Clayton DD, Deneault EAN, Meyer BS (2001) Condensation of carbon in radioactive supernova gas. Astrophys J 562:480–493. https://doi.org/10.1086/323467

Coc A, Hernanz M, José J, Thibaud J (2000) Influence of new reaction rates on ^{18}F production in novae. Astron Astrophys 357:561–571. arXiv:astro-ph/0003166

Colgate SA, McKee C (1969) Early supernova luminosity. Astrophys J 157:623–644. 10.1086/150102

Cornelisse R, Heise J, Kuulkers E, Verbunt F, in't Zand JJM (2000) The longest thermonuclear X-ray burst ever observed? A BeppoSAX Wide Field Camera observation of 4U 1735-44. Astron Astrophys 357:L21–L24. arXiv:astro-ph/0003454

Cottam J, Paerels F, Mendez M (2002) Gravitationally redshifted absorption lines in the X-ray burst spectra of a neutron star. Nature 420:51–54. https://doi.org/10.1038/nature01159, arXiv:astro-ph/0211126

Cottam J, Paerels F, Méndez M, Boirin L, Lewin WHG, Kuulkers E, Miller JM (2008) The Burst Spectra of EXO 0748-676 during a Long 2003 XMM-Newton Observation. Astrophys J 672:504–509. https://doi.org/10.1086/524186, arXiv:0709.4062

Cumming A (2005) Superbursts: a new probe of the rp-process. Nucl Phys A 758:439–446. https://doi.org/10.1016/j.nuclphysa.2005.05.081

Cumming A, Bildsten L (2001) Carbon flashes in the heavy-element ocean on accreting neutron stars. Astrophys J 559:L127–L130. https://doi.org/10.1086/323937, arXiv:astro-ph/0107213

D'Antona F, Mazzitelli I (1989) The fastest evolving white dwarfs. Astrophys J 347:934–949. https://doi.org/10.1086/168185

Damen E, Magnier E, Lewin WHG, Tan J, Penninx W, van Paradijs J (1990) X-ray bursts with photospheric radius expansion and the gravitational redshift of neutron stars. Astron Astrophys 237:103–109

Darnley MJ, Henze M, Steele IA, Bode MF, Ribeiro VARM, Rodríguez-Gil P, Shafter AW, Williams SC, Baer D, Hachisu I, Hernanz M, Hornoch K, Hounsell R, Kato M, Kiyota S, Kučáková H, Maehara H, Ness JU, Piascik AS, Sala G, Skillen I, Smith RJ, Wolf M (2015) A remarkable recurrent nova in M31: discovery and optical/UV observations of the predicted 2014 eruption. Astron Astrophys 580:A45. https://doi.org/10.1051/0004-6361/201526027, arXiv:1506.04202

Darnley MJ, Henze M, Bode MF, Hachisu I, Hernanz M, Hornoch K, Hounsell R, Kato M, Ness JU, Osborne JP, Page KL, Ribeiro VARM, Rodríguez-Gil P, Shafter AW, Shara MM, Steele IA, Williams SC, Arai A, Arcavi I, Barsukova EA, Boumis P, Chen T, Fabrika S, Figueira J, Gao X, Gehrels N, Godon P, Goranskij VP, Harman DJ, Hartmann DH, Hosseinzadeh G, Horst JC, Itagaki K, José J, Kabashima F, Kaur A, Kawai N, Kennea JA, Kiyota S, Kučáková H, Lau KM, Maehara H, Naito H, Nakajima K, Nishiyama K, O'Brien TJ, Quimby R, Sala G, Sano Y, Sion EM, Valeev AF, Watanabe F, Watanabe M, Williams BF, Xu Z (2016a) M31N 2008-12a – the remarkable recurrent nova in M31: panchromatic observations of the 2015 eruption. Astrophys J 833:149. https://doi.org/10.3847/1538-4357/833/2/149, arXiv:1607.08082

Darnley MJ, Henze M, Steele IA, Bode MF, Ribeiro VARM, Rodríguez-Gil P, Shafter AW, Williams SC, Baer D, Hachisu I, Hernanz M, Hornoch K, Hounsell R, Kato M, Kiyota S, Kučáková H, Maehara H, Ness JU, Piascik AS, Sala G, Skillen I, Smith RJ, Wolf M (2016b) A remarkable recurrent nova in M31: discovery and optical/UV observations of the predicted 2014 eruption (Corrigendum). Astron Astrophys 593:C3. https://doi.org/10.1051/0004-6361/201526027e

Darnley MJ, Hounsell R, Godon P, Perley DA, Henze M, Kuin NPM, Williams BF, Williams SC, Bode MF, Harman DJ, Hornoch K, Link M, Ness JU, Ribeiro VARM, Sion EM, Shafter AW, Shara MM (2017b) Inflows, outflows, and a giant donor in the remarkable recurrent nova M31N 2008-12a? – Hubble space telescope photometry of the 2015 eruption. Astrophys J 849:96. https://doi.org/10.3847/1538-4357/aa9062, arXiv:1709.10145

Darnley MJ, Hounsell R, Godon P, Perley DA, Henze M, Kuin NPM, Williams BF, Williams SC, Bode MF, Harman DJ, Hornoch K, Link M, Ness JU, Ribeiro VARM, Sion EM, Shafter AW, Shara MM (2017a) No neon, but jets in the remarkable recurrent nova M31N 2008-12a? – Hubble space telescope spectroscopy of the 2015 eruption. Astrophys J 847:35. https://doi.org/10.3847/1538-4357/aa8867, arXiv:1708.06795

De Angelis A, Tatischeff V, Grenier IA, McEnery J, Mallamaci M, Tavani M, Oberlack U, Hanlon L, Walter R, Argan A, et al (2017a) Science with e-ASTROGAM (A space mission for MeV-GeV gamma-ray astrophysics). arXiv:1711.01265

De Angelis A, Tatischeff V, Tavani M, Oberlack U, Grenier I, Hanlon L, Walter R, Argan A, von Ballmoos P, Bulgarelli A, Donnarumma I, Hernanz M, Kuvvetli I, Pearce M, Zdziarski A, Aboudan A, Ajello M, Ambrosi G, Bernard D, Bernardini E, Bonvicini V, Brogna A, Branchesi M, Budtz-Jorgensen C, Bykov A, Campana R, Cardillo M, Coppi P, De Martino D, Diehl R, Doro M, Fioretti V, Funk S, Ghisellini G, Grove E, Hamadache C, Hartmann DH, Hayashida M, Isern J, Kanbach G, Kiener J, Knödlseder J, Labanti C, Laurent P, Limousin O, Longo F, Mannheim K, Marisaldi M, Martinez M, Mazziotta MN, McEnery J, Mereghetti S, Minervini G, Moiseev A, Morselli A, Nakazawa K, Orleanski P, Paredes JM, Patricelli B, Peyré J, Piano G, Pohl M, Ramarijaona H, Rando R, Reichardt I, Roncadelli M, Silva R, Tavecchio F, Thompson DJ, Turolla R, Ulyanov A, Vacchi A, Wu X, Zoglauer A (2017b) The e-ASTROGAM mission. Exploring the extreme Universe with gamma rays in the MeV–GeV range. Exp Astron 44:25–82. https://doi.org/10.1007/s10686-017-9533-6, arXiv:1611.02232

de Plaa J, Werner N, Bleeker JAM, Vink J, Kaastra JS, Méndez M (2007) Constraining supernova models using the hot gas in clusters of galaxies. Astron Astrophys 465:345–355. https://doi.org/10.1051/0004-6361:20066382, arXiv:astro-ph/0701553

Della Valle M (2002) Nova populations. In: Hernanz M, José J (eds) Classical nova explosions, American Institute of Physics conference series, vol 637, pp 443–456. https://doi.org/10.1063/1.1518244

Della Valle M, Livio M (1994) On the nova rate in the Galaxy. Astron Astrophys 286:786–788

Della Valle M, Livio M (1995) The calibration of novae as distance indicators. Astrophys J 452:704–+. https://doi.org/10.1086/176342

Della Valle M, Livio M (1998) The spectroscopic differences between disk and thick-disk/bulge novae. Astrophys J 506:818–823. https://doi.org/10.1086/306275

Della Valle M, Bianchini A, Livio M, Orio M (1992) On the possible existence of two classes of progenitors for classical novae. Astron Astrophys 266:232–236

Della Valle M, Pasquini L, Daou D, Williams RE (2002) The evolution of Nova V382 Velorum 1999. Astron Astrophys 390:155–166. https://doi.org/10.1051/0004-6361:20020611, arXiv:astro-ph/0205135

Diehl R, Dupraz C, Bennett K, Bloemen H, Hermsen W, Knoedlseder J, Lichti G, Morris D, Ryan J, Schoenfelder V, Steinle H, Strong A, Swanenburg B, Varendorff M, Winkler C (1995) COMPTEL observations of Galactic ^{26}Al emission. Astron Astrophys 298:445–+

Diehl R, Siegert T, Hillebrandt W, Grebenev SA, Greiner J, Krause M, Kromer M, Maeda K, Röpke F, Taubenberger S (2014) Early ^{56}Ni decay gamma rays from SN2014J suggest an unusual explosion. Science 345:1162–1165. https://doi.org/10.1126/science.1254738, arXiv:1407.3061

Dominguez I, Tornambe A, Isern J (1993) On the formation of O-Ne white dwarfs in metal-rich close binary systems. Astrophys J 419:268–+. https://doi.org/10.1086/173480

Domínguez I, Höflich P, Straniero O (2001) Constraints on the progenitors of Type Ia supernovae and implications for the cosmological equation of state. Astrophys J 557:279–291. https://doi.org/10.1086/321661, arXiv:astro-ph/0104257

Domínguez I, Piersanti L, Bravo E, Tornambé A, Straniero O, Gagliardi S (2006) Rotating Type Ia SN progenitors: explosion and light curves. Astrophys J 644:21–29. https://doi.org/10.1086/503534

Elias JH, Matthews K, Neugebauer G, Persson SE (1985) Type I supernovae in the infrared and their use as distance indicators. Astrophys J 296:379–389. https://doi.org/10.1086/163456

Elomaa V, Vorobjev GK, Kankainen A, Batist L, Eliseev S, Eronen T, Hakala J, Jokinen A, Moore ID, Novikov YN, Penttilä H, Popov A, Rahaman S, Rissanen J, Saastamoinen A, Schatz H, Seliverstov DM, Weber C, Äystö J (2009) Quenching of the SnSbTe cycle in the rp process. Phys Rev Lett 102(25):252501/1–252501/4. https://doi.org/10.1103/PhysRevLett.102.252501

Falanga M, Chenevez J, Cumming A, Kuulkers E, Trap G, Goldwurm A (2008) Intermediate long X-ray bursts from the ultra-compact binary candidate SLX 1737-282. Astron Astrophys 484:43–50. https://doi.org/10.1051/0004-6361:20078982, arXiv:0711.0328

Fan YZ, Yu YW, Xu D, Jin ZP, Wu XF, Wei DM, Zhang B (2013) A supramassive magnetar central engine for GRB 130603B. Astrophys J 779:L25. https://doi.org/10.1088/2041-8205/779/2/L25, arXiv:1311.7185

Fernández R, Metzger BD (2016) Electromagnetic signatures of neutron star mergers in the advanced LIGO era. Ann Rev Nucl Part Sci 66:23–45. https://doi.org/10.1146/annurev-nucl-102115-044819, arXiv:1512.05435

Filippenko AV, Richmond MW, Branch D, Gaskell M, Herbst W, Ford CH, Treffers RR, Matheson T, Ho LC, Dey A, Sargent WLW, Small TA, van Breugel WJM (1992) The subluminous, spectroscopically peculiar Type IA supernova 1991bg in the elliptical galaxy NGC 4374. Astron J 104:1543–1556. https://doi.org/10.1086/116339

Fink M, Hillebrandt W, Röpke FK (2007) Double-detonation supernovae of sub-Chandrasekhar mass white dwarfs. Astron Astrophys 476:1133–1143. https://doi.org/10.1051/0004-6361:20078438, arXiv:0710.5486

Fishman GJ, Wilson RB, Meegan CA, Brock MN, Horack JM, Paciesas WS, Pendleton GN, Harmon BA, Leising M (1991) Detectability of early low-energy gamma rays from nearby novae by BATSE/GRO. In: Durouchoux P, Prantzos N (eds) Gamma-ray line astrophysics. American Institute of Physics conference series, vol 232, pp 190–192. https://doi.org/10.1063/1.40956

Fisker JL, Görres J, Wiescher M, Davids B (2006) The importance of $^{15}O(\alpha,\gamma)^{19}Ne$ to X-Ray bursts and superbursts. Astrophys J 650:332–337. https://doi.org/10.1086/507083, arXiv:astro-ph/0410561

Fisker JL, Schatz H, Thielemann F (2008) Explosive hydrogen burning during Type I X-ray bursts. Astrophys J Suppl Ser 174:261–276. https://doi.org/10.1086/521104

Fossey SJ, Cooke B, Pollack G, Wilde M, Wright T (2014) Supernova 2014J in M82 = Psn J09554214+6940260. Central Bureau Electronic Telegrams 3792

Fryxell BA, Woosley SE (1982a) A two-dimensional model for gamma-ray bursts. Astrophys J 258:733–739. https://doi.org/10.1086/160121

Fryxell BA, Woosley SE (1982b) Finite propagation time in multidimensional thermonuclear runaways. Astrophys J 261:332–336. https://doi.org/10.1086/160344

Fujimoto MY, Hanawa T, Miyaji S (1981) Shell flashes on accreting neutron stars and X-ray bursts. Astrophys J 247:267–278. https://doi.org/10.1086/159034

Fuller GM, Fowler WA, Newman MJ (1985) Stellar weak interaction rates for intermediate-mass nuclei. IV – interpolation procedures for rapidly varying lepton capture rates using effective log (ft)-values. Astrophys J 293:1–16. https://doi.org/10.1086/163208

Fushiki I, Lamb DQ (1987) New insights from a global view of X-ray bursts. Astrophys J 323:L55–L60. https://doi.org/10.1086/185056

Gallino R, Raiteri CM, Busso M (1993) Carbon stars and isotopic BA anomalies in meteoritic SiC grains. Astrophys J 410:400–411. https://doi.org/10.1086/172757

Galloway DK, Muno MP, Hartman JM, Psaltis D, Chakrabarty D (2008) Thermonuclear (Type I) X-ray bursts observed by the Rossi X-ray timing explorer. Astrophys J Suppl Ser 179:360–422. https://doi.org/10.1086/592044, arXiv:astro-ph/0608259

Gamezo VN, Khokhlov AM, Oran ES, Chtchelkanova AY, Rosenberg RO (2003) Thermonuclear supernovae: simulations of the deflagration stage and their implications. Science 299:77–81. https://doi.org/10.1126/science.1078129, arXiv:astro-ph/0212054

García-Senz D, Bravo E (2005) Type Ia Supernova models arising from different distributions of igniting points. Astron Astrophys 430:585–602. https://doi.org/10.1051/0004-6361:20041628, arXiv:astro-ph/0409480

García-Senz D, Cabezón RM, Arcones A, Relaño A, Thielemann FK (2013) High-resolution simulations of the head-on collision of white dwarfs. Mon Not R Astron Soc 436:3413–3429. https://doi.org/10.1093/mnras/stt1821, arXiv:1309.6884

Gehrz RD (2002) Infrared and radio observations of classical novae: physical parameters and abundances in the ejecta. In: Hernanz M, José J (eds) Classical nova explosions. American Institute of Physics conference series, vol 637, pp 198–207. https://doi.org/10.1063/1.1518200

Gehrz RD, Truran JW, Williams RE, Starrfield S (1998) Nucleosynthesis in classical novae and its contribution to the interstellar medium. Publ Astron Soc Pac 110:3–26. https://doi.org/10.1086/316107

Glasner SA, Livne E (1995) Convective hydrogen burning down a nova outburst. Astrophys J 445:L149–L151. https://doi.org/10.1086/187911

Glasner SA, Truran JW (2009) Carbon-nitrogen-oxygen “breakout” and nucleosynthesis in classical novae. Astrophys J 692:L58–L61. https://doi.org/10.1088/0004-637X/692/1/L58, arXiv:0812.3984

Glasner SA, Livne E, Truran JW (1997) Reactive flow in nova outbursts. Astrophys J 475:754–762. https://doi.org/10.1086/303561

Glasner SA, Livne E, Truran JW (2005) The sensitivity of multidimensional nova calculations to the outer boundary condition. Astrophys J 625:347–350. https://doi.org/10.1086/429482, arXiv:astro-ph/0504054

Goldstein DA, Kasen D (2018) Evidence for sub-Chandrasekhar mass Type Ia supernovae from an extensive survey of radiative transfer models. Astrophys J 852:L33. https://doi.org/10.3847/2041-8213/aaa409, arXiv:1801.00789

Gómez-Gomar J, Hernanz M, Jose J, Isern J (1998a) Gamma-ray emission from individual classical novae. Mon Not R Astron Soc 296:913–920. https://doi.org/10.1046/j.1365-8711.1998.01421.x, arXiv:astro-ph/9711322

Gómez-Gomar J, Isern J, Jean P (1998b) Prospects for Type IA supernova explosion mechanism identification with gamma rays. Mon Not R Astron Soc 295:1–+. https://doi.org/10.1046/j.1365-8711.1998.29511115.x, arXiv:astro-ph/9709048

Grindlay J, Gursky H (1976) Scattering model for X-ray bursts – massive black holes in globular clusters. Astrophys J 205:L131–L133. https://doi.org/10.1086/182106

Grindlay JE, McClintock JE, Canizares CR, Cominsky L, Li FK, Lewin WHG, van Paradijs J (1978) Discovery of optical bursts from an X-ray burst source, MXB1735-44. Nature 274:567–+. https://doi.org/10.1038/274567a0

Guerrero J, García-Berro E, Isern J (2004) Smoothed particle hydrodynamics simulations of merging white dwarfs. Astron Astrophys 413:257–272. https://doi.org/10.1051/0004-6361:20031504

Gutierrez J, Garcia-Berro E, Iben I Jr, Isern J, Labay J, Canal R (1996) The final evolution of ONeMg electron-degenerate cores. Astrophys J 459:701–705. https://doi.org/10.1086/176934

Gyngard F, Nittler LR, Zinner E, Jose J, Cristallo S (2011) New reaction rates and implications for nova nucleosynthesis and presolar grains. In: Lunar and planetary science conference, vol 42, p 2675

Hachisu I, Kato M, Nomoto K (1999) A wide symbiotic channel to Type IA supernovae. Astrophys J 522:487–503. https://doi.org/10.1086/307608, arXiv:astro-ph/9902304

Hachisu I, Saio H, Kato M (2016) Shortest recurrence periods of forced novae. Astrophys J 824:22. https://doi.org/10.3847/0004-637X/824/1/22, arXiv:1604.02965

Hackwell JA, Grasdalen GL, Gehrz RD, Cominsky L, Lewin WHG, van Paradijs J (1979) The detection of an optical burst coincident with an X-ray burst from MXB 1837 + 05 /Ser X-1/. Astrophys J 233:L115–L119. https://doi.org/10.1086/183088

Haenecour P, Floss C, José J, Amari S, Lodders K, Jadhav M, Wang A, Gyngard F (2016) Coordinated analysis of two graphite grains from the CO3.0 LAP 031117 meteorite: first identification of a CO nova graphite and a presolar iron sulfide subgrain. Astrophys J 825:88. https://doi.org/10.3847/0004-637X/825/2/88, arXiv:1606.08310

Hamuy M, Phillips MM, Maza J, Suntzeff NB, Schommer RA, Aviles R (1995) A Hubble diagram of distant Type IA supernovae. Astron J 109:1–13. https://doi.org/10.1086/117251

Hamuy M, Phillips MM, Suntzeff NB, Schommer RA, Maza J, Antezan AR, Wischnjewsky M, Valladares G, Muena C, Gonzales LE, Aviles R, Wells LA, Smith RC, Navarrete M, Covarrubias R, Williger GM, Walker AR, Layden AC, Elias JH, Baldwin JA, Hernandez M, Tirado H, Ugarte P, Elston R, Saavedra N, Barrientos F, Costa E, Lira P, Ruiz MT, Anguita C, Gomez X, Ortiz P, Della Valle M, Danziger J, Storm J, Kim Y, Bailyn C, Rubenstein EP, Tucker D, Cersosimo S, Mendez RA, Siciliano L, Sherry W, Chaboyer B, Koopmann RA, Geisler D, Sarajedini A, Dey A, Tyson N, Rich RM, Gal R, Lamontagne R, Caldwell N, Guhathakurta P, Phillips AC, Szkody P, Prosser C, Ho LC, McMahan R, Baggley G, Cheng K, Havlen R, Wakamatsu K, Janes K, Malkan M, Baganoff F, Seitzer P, Shara M, Sturch C, Hesser J, Hartig ANP, Hughes J, Welch D, Williams TB, Ferguson H, Francis PJ, French L, Bolte M, Roth J, Odewahn S, Howell S, Krzeminski W (1996) BVRI light curves for 29 Type IA supernovae. Astron J 112:2408–2437. https://doi.org/10.1086/118192, arXiv:astro-ph/9609064

Hamuy M, Phillips MM, Suntzeff NB, Maza J, González LE, Roth M, Krisciunas K, Morrell N, Green EM, Persson SE, McCarthy PJ (2003) An asymptotic-giant-branch star in the progenitor system of a Type Ia supernova. Nature 424:651–654. https://doi.org/10.1038/nature01854, arXiv:astro-ph/0306270

Hanawa T, Sugimoto D, Hashimoto M (1983) Nucleosynthesis in explosive hydrogen burning and its implications in ten-minute interval of X-ray bursts. Publ Astron Soc Jpn 35:491–506

Hansen CJ, van Horn HM (1975) Steady-state nuclear fusion in accreting neutron-star envelopes. Astrophys J 195:735–741. https://doi.org/10.1086/153375

Harkness R (1991) Type Ia Supernovae. In: Danziger IJ, Kjaer K (eds) European southern observatory astrophysics symposia, vol 37, pp 447–456

Harris MJ, Leising MD, Share GH (1991) A search for the 478 keV line from the decay of nucleosynthetic Be-7. Astrophys J 375:216–220. https://doi.org/10.1086/170183

Harris MJ, Naya JE, Teegarden BJ, Cline TL, Gehrels N, Palmer DM, Ramaty R, Seifert H (1999) Transient gamma ray spectrometer observations of gamma-ray lines from novae. I. Limits on the positron annihilation line in five individual novae. Astrophys J 522:424–432. https://doi.org/10.1086/307625, arXiv:astro-ph/0004164

Harris MJ, Teegarden BJ, Weidenspointner G, Palmer DM, Cline TL, Gehrels N, Ramaty R (2001) Transient gamma-ray spectrometer observations of gamma-ray lines from novae. III. The 478 keV line from ^{7}Be decay. Astrophys J 563:950–957. https://doi.org/10.1086/323951

Hatano K, Branch D, Fisher A, Starrfield S (1997) On the spatial distribution and occurrence rate of Galactic classical novae. Mon Not R Astron Soc 290:113–118

Hayakawa S (1981) Galactic X-rays observed with X-ray astronomy satellite 'Hakucho'. Space Sci Rev 29:221–290. https://doi.org/10.1007/BF00229297

Heger A, Cumming A, Galloway DK, Woosley SE (2007) Models of Type I X-ray bursts from GS 1826-24: a probe of rp-process hydrogen burning. Astrophys J 671:L141–L144. https://doi.org/10.1086/525522, arXiv:0711.1195

Henyey L, L'Ecuyer J (1969) Studies in stellar evolution. VIII. The time scale for the diffusion of energy in the stellar interior. Astrophys J 156:549–558. https://doi.org/10.1086/149988

Henze M, Ness JU, Darnley MJ, Bode MF, Williams SC, Shafter AW, Sala G, Kato M, Hachisu I, Hernanz M (2015) A remarkable recurrent nova in M 31: the predicted 2014 outburst in

X-rays with Swift. Astron Astrophys 580:A46. https://doi.org/10.1051/0004-6361/201526028, arXiv:1504.06237

Hernanz M (2002) Gamma-ray emission from classical novae. In: Hernanz M, José J (eds) Classical nova explosions. American Institute of Physics conference series, vol 637, pp 399–408. https://doi.org/10.1063/1.1518237

Hernanz M (2012) Novae in γ-rays. Bull Astron Soc India 40:377. arXiv:1301.1660

Hernanz M (2014) Gamma-ray emission from nova outbursts. In: Woudt PA, Ribeiro VARM (eds) Stellar novae: past and future decades. Astronomical Society of the Pacific conference series, vol 490, p 319. arXiv:1305.0769

Hernanz M (2015) Astrophysics: a lithium-rich stellar explosion. Nature 518:307–308. https://doi.org/10.1038/518307a

Hernanz M, José J (2004) γ-Rays from classical novae: expectations from present and future missions. New Astron Rev 48:35–39. https://doi.org/10.1016/j.newar.2003.11.005

Hernanz M, Isern J, Canal R, Labay J, Mochkovitch R (1988) The final stages of evolution of cold, mass-accreting white dwarfs. Astrophys J 324:331–344. https://doi.org/10.1086/165898

Hernanz M, Jose J, Coc A, Isern J (1996) On the synthesis of 7Li and 7Be in novae. Astrophys J 465:L27+. https://doi.org/10.1086/310122

Hernanz M, José J, Coc A, Gómez-Gomar J, Isern J (1999) Gamma-ray emission from novae related to positron annihilation: constraints on its observability posed by new experimental nuclear data. Astrophys J 526:L97–L100. https://doi.org/10.1086/312372, arXiv:astro-ph/9910111

Hernanz M, Smith DM, Fishman J, Harmon A, Gómez-Gomar J, José J, Isern J, Jean P (2000) BATSE observations of classical novae. In: McConnell ML, Ryan JM (eds) American Institute of Physics conference series, vol 510, pp 82–86. https://doi.org/10.1063/1.1303179

Hernanz M, Gómez-Gomar J, José J (2002) The prompt gamma-ray emission of novae. New Astron Rev 46:559–563. https://doi.org/10.1016/S1387-6473(02)00201-4, arXiv:astro-ph/0110203

Higdon JC, Fowler WA (1987) Gamma-ray constraints on Na-22 yields in nova explosions. Astrophys J 317:710–716. https://doi.org/10.1086/165317

Hillebrandt W, Thielemann F (1982) Nucleosynthesis in novae – a source of Ne-E and Al-26. Astrophys J 255:617–623. https://doi.org/10.1086/159864

Hillman Y, Prialnik D, Kovetz A, Shara MM (2016) Growing white dwarfs to the Chandrasekhar limit: the parameter space of the single degenerate SNIa channel. Astrophys J 819:168. https://doi.org/10.3847/0004-637X/819/2/168, arXiv:1508.03141

Hoeflich P, Khokhlov A (1996) Explosion models for Type IA supernovae: a comparison with observed light curves, distances, H 0, and Q 0. Astrophys J 457:500. https://doi.org/10.1086/176748, arXiv:astro-ph/9602025

Hoffman JA, Marshall HL, Lewin WHG (1978) Dual character of the rapid burster and a classification of X-ray bursts. Nature 271:630–633. https://doi.org/10.1038/271630a0

Hoppe P, Ott U (1997) Mainstream silicon carbide grains from meteorites. In: Bernatowicz TJ, Zinner E (eds) American Institute of Physics conference series, vol 402, pp 27–58. https://doi.org/10.1063/1.53314

Hoppe P, Annen P, Strebel R, Eberhardt P, Gallino R, Lugaro M, Amari S, Lewis RS (1997) Meteoritic silicon carbide grains with unusual Si isotopic compositions: evidence for an origin in low-mass, low-metallicity asymptotic giant branch stars. Astrophys J 487:L101–L104. https://doi.org/10.1086/310869

Hoppe P, Strebel R, Eberhardt P, Amari S, Lewis RS (2000) Isotopic properties of silicon carbide X grains from the Murchison meteorite in the size range 0.5–1.5 µm. Meteoritics and Planetary Science 35:1157–1176

Hounsell R, Bode MF, Hick PP, Buffington A, Jackson BV, Clover JM, Shafter AW, Darnley MJ, Mawson NR, Steele IA, Evans A, Eyres SPS, O'Brien TJ (2010) Exquisite nova light curves from the Solar Mass Ejection Imager (SMEI). Astrophys J 724:480–486. https://doi.org/10.1088/0004-637X/724/1/480, arXiv:1009.1737

Hounsell R, Darnley MJ, Bode MF, Harman DJ, Surina F, Starrfield S, Holdsworth DL, Bewsher D, Hick PP, Jackson BV, Buffington A, Clover JM, Shafter AW (2016) Nova light curves from the Solar Mass Ejection Imager (SMEI) – II. The extended catalog. Astrophys J 820:104. https://doi.org/10.3847/0004-637X/820/2/104, arXiv:1512.03321

Howell DA, Sullivan M, Nugent PE, Ellis RS, Conley AJ, Le Borgne D, Carlberg RG, Guy J, Balam D, Basa S, Fouchez D, Hook IM, Hsiao EY, Neill JD, Pain R, Perrett KM, Pritchet CJ (2006) The Type Ia supernova SNLS-03D3bb from a super-Chandrasekhar-mass white dwarf star. Nature 443:308–311. https://doi.org/10.1038/nature05103, arXiv:astro-ph/0609616

Hoyle F, Fowler WA (1960) Nucleosynthesis in supernovae. Astrophys J 132:565–590. https://doi.org/10.1086/146963

Hutcheon ID, Huss GR, Fahey AJ, Wasserburg GJ (1994) Extreme Mg-26 and O-17 enrichments in an Orgueil corundum: identification of a presolar oxide grain. Astrophys J 425:L97–L100. https://doi.org/10.1086/187319

Iben I Jr, Tutukov AV (1985) On the evolution of close binaries with components of initial mass between 3 solar masses and 12 solar masses. Astrophys J Suppl Ser 58:661–710. https://doi.org/10.1086/191054

Iliadis C (2007) Nuclear physics of stars. Wiley-VCH, Weinheim

Iliadis C, Endt PM, Prantzos N, Thompson WJ (1999) Explosive hydrogen burning of ^{27}Si, ^{31}S, ^{35}Ar, and ^{39}Ca in novae and X-ray bursts. Astrophys J 524:434–453. https://doi.org/10.1086/307778

Iliadis C, Downen LN, José J, Nittler LR, Starrfield S (2018) On presolar stardust grains from CO classical novae. Astrophys J, arXiv:1801.09568

in't Zand J (2017) Understanding superbursts. In: Serino M, Shidatsu M, Iwakiri W, Mihara T (eds) 7 years of MAXI: monitoring X-ray transients, p 121. arXiv:1702.04899

in't Zand JJM, Weinberg NN (2010) Evidence of heavy-element ashes in thermonuclear X-ray bursts with photospheric superexpansion. Astron Astrophys 520:A81. https://doi.org/10.1051/0004-6361/200913952, arXiv:1001.0900

in't Zand JJM, Kuulkers E, Verbunt F, Heise J, Cornelisse R (2003) A superburst from 4U 1254-69. Astron Astrophys 411:L487–L491. https://doi.org/10.1051/0004-6361:20031586, arXiv:astro-ph/0310364

in't Zand JJM, Cumming A, van der Sluys MV, Verbunt F, Pols OR (2005) On the possibility of a helium white dwarf donor in the presumed ultracompact binary 2S 0918-549. Astron Astrophys 441:675–684. https://doi.org/10.1051/0004-6361:20053002, arXiv:astro-ph/0506666

Isern J, Jean P, Bravo E, Knödlseder J, Lebrun F, Churazov E, Sunyaev R, Domingo A, Badenes C, Hartmann DH, Hoeflich P, Renaud M, Soldi S, Elias-Rosa N, Hernanz M, Domínguez I, García-Senz D, Lichti GG, Vedrenne G, Von Ballmoos P (2016) Gamma-ray emission from SN2014J near maximum optical light. Astron Astrophys 588:A67. https://doi.org/10.1051/0004-6361/201526941, arXiv:1602.02918

Ivanova LN, Imshennik VS, Chechetkin VM (1974) Pulsation regime of the thermonuclear explosion of a star's dense carbon core. Astrophys Space Sci 31:497–514. https://doi.org/10.1007/BF00644102

Iyudin AF, Bennett K, Bloemen H, Diehl R, Hermsen W, Lichti GG, Morris D, Ryan J, Schoenfelder V, Steinle H, Strong A, Varendorff M, Winkler C (1995) COMPTEL search for ^{22}Na line emission from recent novae. Astron Astrophys 300:422–428

Izzo L, Della Valle M, Mason E, Matteucci F, Romano D, Pasquini L, Vanzi L, Jordan A, Fernandez JM, Bluhm P, Brahm R, Espinoza N, Williams R (2015) Early optical spectra of nova V1369 Cen show the presence of lithium. Astrophys J 808:L14. https://doi.org/10.1088/2041-8205/808/1/L14, arXiv:1506.08048

Jean P, Hernanz M, Gómez-Gomar J, José J (2000) Galactic 1.275-MeV emission from ONe novae and its detectability by INTEGRAL/SPI. Mon Not R Astron Soc 319:350–364. https://doi.org/10.1046/j.1365-8711.2000.03587.x, arXiv:astro-ph/0004126

Jiang JA, Doi M, Maeda K, Shigeyama T, Nomoto K, Yasuda N, Jha SW, Tanaka M, Morokuma T, Tominaga N, Ivezić Ž, Ruiz-Lapuente P, Stritzinger MD, Mazzali PA, Ashall C, Mould J, Baade D, Suzuki N, Connolly AJ, Patat F, Wang L, Yoachim P, Jones D, Furusawa H, Miyazaki

S (2017) A hybrid Type Ia supernova with an early flash triggered by helium-shell detonation. Nature 550:80–83. https://doi.org/10.1038/nature23908, arXiv:1710.01824

Jose J (2016) Stellar explosions: hydrodynamics and nucleosynthesis. CRC Press/Taylor and Francis, Boca Raton. https://doi.org/10.1201/b19165

José J, Hernanz M (1998) Nucleosynthesis in classical novae: CO versus ONe white dwarfs. Astrophys J 494:680–690. https://doi.org/10.1086/305244, arXiv:astro-ph/9709153

José J, Hernanz M (2007a) The origin of presolar nova grains. Meteorit Planet Sci 42:1135–1143

José J, Hernanz M (2007b) TOPICAL REVIEW: nucleosynthesis in classical nova explosions. J Phys G Nucl Phys 34:431–458. https://doi.org/10.1088/0954-3899/34/12/R01

José J, Hernanz M, Coc A (1997) New results on 26Al production in classical novae. Astrophys J 479:L55–L58. https://doi.org/10.1086/310575, arXiv:astro-ph/9701181

José J, Coc A, Hernanz M (1999) Nuclear uncertainties in the NENA-MGAL cycles and production of ^{22}Na and ^{26}Al during nova outbursts. Astrophys J 520:347–360. https://doi.org/10.1086/307445, arXiv:astro-ph/9902357

José J, Hernanz M, García-Berro E, Gil-Pons P (2003) The impact of the chemical stratification of white dwarfs on the classification of classical novae. Astrophys J 597:L41–L44. https://doi.org/10.1086/379782, arXiv:astro-ph/0309451

José J, Hernanz M, Amari S, Lodders K, Zinner E (2004) The imprint of nova nucleosynthesis in presolar grains. Astrophys J 612:414–428. https://doi.org/10.1086/422569, arXiv:astro-ph/0405332

José J, García-Berro E, Hernanz M, Gil-Pons P (2007) The first nova explosions. Astrophys J 662:L103–L106. https://doi.org/10.1086/519521

José J, Moreno F, Parikh A, Iliadis C (2010) Hydrodynamic models of Type I X-ray bursts: metallicity effects. Astrophys J Suppl Ser 189:204–239. https://doi.org/10.1088/0067-0049/189/1/204, arXiv:1005.4767

Joss PC (1977) X-ray bursts and neutron-star thermonuclear flashes. Nature 270:310–314. https://doi.org/10.1038/270310a0

Joss PC (1978) Helium-burning flashes on an accreting neutron star – a model for X-ray burst sources. Astrophys J 225:L123–L127. https://doi.org/10.1086/182808

Kashi A, Soker N (2011) A circumbinary disc in the final stages of common envelope and the core-degenerate scenario for Type Ia supernovae. Mon Not R Astron Soc 417:1466–1479. https://doi.org/10.1111/j.1365-2966.2011.19361.x, arXiv:1105.5698

Kasliwal MM, Cenko SB, Kulkarni SR, Ofek EO, Quimby R, Rau A (2011) Discovery of a new photometric sub-class of faint and fast classical novae. Astrophys J 735:94. https://doi.org/10.1088/0004-637X/735/2/94, arXiv:1003.1720

Kato M, Hachisu I (1994) Optically thick winds in nova outbursts. Astrophys J 437:802–826. https://doi.org/10.1086/175041

Kato M, Saio H, Hachisu I, Nomoto K (2014) Shortest recurrence periods of novae. Astrophys J 793:136. https://doi.org/10.1088/0004-637X/793/2/136, arXiv:1404.0582

Keek L, in't Zand JJM (2008) On burning regimes and long duration X-ray bursts. In: Proceedings of the 7th INTEGRAL workshop, p 32. arXiv:0811.4574

Keek L, Galloway DK, in't Zand JJM, Heger A (2010) Multi-instrument X-ray observations of thermonuclear bursts with short recurrence times. Astrophys J 718:292–305. https://doi.org/10.1088/0004-637X/718/1/292, arXiv:1005.3302

Keek L, Heger A, in't Zand JJM (2012) Superburst models for neutron stars with hydrogen- and helium-rich atmospheres. Astrophys J 752:150. https://doi.org/10.1088/0004-637X/752/2/150, arXiv:1204.1343

Kercek A, Hillebrandt W, Truran JW (1998) Two-dimensional simulations of the thermonuclear runaway in an accreted atmosphere of a C+O White Dwarf. Astron Astrophys 337:379–392. arXiv:astro-ph/9801054

Kercek A, Hillebrandt W, Truran JW (1999) Three-dimensional simulations of classical novae. Astron Astrophys 345:831–840. arXiv:astro-ph/9811259

Khokhlov AM (1991) Delayed detonation model for Type IA supernovae. Astron Astrophys 245:114–128

Khokhlov AM (1995) Propagation of turbulent flames in supernovae. Astrophys J 449:695–713. https://doi.org/10.1086/176091

Khokhlov A, Mueller E, Hoeflich P (1993) Light curves of Type IA supernova models with different explosion mechanisms. Astron Astrophys 270:223–248

Khokhlov AM, Oran ES, Wheeler JC (1997) Deflagration-to-detonation transition in thermonuclear supernovae. Astrophys J 478:678–688. https://doi.org/10.1086/303815, arXiv:astro-ph/9612226

Knödlseder J (1999) Implications of 1.8 MEV gamma-ray observations for the origin of ^{26}Al. Astrophys J 510:915–929. https://doi.org/10.1086/306601

Koike O, Hashimoto M, Kuromizu R, Fujimoto S (2004) Final products of the rp-process on accreting neutron stars. Astrophys J 603:242–251. https://doi.org/10.1086/381354

Kolb U, Politano M (1997) The contribution of O-Ne-Mg novae to the ^{26}Al production in the Galaxy. Astron Astrophys 319:909–922

Kong AKH, Miller JM, Méndez M, Cottam J, Lewin WHG, Paerels F, Kuulkers E, Wijnands R, van der Klis M (2007) Nondetection of gravitationally redshifted absorption lines in the X-ray burst spectra of GS 1826-24. Astrophys J 670:L17–L20. https://doi.org/10.1086/524137, arXiv:0708.0413

Kovetz A, Prialnik D (1985) CNO abundances resulting from diffusion in accreting nova progenitors. Astrophys J 291:812–821. https://doi.org/10.1086/163117

Kovetz A, Prialnik D (1997) The composition of nova ejecta from multicycle evolution models. Astrophys J 477:356–367. https://doi.org/10.1086/303675

Kraft RP (1964) Are all novae binary stars? Leaflet Astronom Soc Pac 9:137–144

Krautter J, Oegelman H, Starrfield S, Wichmann R, Pfeffermann E (1996) ROSAT X-ray observations of nova V1974 Cygni: the rise and fall of the brightest supersoft X-ray source. Astrophys J 456:788–+. https://doi.org/10.1086/176697

Kuchner MJ, Kirshner RP, Pinto PA, Leibundgut B (1994) Evidence for Ni-56 yields Co-56 yields Fe-56 decay in Type IA supernovae. Astrophys J 426:L89–L92. https://doi.org/10.1086/187347

Kulkarni PV, Ashok NM, Apparao KMV, Chitre SM (1979) Discovery of IR bursts from Liller I/MXB1730-333. Nature 280:819–820. https://doi.org/10.1038/280819a0

Kumagai S, Nomoto K (1997) Gamma-rays and X-rays from Type Ia supernovae. In: Ruiz-Lapuente P, Canal R, Isern J (eds) NATO ASIC Proc. 486: thermonuclear supernovae, pp 515–540

Kushnir D, Katz B, Dong S, Livne E, Fernández R (2013) Head-on collisions of white dwarfs in triple systems could explain Type Ia supernovae. Astrophys J 778:L37. https://doi.org/10.1088/2041-8205/778/2/L37, arXiv:1303.1180

Kuulkers E (2004) The observers' view of (very) long X-ray bursts: they are super! Nucl Phys B Proc Suppl 132:466–475. https://doi.org/10.1016/j.nuclphysbps.2004.04.081, arXiv:astro-ph/0310402

Kuulkers E, in't Zand JJM, van Kerkwijk MH, Cornelisse R, Smith DA, Heise J, Bazzano A, Cocchi M, Natalucci L, Ubertini P (2002) A half-a-day long thermonuclear X-ray burst from KS 1731-260. Astron Astrophys 382:503–512. https://doi.org/10.1051/0004-6361:20011654, arXiv:astro-ph/0111261

Kuulkers E, den Hartog PR, in't Zand JJM, Verbunt FWM, Harris WE, Cocchi M (2003) Photospheric radius expansion X-ray bursts as standard candles. Astron Astrophys 399:663–680. https://doi.org/10.1051/0004-6361:20021781, arXiv:astro-ph/0212028

Landau LD, Lifshitz EM (1959) Fluid mechanics. Pergamon Press, Oxford

Langanke K, Martínez-Pinedo G (2000) Shell-model calculations of stellar weak interaction rates: II. Weak rates for nuclei in the mass range /A=45-65 in supernovae environments. Nucl Phys A 673:481–508. https://doi.org/10.1016/S0375-9474(00)00131-7, arXiv:nucl-th/0001018

Leising MD (1991) Gamma-ray lines from classical novae. In: Durouchoux P, Prantzos N (eds) Gamma-ray line astrophysics, American Institute of Physics conference series, vol 232, pp 173–182. https://doi.org/10.1063/1.40932

Leising MD (1993) Hard emission from classical novae. Astron Astrophys Suppl Ser 97:299–301

Leising MD, Clayton DD (1987) Positron annihilation gamma rays from novae. Astrophys J 323:159–169. https://doi.org/10.1086/165816

Lewin WHG (1977) X-ray burst sources. In: Papagiannis MD (ed) Eighth Texas symposium on relativistic astrophysics. New York Academy Sciences annals, vol 302, pp 210–227. https://doi.org/10.1111/j.1749-6632.1977.tb37050.x

Lewin WHG, Clark G, Doty J (1976) X-ray bursts. IAU Circ 2922:1

Lewin WHG, Cominsky LR, Walker AR, Robertson BSC (1980) Simultaneous IR and X-ray burst observation of SER X-1. Nature 287:27–28. https://doi.org/10.1038/287027a0

Lewin WHG, van Paradijs J, Taam RE (1993) X-ray bursts. Space Sci Rev 62:223–389. https://doi.org/10.1007/BF00196124

Lewin WHG, van Paradijs J, Taam RE (1995) X-ray bursts. In: Lewin WHG, van Paradijs J, van den Heuvel EPJ (eds) X-ray binaries. Cambridge University Press, Cambridge, pp 175–232

Lewis RS, Ming T, Wacker JF, Anders E, Steel E (1987) Interstellar diamonds in meteorites. Nature 326:160–162. https://doi.org/10.1038/326160a0

Linares M, Watts AL, Wijnands R, Soleri P, Degenaar N, Curran PA, Starling RLC, van der Klis M (2009) The Swift capture of a long X-ray burst from XTE J1701-407. Mon Not R Astron Soc 392:L11–L15. https://doi.org/10.1111/j.1745-3933.2008.00572.x, arXiv:0808.3950

Liu N, Nittler LR, O'D Alexander CM, Wang J, Pignatari M, José J, Nguyen A (2016) Stellar origins of extremely 13C- and 15N-enriched Presolar SiC grains: novae or supernovae? Astrophys J 820:140. https://doi.org/10.3847/0004-637X/820/2/140, arXiv:1602.05252

Liu N, Nittler LR, Pignatari M, O'D Alexander CM, Wang J (2017) Stellar Origin of ^{15}N-rich presolar SiC grains of Type AB: supernovae with explosive hydrogen burning. Astrophys J 842:L1. https://doi.org/10.3847/2041-8213/aa74e5, arXiv:1705.08222

Liu N, Nittler LR, Alexander COD, Wang J (2018) Late formation of silicon carbide in Type II supernovae. Astrophys J. arXiv:1801.06463

Livio M (1992) Classical novae and the extragalactic distance scale. Astrophys J 393:516–522. https://doi.org/10.1086/171524

Livio M (1994) Topics in the theory of cataclysmic variables and X-ray binaries. In: Shore SN, Livio M, van den Heuvel EPJ (eds) Saas-Fee Advanced Course 22: interacting binaries, pp 135–262

Lodders K (2005) Presolar grains from meteorites: remnants from the early times of the solar system. Chem Erde-Geochem 65:93–166. https://doi.org/10.1016/j.chemer.2005.01.001, arXiv:astro-ph/0501430

Lorén-Aguilar P, Isern J, García-Berro E (2010) Smoothed particle hydrodynamics simulations of white dwarf collisions and close encounters. Mon Not R Astron Soc 406:2749–2763. https://doi.org/10.1111/j.1365-2966.2010.16878.x, arXiv:1004.4783

Lugaro M, Davis AM, Gallino R, Pellin MJ, Straniero O, Käppeler F (2003) Isotopic compositions of strontium, zirconium, molybdenum, and barium in single presolar SiC grains and asymptotic giant branch stars. Astrophys J 593:486–508. https://doi.org/10.1086/376442

MacAlpine GM, Ecklund TC, Lester WR, Vanderveer SJ, Strolger L (2007) A spectroscopic study of nuclear processing and the production of anomalously strong lines in the crab nebula. Astron J 133:81–88. https://doi.org/10.1086/509504, arXiv:astro-ph/0609803

Mahoney WA, Ling JC, Jacobson AS, Lingenfelter RE (1982) Diffuse galactic gamma-ray line emission from nucleosynthetic Fe-60, Al-26, and Na-22 – preliminary limits from HEAO 3. Astrophys J 262:742–748. https://doi.org/10.1086/160469

Malone CM, Nonaka A, Almgren AS, Bell JB, Zingale M (2011) Multidimensional modeling of Type I X-ray bursts. I. Two-dimensional convection prior to the outburst of a pure ^{4}He accretor. Astrophys J 728:118. https://doi.org/10.1088/0004-637X/728/2/118, arXiv:1012.0609

Malone CM, Zingale M, Nonaka A, Almgren AS, Bell JB (2014) Multidimensional modeling of Type I X-ray bursts. II. Two-dimensional convection in a mixed H/He accretor. Astrophys J 788:115. https://doi.org/10.1088/0004-637X/788/2/115, arXiv:1404.6286

Maraschi L, Cavaliere A (1977) X-ray bursts of nuclear origin? In: X-ray binaries and compact objects, pp 127–128

Matteucci F, Raiteri CM, Busson M, Gallino R, Gratton R (1993) Constraints on the nucleosynthesis of CU and Zn from models of chemical evolution of the Galaxy. Astron Astrophys 272:421–429

Mazurek TJ, Wheeler JC (1980) Thermonuclear explosions in stars. Fundam Cosm Phys 5:193–286

McClintock JE, Canizares CR, Cominsky L, Li FK, Lewin WHG, van Paradijs J, Grindlay JE (1979) A 3-s delay in an optical burst from X-ray burst source MXB1735-44. Nature 279:47–49. https://doi.org/10.1038/279047a0

McCully C, Jha SW, Foley RJ, Bildsten L, Fong WF, Kirshner RP, Marion GH, Riess AG, Stritzinger MD (2014) A luminous, blue progenitor system for the Type Iax supernova 2012Z. Nature 512:54–56. https://doi.org/10.1038/nature13615, arXiv:1408.1089

Messenger S, Keller LP, Stadermann FJ, Walker RM, Zinner E (2003) Samples of stars beyond the solar system: silicate grains in interplanetary dust. Science 300:105–108. https://doi.org/10.1126/science.1080576

Metzger BD (2017) Kilonovae. Living reviews in relativity 20:3. https://doi.org/10.1007/s41114-017-0006-z, arXiv:1610.09381

Metzger BD, Piro AL, Quataert E (2009) Nickel-rich outflows from accretion discs formed by the accretion-induced collapse of white dwarfs. Mon Not R Astron Soc 396:1659–1664. https://doi.org/10.1111/j.1365-2966.2009.14909.x, arXiv:0812.3656

Meyer BS, Zinner E (2006) Nucleosynthesis. The University of Arizona space science series, Tucson, pp 69–108

Milne PA, The L, Leising MD (2001) Late light curves of Type Ia supernovae. Astrophys J 559:1019–1031. https://doi.org/10.1086/322352, arXiv:astro-ph/0104185

Minkowski R (1941) Spectra of supernovae. Publ Astron Soc Pac 53:224–225. https://doi.org/10.1086/125315

Mochkovitch R (1994) An introduction to the physics of Type II supernova explosions. In: Latal H, Schweiger W (eds) Matter under extreme conditions. Lecture notes in physics, vol 440. Springer, Berlin, p 49

Mochkovitch R, Hernanz M, Isern J, Martin X (1993) Gamma-ray bursts as collimated jets from neutron star/black hole mergers. Nature 361:236–238. https://doi.org/10.1038/361236a0

Molaro P, Izzo L, Mason E, Bonifacio P, Della Valle M (2016) Highly enriched ^{7}Be in the ejecta of Nova Sagittarii 2015 No. 2 (V5668 Sgr) and the Galactic ^{7}Li origin. Mon Not R Astron Soc 463:L117–L121. https://doi.org/10.1093/mnrasl/slw169, arXiv:1609.07297

Moll R, Woosley SE (2013) Multi-dimensional models for double detonation in sub-Chandrasekhar mass white dwarfs. Astrophys J 774:137. https://doi.org/10.1088/0004-637X/774/2/137, arXiv:1303.0324

Mostefaoui S, Hoppe P (2004) Discovery of abundant in situ silicate and spinel grains from red giant stars in a primitive meteorite. Astrophys J 613:L149–L152. https://doi.org/10.1086/424842

Mukai K, Nelson T, Sokoloski J, Chomiuk L, Finzell T, Linford J, Weston J, Rupen M, Mioduszewski A (2017) NuSTAR observations of Fermi-detected novae, V339 Delphini and V5668 Sagitarii. In: Ness JU, Migliari S (eds) The X-ray Universe 2017, p 152

Narayan R, Paczynski B, Piran T (1992) Gamma-ray bursts as the death throes of massive binary stars. Astrophys J 395:L83–L86. https://doi.org/10.1086/186493, arXiv:astro-ph/9204001

Ness JU (2012) High-resolution spectroscopy and high-density monitoring in X-rays of novae. Bull Astron Soc India 40:353. arXiv:1209.2153

Ness JU, Schwarz GJ, Retter A, Starrfield S, Schmitt JHMM, Gehrels N, Burrows D, Osborne JP (2007) Swift X-ray observations of classical novae. Astrophys J 663:505–515. https://doi.org/10.1086/518084, arXiv:astro-ph/0703286

Nguyen AN, Zinner E (2004) Discovery of ancient silicate stardust in a meteorite. Science 303:1496–1499. https://doi.org/10.1126/science.1094389

Niemeyer JC, Woosley SE (1997) The thermonuclear explosion of Chandrasekhar mass white dwarfs. Astrophys J 475:740–753. https://doi.org/10.1086/303544, arXiv:astro-ph/9607032

Nittler LR (1997) Presolar oxide grains in meteorites. In: Bernatowicz TJ, Zinner v (eds) American Institute of Physics conference series, vol 402, pp 59–82. https://doi.org/10.1063/1.53320

Nittler LR, Ciesla F (2016) Astrophysics with extraterrestrial materials. Annu Rev Astron Astrophys 54:53–93. https://doi.org/10.1146/annurev-astro-082214-122505

Nittler LR, Hoppe P (2005) Are presolar silicon carbide grains from novae actually from supernovae? Astrophys J 631:L89–L92. https://doi.org/10.1086/497029

Nittler LR, O'D Alexander CM, Gao X, Walker RM, Zinner EK (1994) Interstellar oxide grains from the Tieschitz ordinary chondrite. Nature 370:443–446. https://doi.org/10.1038/370443a0

Nittler LR, Hoppe P, Alexander CMO, Amari S, Eberhardt P, Gao X, Lewis RS, Strebel R, Walker RM, Zinner E (1995) Silicon nitride from supernovae. Astrophys J 453:L25–L28. https://doi.org/10.1086/309743

Nittler LR, Alexander CMO, Gao X, Walker RM, Zinner E (1997) Stellar sapphires: the properties and origins of presolar AL 2O 3 in meteorites. Astrophys J 483:475–495. https://doi.org/10.1086/304234

Nittler LR, Alexander CMO, Nguyen AN (2006) Extreme 13C and 15N enrichments in a Murchison presolar SiC grain. Meteorit Planet Sci Suppl 41:5316

Nofar I, Shaviv G, Starrfield S (1991) The formation of Al-26 in nova explosions. Astrophys J 369:440–450. https://doi.org/10.1086/169772

Nomoto K (1982) Accreting white dwarf models for Type 1 supernovae. II – Off-center detonation supernovae. Astrophys J 257:780–792. https://doi.org/10.1086/160031

Nomoto K, Kondo Y (1991) Conditions for accretion-induced collapse of white dwarfs. Astrophys J 367:L19–L22. https://doi.org/10.1086/185922

Nomoto K, Sugimoto D, Neo S (1976) Carbon deflagration supernova, an alternative to carbon detonation. Astrophys Space Sci 39:L37–L42. https://doi.org/10.1007/BF00648354

Nomoto K, Thielemann F, Yokoi K (1984) Accreting white dwarf models of Type I supernovae. III – carbon deflagration supernovae. Astrophys J 286:644–658. https://doi.org/10.1086/162639

Ore A, Powell JL (1949) Three-photon annihilation of an electron-positron pair. Phys Rev 75:1696–1699. https://doi.org/10.1103/PhysRev.75.1696

Orio M, Covington J, Ögelman H (2001) X-ray emission from classical and recurrent novae observed with ROSAT. Astron Astrophys 373:542–554. https://doi.org/10.1051/0004-6361:20010537, arXiv:astro-ph/0104219

Orio M, Rana V, Page KL, Sokoloski J, Harrison F (2015) A NuSTAR observation of the fast symbiotic nova V745 Sco in outburst. Mon Not R Astron Soc 448:L35–L39. https://doi.org/10.1093/mnrasl/slu195, arXiv:1412.2088

Osborne JP (2015) Getting to know classical novae with Swift. J High Energy Astrophys 7:117–125. https://doi.org/10.1016, arXiv:1507.02153

Ott U, Begemann F (1990) Discovery of s-process barium in the Murchison meteorite. Astrophys J 353:L57–L60. https://doi.org/10.1086/185707

Page D, Cumming A (2005) Superbursts from strange stars. Astrophys J 635:L157–L160. https://doi.org/10.1086/499520, arXiv:astro-ph/0508444

Papish O, Perets HB (2016) Supernovae from direct collisions of white dwarfs and the role of helium shell ignition. Astrophys J 822:19. https://doi.org/10.3847/0004-637X/822/1/19, arXiv:1502.03453

Parikh A, José J, Moreno F, Iliadis C (2008) The effects of variations in nuclear processes on Type I X-ray burst nucleosynthesis. Astrophys J Suppl Ser 178:110–136. https://doi.org/10.1086/589879, arXiv:0802.2819

Payne Gaposchkin CH (1957) The galactic novae. Interscience Publishers, Amsterdam

Perlmutter S, Gabi S, Goldhaber G, Goobar A, Groom DE, Hook IM, Kim AG, Kim MY, Lee JC, Pain R, Pennypacker CR, Small IA, Ellis RS, McMahon RG, Boyle BJ, Bunclark PS, Carter D, Irwin MJ, Glazebrook K, Newberg HJM, Filippenko AV, Matheson T, Dopita M, Couch WJ, The Supernova Cosmology Project (1997) Measurements of the cosmological parameters omega and lambda from the first seven supernovae at $Z \geq 0.35$. Astrophys J 483:565–581. https://doi.org/10.1086/304265, arXiv:astro-ph/9608192

Phillips MM (1993) The absolute magnitudes of Type IA supernovae. Astrophys J 413:L105–L108. https://doi.org/10.1086/186970

Phillips MM, Wells LA, Suntzeff NB, Hamuy M, Leibundgut B, Kirshner RP, Foltz CB (1992) SN 1991T – further evidence of the heterogeneous nature of Type IA supernovae. Astron J 103:1632–1637. https://doi.org/10.1086/116177

Piersanti L, Gagliardi S, Iben I Jr, Tornambé A (2003a) Carbon-oxygen white dwarf accreting CO-rich matter. II. Self-regulating accretion process up to the explosive stage. Astrophys J 598:1229–1238. https://doi.org/10.1086/378952

Piersanti L, Gagliardi S, Iben I Jr, Tornambé A (2003b) Carbon-oxygen white dwarfs accreting CO-rich matter. I. A comparison between rotating and nonrotating models. Astrophys J 583:885–901. https://doi.org/10.1086/345444, arXiv:astro-ph/0210624

Pietsch W, Haberl F (2005) XMM-Newton detection of Type I X-ray bursts in M 31. Astron Astrophys 430:L45–L48. https://doi.org/10.1051/0004-6361:200400128, arXiv:astro-ph/0412373

Pignatari M, Wiescher M, Timmes FX, de Boer RJ, Thielemann FK, Fryer C, Heger A, Herwig F, Hirschi R (2013) Production of carbon-rich presolar grains from massive stars. Astrophys J 767:L22. yhttps://doi.org/10.1088/2041-8205/767/2/L22, arXiv:1303.3374

Pinto PA, Eastman RG, Rogers T (2001) A test for the nature of the Type IA supernova explosion mechanism. Astrophys J 551:231–243. https://doi.org/10.1086/320059, arXiv:astro-ph/0008330

Politano M, Starrfield S, Truran JW, Weiss A, Sparks WM (1995) Hydrodynamic studies of accretion onto massive white dwarfs: ONeMg-enriched nova outbursts. I. Dependence on white dwarf mass. Astrophys J 448:807–821. https://doi.org/10.1086/176009

Pope SB (2000) Turbulent flows. Cambridge University press, Cambridge

Pozdnyakov LA, Sobol IM, Syunyaev RA (1983) Comptonization and the shaping of X-ray source spectra – Monte Carlo calculations. Astrophys Space Phys Rev 2:189–331

Prantzos N, Diehl R (1996) Radioactive 26Al in the galaxy: observations versus theory. Phys Rep 267:1–69. https://doi.org/10.1016/0370-1573(95)00055-0

Prialnik D, Kovetz A (1984) The effect of diffusion on prenova evolution – CNO-enriched envelopes. Astrophys J 281:367–374. https://doi.org/10.1086/162107

Prialnik D, Kovetz A (1995) An extended grid of multicycle nova evolution models. Astrophys J 445:789–810. https://doi.org/10.1086/175741

Prialnik D, Shara MM, Shaviv G (1978) The evolution of a slow nova model with a Z = 0.03 envelope from pre-explosion to extinction. Astron Astrophys 62:339–348

Prialnik D, Shara MM, Shaviv G (1979) The evolution of a fast nova model with a Z = 0.03 envelope from pre-explosion to decline. Astron Astrophys 72:192–203

Pskovskii IP (1977) Light curves, color curves, and expansion velocity of Type I supernovae as functions of the rate of brightness decline. Sov Astron 21:675–682

Rakowski CE, Badenes C, Gaensler BM, Gelfand JD, Hughes JP, Slane PO (2006) Can ejecta-dominated supernova remnants be typed from their X-ray spectra? The case of G337.2-0.7. Astrophys J 646:982–1000. https://doi.org/10.1086/505018, arXiv:astro-ph/0604246

Raskin C, Timmes FX, Scannapieco E, Diehl S, Fryer C (2009) On Type Ia supernovae from the collisions of two white dwarfs. Mon Not R Astron Soc 399:L156–L159. https://doi.org/10.1111/j.1745-3933.2009.00743.x, arXiv:0907.3915

Rauch T, Suleimanov V, Werner K (2008) Absorption features in the spectra of X-ray bursting neutron stars. Astron Astrophys 490:1127–1134. https://doi.org/10.1051/0004-6361:200810129, arXiv:0809.2170

Riess AG, Press WH, Kirshner RP (1996) A precise distance indicator: Type IA supernova multicolor light-curve shapes. Astrophys J 473:88–109. https://doi.org/10.1086/178129, arXiv:astro-ph/9604143

Riess AG, Filippenko AV, Li W, Treffers RR, Schmidt BP, Qiu Y, Hu J, Armstrong M, Faranda C, Thouvenot E, Buil C (1999) The rise time of nearby Type IA supernovae. Astron J 118:2675–2688. https://doi.org/10.1086/301143, arXiv:astro-ph/9907037

Ritossa C, Garcia-Berro E, Iben I Jr (1996) On the evolution of stars that form electron-degenerate cores processed by carbon burning. II. Isotope abundances and thermal pulses in a 10 M_{sun}

model with an ONe core and applications to long-period variables, classical novae, and accretion-induced collapse. Astrophys J 460:489–505. https://doi.org/10.1086/176987

Romano D, Matteucci F, Molaro P, Bonifacio P (1999) The galactic lithium evolution revisited. Astron Astrophys 352:117–128. arXiv:astro-ph/9910151

Röpke FK, Hillebrandt W, Niemeyer JC, Woosley SE (2006) Multi-spot ignition in Type Ia supernova models. Astron Astrophys 448:1–14. https://doi.org/10.1051/0004-6361:20053926, arXiv:astro-ph/0510474

Rosswog S, Kasen D, Guillochon J, Ramirez-Ruiz E (2009a) Collisions of white dwarfs as a new progenitor channel for Type Ia supernovae. Astrophys J 705:L128–L132. https://doi.org/10.1088/0004-637X/705/2/L128, arXiv:0907.3196

Rosswog S, Ramirez-Ruiz E, Hix WR (2009b) Tidal disruption and ignition of white dwarfs by moderately massive black holes. Astrophys J 695:404–419. https://doi.org/10.1088/0004-637X/695/1/404, arXiv:0808.2143

Ruiz-Lapuente P, Cappellaro E, Turatto M, Gouiffes C, Danziger IJ, Della Valle M, Lucy LB (1992) Modeling the iron-dominated spectra of the Type IA supernova SN 1991T at premaximum. Astrophys J 387:L33–L36. https://doi.org/10.1086/186299

Salaris M, Dominguez I, Garcia-Berro E, Hernanz M, Isern J, Mochkovitch R (1997) The cooling of CO white dwarfs: influence of the internal chemical distribution. Astrophys J 486:413–419. https://doi.org/10.1086/304483, arXiv:astro-ph/9704038

Schatz H, Aprahamian A, Goerres J, Wiescher M, Rauscher T, Rembges JF, Thielemann F, Pfeiffer B, Moeller P, Kratz K, Herndl H, Brown BA, Rebel H (1998) rp-Process nucleosynthesis at extreme temperature and density conditions. Phys Rep 294:167–264. https://doi.org/10.1016/S0370-1573(97)00048-3

Schatz H, Bildsten L, Cumming A, Wiescher M (1999) The rapid proton process ashes from stable nuclear burning on an accreting neutron star. Astrophys J 524:1014–1029. https://doi.org/10.1086/307837, arXiv:astro-ph/9905274

Schatz H, Aprahamian A, Barnard V, Bildsten L, Cumming A, Ouellette M, Rauscher T, Thielemann F, Wiescher M (2001) End point of the rp process on accreting neutron stars. Phys Rev Lett 86:3471–3474. https://doi.org/10.1103/PhysRevLett.86.3471, arXiv:astro-ph/0102418

Schmidt W, Niemeyer JC (2006) Thermonuclear supernova simulations with stochastic ignition. Astron Astrophys 446:627–633. https://doi.org/10.1051/0004-6361:20054145, arXiv:astro-ph/0510427

Schmidt W, Niemeyer JC, Hillebrandt W, Röpke FK (2006) A localised subgrid scale model for fluid dynamical simulations in astrophysics. II. Application to Type Ia supernovae. Astron Astrophys 450:283–294. https://doi.org/10.1051/0004-6361:20053618, arXiv:astro-ph/0601500

Schwarz GJ, Ness JU, Osborne JP, Page KL, Evans PA, Beardmore AP, Walter FM, Helton LA, Woodward CE, Bode M, Starrfield S, Drake JJ (2011) Swift X-ray observations of classical novae. II. The super soft source sample. Astrophys J Suppl Ser 197:31. https://doi.org/10.1088/0067-0049/197/2/31, arXiv:1110.6224

Shafter AW (1997) On the nova rate in the galaxy. Astrophys J 487:226–236. https://doi.org/10.1086/304609

Shafter AW (2002) The galactic nova rate. In: Hernanz M, José J (eds) Classical nova explosions. American Institute of Physics conference series, vol 637, pp 462–471. https://doi.org/10.1063/1.1518246

Shafter AW, Ciardullo R, Pritchet CJ (2000) Novae in external galaxies: M51, M87, and M101. Astrophys J 530:193–206. https://doi.org/10.1086/308349

Shara MM (1982) Localized thermonuclear runaways and volcanoes on degenerate dwarf stars. Astrophys J 261:649–660. https://doi.org/10.1086/160376

Shara MM, Doyle T, Lauer TR, Zurek D, Baltz EA, Kovetz A, Madrid JP, Mikołajewska J, Neill JD, Prialnik D, Welch DL, Yaron O (2017) A Hubble space telescope survey for novae in M87. II. Snuffing out the maximum magnitude-rate of decline relation for novae as a non-standard candle, and a prediction of the existence of ultrafast novae. Astrophys J 839:109. https://doi.org/10.3847/1538-4357/aa65cd, arXiv:1702.05788

Shen KJ, Moore K (2014) The initiation and propagation of helium detonations in white dwarf envelopes. Astrophys J 797:46. https://doi.org/10.1088/0004-637X/797/1/46, arXiv:1409.3568

Shen KJ, Kasen D, Weinberg NN, Bildsten L, Scannapieco E (2010) Thermonuclear .Ia supernovae from helium shell detonations: explosion models and observables. Astrophys J 715:767–774. https://doi.org/10.1088/0004-637X/715/2/767, arXiv:1002.2258

Shore SN (2007) Astrophysical hydrodynamics: an introduction. Wiley, Hoboken

Shore SN, Schwarz G, Bond HE, Downes RA, Starrfield S, Evans A, Gehrz RD, Hauschildt PH, Krautter J, Woodward CE (2003) The early ultraviolet evolution of the ONeMg Nova V382 Velorum 1999. Astron J 125:1507–1518. https://doi.org/10.1086/367803, arXiv:astro-ph/0301415

Silverman JM, Foley RJ, Filippenko AV, Ganeshalingam M, Barth AJ, Chornock R, Griffith CV, Kong JJ, Lee N, Leonard DC, Matheson T, Miller EG, Steele TN, Barris BJ, Bloom JS, Cobb BE, Coil AL, Desroches LB, Gates EL, Ho LC, Jha SW, Kandrashoff MT, Li W, Mandel KS, Modjaz M, Moore MR, Mostardi RE, Papenkova MS, Park S, Perley DA, Poznanski D, Reuter CA, Scala J, Serduke FJD, Shields JC, Swift BJ, Tonry JL, Van Dyk SD, Wang X, Wong DS (2012) Berkeley Supernova Ia Program – I. Observations, data reduction and spectroscopic sample of 582 low-redshift Type Ia supernovae. Mon Not R Astron Soc 425:1789–1818. https://doi.org/10.1111/j.1365-2966.2012.21270.x, arXiv:1202.2128

Sim SA, Sauer DN, Röpke FK, Hillebrandt W (2007) Light curves for off-centre ignition models of Type Ia supernovae. Mon Not R Astron Soc 378:2–12. https://doi.org/10.1111/j.1365-2966.2007.11795.x, arXiv:astro-ph/0703764

Sim SA, Röpke FK, Hillebrandt W, Kromer M, Pakmor R, Fink M, Ruiter AJ, Seitenzahl IR (2010) Detonations in sub-Chandrasekhar-mass C+O white dwarfs. Astrophys J 714:L52–L57. https://doi.org/10.1088/2041-8205/714/1/L52, arXiv:1003.2917

Sim SA, Fink M, Kromer M, Röpke FK, Ruiter AJ, Hillebrandt W (2012) 2D simulations of the double-detonation model for thermonuclear transients from low-mass carbon-oxygen white dwarfs. Mon Not R Astron Soc 420:3003–3016. https://doi.org/10.1111/j.1365-2966.2011.20162.x, arXiv:1111.2117

Simonenko VA, Gryaznykh DA, Litvinenko IA, Lykov VA, Shushlebin AN (2012a) Mechanism of thermonuclear burning propagation in a helium layer on a neutron star surface: a refined model with heat conduction and subgrid turbulence. Astron Lett 38:305–320. https://doi.org/10.1134/S1063773712050088

Simonenko VA, Gryaznykh DA, Litvinenko IA, Lykov VA, Shushlebin AN (2012b) Mechanism of thermonuclear burning propagation in a helium layer on a neutron star surface: a simplified adiabatic model. Astron Lett 38:231–237. https://doi.org/10.1134/S1063773712040056

Smale AP (2001) A second intense burst with photospheric radius expansion from X2127+119 in M15. Astrophys J 562:957–962. https://doi.org/10.1086/323517, arXiv:astro-ph/0107593

Starrfield S (1989) Thermonuclear processes and the classical nova outburst. In: Classical novae. Wiley, Chichester, pp 39–60

Starrfield S, Truran JW, Sparks WM (1978a) CNO abundances and hydrodynamic studies of the Nova outburst. V – 1.00-solar-mass models with small mass envelopes. Astrophys J 226:186–202. https://doi.org/10.1086/156598

Starrfield S, Truran JW, Sparks WM, Arnould M (1978b) On Li-7 production in nova explosions. Astrophys J 222:600–603. https://doi.org/10.1086/156175

Starrfield S, Shore SN, Sparks WM, Sonneborn G, Truran JW, Politano M (1992) A prediction of the gamma-ray flux from Nova Herculis 1991. Astrophys J 391:L71–L74. https://doi.org/10.1086/186401

Starrfield S, Truran JW, Politano M, Sparks WM, Nofar I, Shaviv G (1993) ^{22}Na and ^{26}Al production in nova outbursts. Phys Rep 227:223–234. https://doi.org/10.1016/0370-1573(93)90067-N

Starrfield S, Truran JW, Wiescher MC, Sparks WM (1998) Evolutionary sequences for Nova V1974 Cygni using new nuclear reaction rates and opacities. Mon Not R Astron Soc 296:502–522. https://doi.org/10.1046/j.1365-8711.1998.01312.x

Starrfield S, Iliadis C, Hix WR, Timmes FX, Sparks WM (2009) The effects of the pep nuclear reaction and other improvements in the nuclear reaction rate library on simulations of the classical nova outburst. Astrophys J 692:1532–1542. https://doi.org/10.1088/0004-637X/692/2/1532, arXiv:0811.0197

Starrfield S, Iliadis C, Hix WR (2016) The thermonuclear runaway and the classical nova outburst. Publ Astron Soc Pac 128(5):051001. https://doi.org/10.1088/1538-3873/128/963/051001, arXiv:1605.04294

Stritzinger M, Leibundgut B, Walch S, Contardo G (2006) Constraints on the progenitor systems of Type Ia supernovae. Astron Astrophys 450:241–251. https://doi.org/10.1051/0004-6361:20053652, arXiv:astro-ph/0506415

Strohmayer T, Bildsten L (2006) New views of thermonuclear bursts. Cambridge University Press, Cambridge, pp 113–156

Strohmayer TE, Brown EF (2002) A remarkable 3 hour thermonuclear burst from 4U 1820-30. Astrophys J 566:1045–1059. https://doi.org/10.1086/338337, arXiv:astro-ph/0108420

Strohmayer TE, Zhang W, Swank JH, Smale A, Titarchuk L, Day C, Lee U (1996) Millisecond X-ray variability from an accreting neutron star system. Astrophys J 469:L9–L12. https://doi.org/10.1086/310261

Strope RJ, Schaefer BE, Henden AA (2010) Catalog of 93 nova light curves: classification and properties. Astron J 140:34–62. https://doi.org/10.1088/0004-6256/140/1/34, arXiv:1004.3698

Swank JH, Becker RH, Boldt EA, Holt SS, Pravdo SH, Serlemitsos PJ (1977) Spectral evolution of a long X-ray burst. Astrophys J 212:L73–L76. https://doi.org/10.1086/182378

Taam RE (1980) X-ray bursts from thermonuclear runaways on accreting neutron stars. Astrophys J 241:358–366. https://doi.org/10.1086/158348

Taam RE, Picklum RE (1978) Nuclear fusion and carbon flashes on neutron stars. Astrophys J 224:210–216. https://doi.org/10.1086/156367

Tajitsu A, Sadakane K, Naito H, Arai A, Aoki W (2015) Explosive lithium production in the classical nova V339 Del (Nova Delphini 2013). Nature 518:381–384. https://doi.org/10.1038/nature14161, arXiv:1502.05598

Tajitsu A, Sadakane K, Naito H, Arai A, Kawakita H, Aoki W (2016) The ^{7}Be II resonance lines in two classical novae V5668 Sgr and V2944 Oph. Astrophys J 818:191. https://doi.org/10.3847/0004-637X/818/2/191, arXiv:1601.05168

Takei D, Tsujimoto M, Kitamoto S, Ness JU, Drake JJ, Takahashi H, Mukai K (2009) Suzaku detection of superhard X-ray emission from the classical nova V2491 Cygni. Astrophys J 697:L54–L57. https://doi.org/10.1088/0004-637X/697/1/L54, arXiv:0904.1693

Tammann GA (1970) On the frequency of supernovae as a function of the integral properties of inter mediate and late type spiral galaxies. Astron Astrophys 8:458–475

Tan WP, Fisker JL, Görres J, Couder M, Wiescher M (2007) O15(α,γ)Ne19 breakout reaction and impact on X-ray bursts. Phys Rev Lett 98(24):242503/1–242503/4. https://doi.org/10.1103/PhysRevLett.98.242503, arXiv:0706.2349

Tang M, Anders E (1988) Interstellar silicon carbide – how much older than the solar system? Astrophys J 335:L31–L34. https://doi.org/10.1086/185333

Tanvir NR, Levan AJ, Fruchter AS, Hjorth J, Hounsell RA, Wiersema K, Tunnicliffe RL (2013) A 'kilonova' associated with the short-duration γ-ray burst GRB 130603B. Nature 500:547–549. https://doi.org/10.1038/nature12505, arXiv:1306.4971

Tatischeff V, Hernanz M (2007) Evidence for nonlinear diffusive shock acceleration of cosmic rays in the 2006 outburst of the recurrent nova RS Ophiuchi. Astrophys J 663:L101–L104. https://doi.org/10.1086/520049, arXiv:0705.4422

Tatischeff V, Tavani M, von Ballmoos P, Hanlon L, Oberlack U, Aboudan A, Argan A, Bernard D, Brogna A, Bulgarelli A, Bykov A, Campana R, Caraveo P, Cardillo M, Coppi P, De Angelis A, Diehl R, Donnarumma I, Fioretti V, Giuliani A, Grenier I, Grove JE, Hamadache C, Hartmann D, Hernanz M, Isern J, Kanbach G, Kiener J, Knödlseder J, Labanti C, Laurent P, Limousin O, Longo F, Marisaldi M, McBreen S, McEnery JE, Mereghetti S, Mirabel F, Morselli A, Nakazawa K, Peyré J, Piano G, Pittori C, Sabatini S, Stawarz L, Thompson DJ, Ulyanov A, Walter R, Wu X, Zdziarski A, Zoglauer A (2016) The e-ASTROGAM gamma-ray space mission. In: Space telescopes and instrumentation 2016: ultraviolet to gamma ray, Proc SPIE, vol 9905, p 99052N. https://doi.org/10.1117/12.2231601, arXiv:1608.03739

Taubenberger S (2017) The extremes of thermonuclear supernovae. arXiv:1703.00528

Thielemann F, Brachwitz F, Freiburghaus C, Kolbe E, Martinez-Pinedo G, Rauscher T, Rembges F, Hix WR, Liebendörfer M, Mezzacappa A, Kratz K, Pfeiffer B, Langanke K, Nomoto K, Rosswog S, Schatz H, Wiescher W (2001) Element synthesis in stars. Prog Part Nucl Phys 46:5–22. https://doi.org/10.1016/S0146-6410(01)00103-X, arXiv:astro-ph/0101476

Thielemann F, Brachwitz F, Höflich P, Martinez-Pinedo G, Nomoto K (2004) The physics of Type Ia supernovae. New Astron Rev 48:605–610. https://doi.org/10.1016/j.newar.2003.12.038

Timmes FX, Woosley SE (1992) The conductive propagation of nuclear flames. I – degenerate C + O and O + NE + MG white dwarfs. Astrophys J 396:649–667. https://doi.org/10.1086/171746

Truran JW, Arnett WD, Cameron AGW (1967) Nucleosynthesis in supernova shock waves. Can J Phys 45:2315–2332

van den Bergh S, Tammann GA (1991) Galactic and extragalactic supernova rates. Annu Rev Astron Astrophys 29:363–407. https://doi.org/10.1146/annurev.aa.29.090191.002051

van Horn HM, Hansen CJ (1974) A model for the transient X-ray sources. Astrophys J 191:479–482. https://doi.org/10.1086/152987

van Paradijs J, McClintock JE (1995) Optical and ultraviolet observations of X-ray binaries. In: Lewin WHG, van Paradijs J, van den Heuvel EPJ (eds) X-ray binaries. Cambridge University Press, Cambridge, pp 58–125

Villarreal AR, Strohmayer TE (2004) Discovery of the neutron star spin frequency in EXO 0748-676. Astrophys J 614:L121–L124. https://doi.org/10.1086/425737, arXiv:astro-ph/0409384

Vurm I, Metzger BD (2018) High-energy emission from nonrelativistic radiative shocks: application to Gamma-ray novae. Astrophys J 852:62. https://doi.org/10.3847/1538-4357/aa9c4a

Waki I, Inoue H, Koyama K, Matsuoka M, Murakami T, Ogawara Y, Ohashi T, Tanaka Y, Hayakawa S, Tawara Y, Miyamoto S, Tsunemi H, Kondo I (1984) Discovery of absorption lines in X-ray burst spectra from X1636-536. Publ Astron Soc Jpn 36:819–830

Walker MF (1954) Nova DQ Herculis (1934): an eclipsing binary with very short period. Publ Astron Soc Pac 66:230. https://doi.org/10.1086/126703

Ward RA, Fowler WA (1980) Thermalization of long-lived nuclear isomeric states under stellar conditions. Astrophys J 238:266–286. https://doi.org/10.1086/157983

Warner B (1995) Cataclysmic variable stars. Cambridge University Press, Cambridge

Webbink RF (1984) Double white dwarfs as progenitors of R Coronae Borealis stars and Type I supernovae. Astrophys J 277:355–360. https://doi.org/10.1086/161701

Weinberg NN, Bildsten L (2007) Carbon detonation and shock-triggered helium burning in neutron star superbursts. Astrophys J 670:1291–1300. https://doi.org/10.1086/522111, arXiv:0706.3062

Weinberg NN, Bildsten L, Schatz H (2006) Exposing the nuclear burning ashes of radius expansion Type I X-ray bursts. Astrophys J 639:1018–1032. https://doi.org/10.1086/499426, arXiv:astro-ph/0511247

Weiss A, Truran JW (1990) Na-22 and Al-26 production and nucleosynthesis in novae explosions. Astron Astrophys 238:178–186

Wheeler JC, Harkness RP (1990) Type I supernovae. Rep Prog Phys 53:1467–1557. https://doi.org/10.1088/0034-4885/53/12/001

Whelan J, Iben I Jr (1973) Binaries and supernovae of Type I. Astrophys J 186:1007–1014. https://doi.org/10.1086/152565

White NE, Nagase F, Parmar AN (1995) The properties of X-ray binaries. In: Lewin WHG, van Paradijs J, van den Heuvel EPJ (eds) X-ray binaries. Cambridge University Press, Cambridge, pp 1–57

Wiescher M, Gorres J, Thielemann F, Ritter H (1986) Explosive hydrogen burning in novae. Astron Astrophys 160:56–72

Wijnands R (2001) Recurrent very long Type I X-ray bursts in the low-mass X-Ray binary 4U 1636-53. Astrophys J 554:L59–L62. https://doi.org/10.1086/320922, arXiv:astro-ph/0103125

Williams RE (1992) The formation of novae spectra. Astron J 104:725–733. https://doi.org/10.1086/116268

Woosley SE (1986) Nucleosynthesis and stellar evolution. In: Audouze J, Chiosi C, Woosley SE (eds) Saas-fee advanced course 16: nucleosynthesis and chemical evolution. Geneva Observatory, Geneva, p 1

Woosley SE, Taam RE (1976) Gamma-ray bursts from thermonuclear explosions on neutron stars. Nature 263:101–103. https://doi.org/10.1038/263101a0

Woosley SE, Weaver TA (1986) The physics of supernova explosions. Annu Rev Astron Astrophys 24:205–253. https://doi.org/10.1146/annurev.aa.24.090186.001225

Woosley SE, Heger A, Cumming A, Hoffman RD, Pruet J, Rauscher T, Fisker JL, Schatz H, Brown BA, Wiescher M (2004) Models for Type I X-ray bursts with improved nuclear physics. Astrophys J Suppl Ser 151:75–102. https://doi.org/10.1086/381533, arXiv:astro-ph/0307425

Yaron O, Prialnik D, Shara MM, Kovetz A (2005) An extended grid of nova models. II. The parameter space of nova outbursts. Astrophys J 623:398–410. https://doi.org/10.1086/428435, arXiv:astro-ph/0503143

Yoon S, Langer N (2005) On the evolution of rapidly rotating massive white dwarfs towards supernovae or collapses. Astron Astrophys 435:967–985. https://doi.org/10.1051/0004-6361:20042542, arXiv:astro-ph/0502133

Zheng W, Shivvers I, Filippenko AV, Itagaki K, Clubb KI, Fox OD, Graham ML, Kelly PL, Mauerhan JC (2014) Estimating the first-light time of the Type Ia supernova 2014J in M82. Astrophys J 783:L24. https://doi.org/10.1088/2041-8205/783/1/L24, arXiv:1401.7968

Zingale M, Dursi LJ (2007) Propagation of the first flames in Type Ia supernovae. Astrophys J 656:333–346. https://doi.org/10.1086/510306, arXiv:astro-ph/0610297

Zingale M, Timmes FX, Fryxell B, Lamb DQ, Olson K, Calder AC, Dursi LJ, Ricker P, Rosner R, MacNeice P, Tufo HM (2001) Helium detonations on neutron stars. Astrophys J Suppl Ser 133:195–220. https://doi.org/10.1086/319182

Zingale M, Malone CM, Nonaka A, Almgren AS, Bell JB (2015) Comparisons of two- and three-dimensional convection in Type I X-ray bursts. Astrophys J 807:60. https://doi.org/10.1088/0004-637X/807/1/60, arXiv:1410.5796

Zinner EK (2005) Presolar grains. Elsevier, Oxford, pp 17–39

Zwicky F (1938) On collapsed neutron stars. Astrophys J 88:522–525. https://doi.org/10.1086/144003

AUTHOR QUERIES

AQ1. Please check the presentation of affiliations and correct if necessary.
AQ2. Please provide subject index term for this chapter.
AQ3. Missing citation for Figs. 5.6, 5.7, 5.8, 5.9, 5.16, 5.17 was inserted in the text. Please check if appropriate. Otherwise, please provide citations for Figs. 5.6, 5.7, 5.8, 5.9, 5.16, 5.17. Note that the order of main citations of figures in the text must be sequential.
AQ4. Please provide revised artwork for Fig. 5.8 as the text quality is blurred.
AQ5. Please provide revised artwork for Fig. 5.13 as the text size is too small.
AQ6. Please check whether the unit "photons/s/cm^2" can be changed to "photons cm^{-2} s^{-1}" in the sentence "The total expected...".
AQ7. Missing citation for Table 5.2 was inserted here. Please check if appropriate. Otherwise, please provide citation for Table 5.2. Note that the order of main citations of tables in the text must be sequential.